



713  
2017

# Berichte

zur Polar- und Meeresforschung

Reports on Polar and Marine Research

## The Expedition PS102 of the Research Vessel POLARSTERN to the Atlantic Ocean in 2016

Edited by

Karen Wiltshire, Eva-Maria Brodte, Annette Wilson and  
Peter Lemke with contributions of the participants

Die Berichte zur Polar- und Meeresforschung werden vom Alfred-Wegener-Institut, Helmholtz-Zentrum für Polar- und Meeresforschung (AWI) in Bremerhaven, Deutschland, in Fortsetzung der vormaligen Berichte zur Polarforschung herausgegeben. Sie erscheinen in unregelmäßiger Abfolge.

Die Berichte zur Polar- und Meeresforschung enthalten Darstellungen und Ergebnisse der vom AWI selbst oder mit seiner Unterstützung durchgeführten Forschungsarbeiten in den Polargebieten und in den Meeren.

Die Publikationen umfassen Expeditionsberichte der vom AWI betriebenen Schiffe, Flugzeuge und Stationen, Forschungsergebnisse (inkl. Dissertationen) des Instituts und des Archivs für deutsche Polarforschung, sowie Abstracts und Proceedings von nationalen und internationalen Tagungen und Workshops des AWI.

Die Beiträge geben nicht notwendigerweise die Auffassung des AWI wider.

Herausgeber

Dr. Horst Bornemann

Redaktionelle Bearbeitung und Layout

Birgit Reimann

Alfred-Wegener-Institut  
Helmholtz-Zentrum für Polar- und Meeresforschung  
Am Handeshafen 12  
27570 Bremerhaven  
Germany

[www.awi.de](http://www.awi.de)  
[www.reports.awi.de](http://www.reports.awi.de)

Der Erstautor bzw. herausgebende Autor eines Bandes der Berichte zur Polar- und Meeresforschung versichert, dass er über alle Rechte am Werk verfügt und überträgt sämtliche Rechte auch im Namen seiner Koautoren an das AWI. Ein einfaches Nutzungsrecht verbleibt, wenn nicht anders angegeben, beim Autor (bei den Autoren). Das AWI beansprucht die Publikation der eingereichten Manuskripte über sein Repository ePIC (electronic Publication Information Center, s. Innenseite am Rückdeckel) mit optionalem print-on-demand.

The Reports on Polar and Marine Research are issued by the Alfred Wegener Institute, Helmholtz Centre for Polar and Marine Research (AWI) in Bremerhaven, Germany, succeeding the former Reports on Polar Research. They are published at irregular intervals.

The Reports on Polar and Marine Research contain presentations and results of research activities in polar regions and in the seas either carried out by the AWI or with its support.

Publications comprise expedition reports of the ships, aircrafts, and stations operated by the AWI, research results (incl. dissertations) of the Institute and the Archiv für deutsche Polarforschung, as well as abstracts and proceedings of national and international conferences and workshops of the AWI.

The papers contained in the Reports do not necessarily reflect the opinion of the AWI.

Editor

Dr. Horst Bornemann

Editorial editing and layout

Birgit Reimann

Alfred-Wegener-Institut  
Helmholtz-Zentrum für Polar- und Meeresforschung  
Am Handeshafen 12  
27570 Bremerhaven  
Germany

[www.awi.de](http://www.awi.de)  
[www.reports.awi.de](http://www.reports.awi.de)

The first or editing author of an issue of Reports on Polar and Marine Research ensures that he possesses all rights of the opus, and transfers all rights to the AWI, including those associated with the co-authors. The non-exclusive right of use (einfaches Nutzungsrecht) remains with the author unless stated otherwise. The AWI reserves the right to publish the submitted articles in its repository ePIC (electronic Publication Information Center, see inside page of verso) with the option to "print-on-demand".

*Titel: Stipendiaten des NoSoAT16 (North South Atlantic Transect) Programms vor Beginn des Trainings an Bord der Polarstern (Foto: Eva Brodte, AWI).*

*Cover: Scholars of the NoSoAT16 (North South Atlantic Transect) programme at the start of the training on board Polarstern (Photo: Eva Brodte, AWI).*

# **The Expedition PS102 of the Research Vessel POLARSTERN to the Atlantic Ocean in 2016**

---

**Edited by**

**Karen Wiltshire, Eva-Maria Brodte, Annette Wilson and Peter Lemke  
with contributions of the participants**

**Please cite or link this publication using the identifiers**

**hdl:10013/epic.52029 or <http://hdl.handle.net/10013/epic.52029> and  
[https://doi.org/10.2312/BzPM\\_0713\\_2017](https://doi.org/10.2312/BzPM_0713_2017)**

**ISSN 1866-3192**

# **PS102**

**12 November 2016 – 12 December 2016**

**Bremerhaven - Cape Town**

**Chief Scientist  
Karen Wiltshire**

**Coordinator  
Rainer Knust**

## Contents

1.	<b>Überblick und Fahrtverlauf</b>	<b>2</b>
	<b>Itinerary and Summary</b>	<b>4</b>
2.	<b>Weather Conditions</b>	<b>5</b>
3.	<b>North South Atlantic Training 2016 (NOSOAT)</b>	<b>7</b>
4.	<b>Genetic and Epigenetic Changes in Organisms Carried in Ballast Water during Trans-Equatorial Travels in the Atlantic Ocean</b>	<b>60</b>
5.	<b>Autonomous Measurement Platforms for Energy and Material Exchange between Ocean and Atmosphere (Oceanet): Atmosphere</b>	<b>63</b>
6.	<b>Column-Integrated Optical Measurements of Aerosol, Water Vapour and Clouds</b>	<b>70</b>
7.	<b>Stable N - Isotopes of Ammonium and Ammonia over the Atlantic Ocean</b>	<b>78</b>
8.	<b>En-Route Test of Upgraded Ship Data Management System Dship</b>	<b>80</b>
9.	<b>Test of New Sea Water Supply and Test of Attached Sensors</b>	<b>81</b>
10.	<b>Integration of New Motion Sensor Ixblue Hydrins (Part 2)</b>	<b>82</b>
11.	<b>Acknowledgements</b>	<b>83</b>
	<b>APPENDIX</b>	<b>84</b>
A.1	<b>Teilnehmende Institute / Participating Institutions</b>	<b>85</b>
A.2	<b>Fahrtteilnehmer / Cruise Participants</b>	<b>89</b>
A.3	<b>Schiffsbesatzung / Ship's Crew</b>	<b>93</b>
A.4	<b>Stationsliste / Station List PS102</b>	<b>94</b>

# 1. ÜBERBLICK UND FAHRTVERLAUF

Karen Wiltshire, Eva Brodte

AWI

Die Transitfahrt von Bremerhaven nach Kapstadt war in zwei Abschnitte geteilt (Bremerhaven – Las Palmas; 12.11.2016 bis 21.11.2016 und Las Palmas – Kapstadt 21.11.2016 bis 12.12.2016; Abb. 1.1). Auf dem ersten Abschnitt wurde u. a. das neue Datenaquisitions- und Managementsystem Dship (DAS) etabliert und erfolgreich getestet.

Beide Fahrtabschnitte standen hauptsächlich im Zeichen der studentischen Ausbildung. An dem Programm NoSoAT (North South Atlantic Transect) nahmen insgesamt 25 Studenten aus 18 Ländern teil. Bord-seitige Probennahmen und Analysen umfassten Küsten und Ozeanische Bereiche von den flachen Schelfgewässern der Nordsee und des Englischen Kanals hindurch zu den tiefen Gewässern der Kanarischen Inseln und des Afrikanischen Kontinents mit den hoch produktiven Gewässern der Auftriebsgebiete vor der Küste Namibias.

Auf der gesamten Fahrt wurden 11 Stationen entlang der Strecke beprobt (Abb. 1.1). Während des Transits wurden die Studenten durch ein internationales Expertenteam in die Grundlagen ozeanographischer und atmosphärischer Wechselwirkungen und ihre Einflüsse auf das Klima unterrichtet. Für die Messungen physikalischer und chemischer Parameter wurden CTD mit Wasserschöpfer, XBTs und Ferrybox eingesetzt. Während der Stationen wurde die Wassersäule mit einer CTD mit Wasserrosette bis in die Nähe des Meeresbodens beprobt. Die gewonnenen Wasserproben wurden auf Nährstoffgehalte und Salzgehalt untersucht. Zusätzlich wurden in den oberen photischen Wasserschichten (photisch Zone bis 50 m unterhalb des Chlorophyllmaximums) ein Planktonnetz-Hol und die Bestimmung der Algenklassenzusammensetzung mit einer fluorometrischen Sonde durchgeführt. Das Phytoplankton wurde qualitativ auf den Stationen und entlang der Route bestimmt. Zudem wurden eingebettet in das Ausbildungs- und Datenerhebungsprogramm *en route* täglich eine Radiosonde zur Temperaturbestimmung in die Atmosphäre und ab Las Palmas XBTs (Expendable Bathythermograph) zur Temperaturprofilierung des Wasserkörpers eingesetzt, mit denen Temperaturmessungen zwischen 1,8 km unter der Wasseroberfläche bis 10 km darüber durchgeführt wurden.

Das Lehrprogramm setzte sich aus den Modulen (i) Klima, (ii) Remote Sensing, (iii) Climate and Ocean Governance, (iv) Art and Science und (v) Ozeanographie zusammen. Das gemeinsame Arbeiten und Lernen wurde durch das Alfred-Wegener-Institut Helmholtz-Zentrum für Polar- und Meeresforschung (AWI) in Kooperation mit der Strategic Marine Alliance for Research & Training (SMART) und der Partnership for Observation of the Global Oceans (POGO) organisiert. Die Summer School wurde durch die Nippon Foundation / POGO Centre of Excellence, durch REKLIM und die FU Berlin unterstützt. Ebenfalls auf beiden Fahrtabschnitten führte das Leibniz-Institut für Troposphärenforschung (TROPOS) chemische und physikalische Messungen zum Energie- und Materialaustausch zwischen Ozean und Atmosphäre durch. Die Arbeiten konnten mit Einlaufen in Kapstadt, wie bereits auf anderen Transittfahrten mit *Polarstern*, sehr erfolgreich abgeschlossen werden.

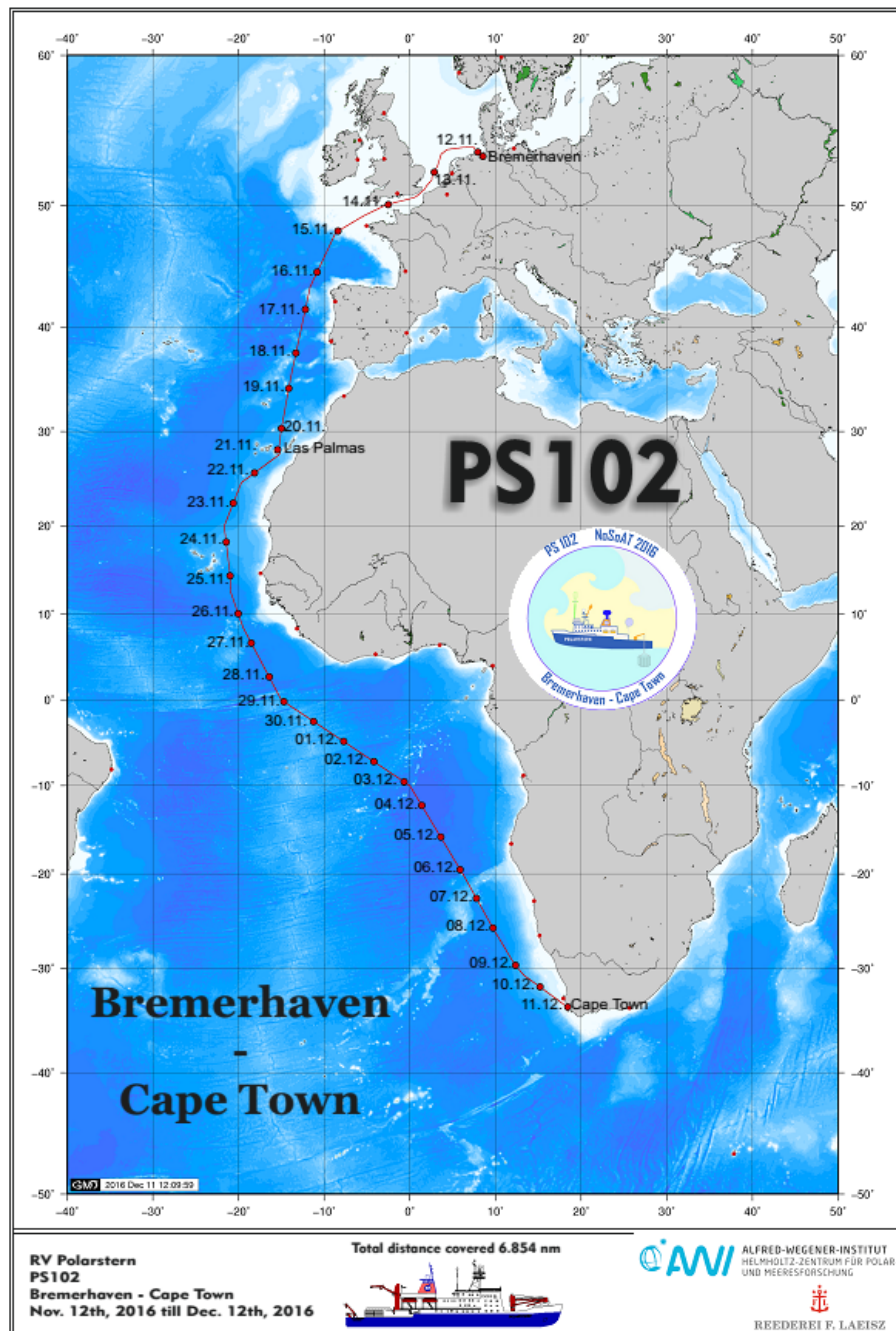


Fig. 1.1: Fahrtroute der Expedition PS102 (Graphik Andreas Winter).  
Siehe <https://doi.pangaea.de/10.1594/PANGAEA.872695> für eine Darstellung des master tracks in Verbindung mit der Stationsliste.

Fig. 1.1: Cruise track of the PS102 expedition (image by Andreas Winter).  
See <https://doi.pangaea.de/10.1594/PANGAEA.872695> to display the master track in conjunction with the list of stations.

## ITINERARY AND SUMMARY

The transit cruise from Bremerhaven to Cape Town (South Africa) was split into two legs (Fig. 1.1). *Polarstern* departed Bremerhaven on 12 November 2016 and arrived in Las Palmas on 21 November, as planned, completing the first leg of the journey. The testing and installation of a new data acquisition (DAS) and management system for Dship was successfully carried out on the first leg. The second leg of the transit cruise began on the same day, 21 November, from Las Palmas after an exchange of scientific personnel. The expedition PS102 ended in Cape Town on 12 December 2016 as scheduled.

The PS102 transit cruise was dedicated to the training and education of 25 ocean and climate science students from 18 different nations. The NoSoAT (North South Atlantic Transect) was designed to train students on-board RV *Polarstern* in a professional environment. Ship-board sampling and analysis were carried out in a range of coastal and oceanic environments; from the shallow shelf waters of the North Sea and English Channel through the deep waters off the Canary Islands and African continent and the highly productive waters of the upwelling areas off the coast of Namibia.

During the transit, the postgraduate students were trained by a team of international experts in the principles of oceanographic and atmospheric interactions and their impacts on climate. A variety of instruments were deployed for ocean and atmospheric measurements, both en-route and at 11 stationary sampling stations. Physical and chemical measurements were carried out using the on-board CTD and rosette water sampler. Expendable bathythermographs were deployed (after Las Palmas) to obtain temperature measurements with a higher resolution. Continuous underway measurements were obtained by means of the thermosalinograph and the ferrybox systems. Plankton net-hauls were carried out to sample the upper water column (photic zone to 50 m below the chlorophyll maximum), with a fluorometric probe additionally deployed to characterize the main algae groups. Daily radiosonde and XBT launches were embedded in the teaching programme and provided temperature measurements ranging from 1.8 km below the surface to 10 km above.

The teaching programme comprised the five different modules: (i) Climate, (ii) Remote Sensing, (iii) Climate and Ocean Governance, (iv) Art and Science and (v) Oceanography. This joint working and learning programme was organized by the Alfred Wegener Institute Helmholtz Center for Polar and Marine Research (AWI) in cooperation with the Strategic Marine Alliance for Research & Training (SMART) and the Partnership for Observation of the Global Oceans (POGO). The summer school was supported by the Nippon Foundation / POGO Centre of Excellence, REKLIM and the FU Berlin. During both cruise legs the Leibniz Institute for Tropospheric Research (TROPOS) carried out chemical and physical measurements of energy and material exchange between ocean and atmosphere. All work was successfully completed on arrival in Cape Town like on previous transit cruises with RV *Polarstern*.

## 2. WEATHER CONDITIONS

Max Miller, Hartmut Sonnabend

DWD

On Saturday morning, November 12, 2016, 09:50 am, *Polarstern* left Bremerhaven for the campaign PS102. Light south-easterly winds, minus 3° C, sunshine and mist were observed.

There was a high over northern Germany. On the other hand the frontal system of a storm near Iceland had reached the English Channel, moved towards the German Bight and weakened. Therefore winds from southeast to south increased rapidly and peaked at Bft 7 during the night to Sunday (Nov. 13) while we steamed the southwestern North Sea. A sea state of 2.5 m was forced. After the passage of the cold front winds veered north and freshened up to Bft 6 for short times.

The high at the Azores already built a ridge towards the English Channel. At first *Polarstern* steamed along its north side at westerly winds Bft 5. From Wednesday (Nov. 16) on we sailed along the east side of the high and winds veered northwest to north. Until our stopover at Las Palmas (Nov. 21) winds did not exceed Bft 4 but moist air masses caused some showers.

From Tuesday (Nov. 22) on we steamed the Northern Trade Wind Zone at a predominant wind force 5 Bft. Up to the Cape Verde Islands isolated showers still occurred. Afterwards the air became enriched with some Sahara dust.

During the night to Sunday (Nov. 27) we arrived at the Inter Tropical Convergence Zone (ITCZ). We observed some showers but no thunderstorm. Already on Monday (Nov. 28) *Polarstern* entered the Southern Trade Wind Zone, crossed the Equator on Tuesday morning and afterwards the showers ended soon.

During the remaining part of the cruise we sailed the Southern Trade Wind Zone and along the Subtropical High over the South Atlantic. Winds did not exceed Bft 5.

On Friday (Dec. 09) a low formed over South Africa and together with the Subtropical High the pressure gradient increased. Therefore south-easterly winds freshened up gradually on Saturday, peaked at Bft 7 for short times during the night to Sunday (Dec. 11) and caused a sea state around 3 m.

On Sunday afternoon, December 11, 2016, *Polarstern* reached Cape Town at moderate and temporarily gusty winds from south to southeast.

For further statistics see attached files (Fig. 2.1 – Fig. 2.3).

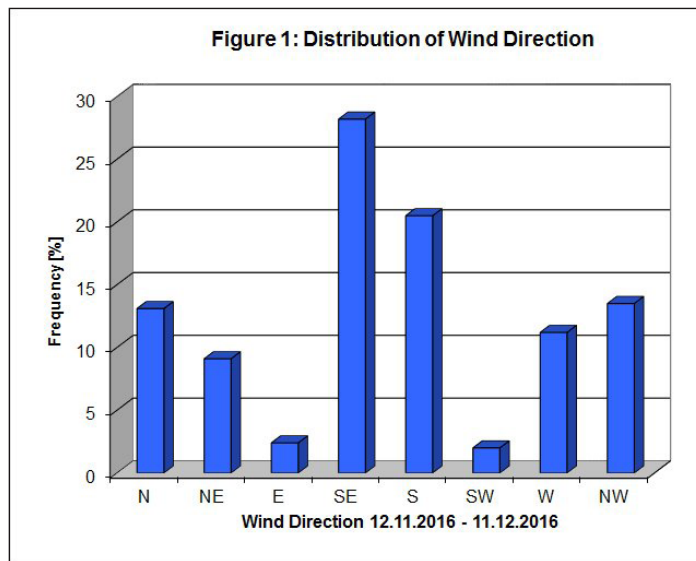


*Fig. 2.1:  
Distribution of  
wind direction*

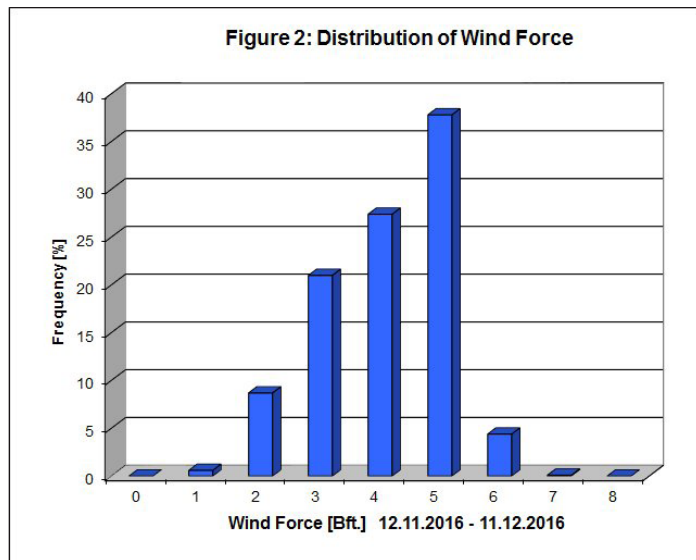


*Fig. 2.2:  
Distribution of  
wind forces*

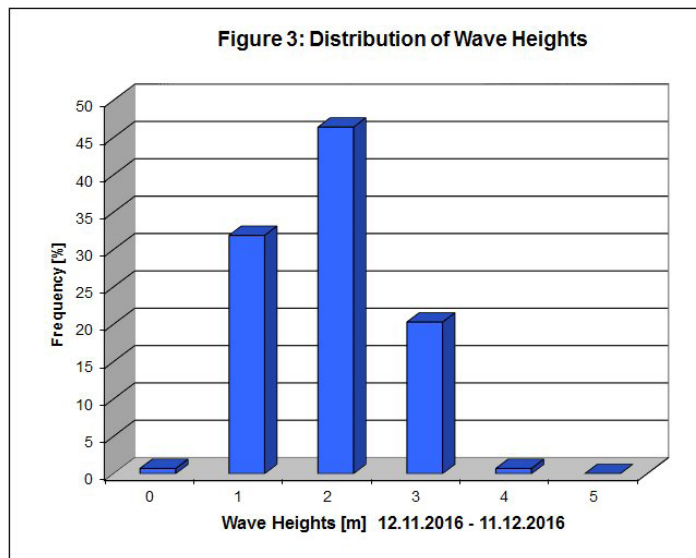


*Fig. 2.3:  
Distribution of  
wave heights*

### 3. NORTH SOUTH ATLANTIC TRAINING 2016 (NOSOAT)

Karen Wiltshire<sup>1</sup>, Peter Lemke<sup>1</sup>, Eva-Maria Brodte<sup>1</sup>, Sabine Schlacke<sup>2</sup>, Peter Croot<sup>3</sup>, P. McGrane (not on board)<sup>3</sup>, Lionel Playford<sup>4</sup>, Kristine Carstens<sup>1</sup>, Thomas Ruhtz<sup>5</sup>, Ulrich Küster<sup>5</sup>, Therese Keck<sup>5</sup>, Rene Preusker<sup>5</sup>, Heike Kalesse<sup>6</sup>, Stephanie Fiedler<sup>7</sup>, Moritz Haarig<sup>6</sup>, Johannes Rick<sup>1</sup>, Annette Wilson<sup>1</sup>, Eva Garcia-Vazquez<sup>9</sup>, Anastasija Zaiko<sup>8</sup>, A. Ardura<sup>9</sup> (not on board), A. Macke<sup>6</sup> (not on board), R Engelmann<sup>6</sup> (not on board), H. Deneke<sup>6</sup> (not on board), S. Kinne<sup>7</sup>(not on board), F. Jansen<sup>7</sup> (not on board), Heidi Witte–Gaedecke<sup>11</sup>, Julia Goedecke<sup>11</sup>, G. Gravenhorst (not on board)<sup>11</sup>, Adedayo Adeleye<sup>12</sup>, William Copeland<sup>12</sup>, Abigail Cronin<sup>12</sup>, Aurelia Reichardt<sup>12</sup>, Subrata Sarker<sup>12</sup>, Michelle Curran<sup>12</sup>, Andrian Gajigan<sup>12</sup>, Carla Geisen<sup>12</sup>, Clynton Gregory<sup>12</sup>, Carla Espinosa Lagunes<sup>12</sup>, Clara Magalhães Loureiro<sup>12</sup>, Daniel Gebregiorgis Yirgaw<sup>12</sup>, Eoghan Daly<sup>12</sup>, Katherine Amorim<sup>12</sup>, Walaa Thabet<sup>12</sup>, Inge Deshepper<sup>12</sup>, Sophie Ehrhardt<sup>12</sup>, Rabie Maarouf<sup>12</sup>, Hugh O’Sullivan<sup>12</sup>, Elena Shestakova<sup>12</sup>, Sarit O’Donovan<sup>12</sup>, Helena Zambalos<sup>12</sup>, Philip Sagero<sup>12</sup>, Valeria Giunta<sup>12</sup>, Sebastian Hoepker<sup>12</sup>

<sup>1</sup>AWI

<sup>2</sup>University Münster

<sup>3</sup>NUIG, MIG

<sup>4</sup>Northumbria University

<sup>5</sup>FUB

<sup>6</sup>TROPOS

<sup>7</sup>MPI-M

<sup>8</sup>UKlaipeda, Cawthron Institute

<sup>9</sup>UOviedo

<sup>11</sup>GAUG

<sup>12</sup>NoSoAT Scholars

#### Grant No AWI\_PS102\_00

#### Objectives

Ocean and shelf seas are pivotal to the future of humankind. Currently oceans provide roughly 20 % of the protein consumed by humans. The world GDP is mainly based on ocean economical aspects. Emerging and developing countries, with a huge need for ocean resources, play an ever-increasing role in defining ocean governance and science. Education founded on a well-managed mix of interests and needs in the field of oceanography and marine science is more imperative than ever in order to secure earths’ future oceans as a sustainable resource. We aim to train ocean experts to address the sustainability of our global ocean, promoting excellence and moral sounding.

In 2015 and 2016, the two North to South transects on *Polarstern* were used to provide a shipboard training to scholars in a professional environment, sampling stations along a transect in the Atlantic Ocean from Bremerhaven to Cape Town. To access this training the students had applied to a call and 25 scholars were selected of more than 400 applications.

The aim of this programme is to chart and characterize different water bodies along a North-South Atlantic Transect, as part of training exercise for capacity building in oceanography. An international group of 25 students was trained in basic oceanographic principles including seagoing methods and sampling associated with these. Using the transit of *Polarstern* from North to South to implement training of students with real scientific data sampling is beneficiary for everyone.

The study objectives of the training included differentiation of different water masses via temperature, salinity, turbidity etc, localization of thermocline, detection of salinity gradients, turbidity, comparison of ground-truth data with remote sensing, measurements of atmospheric properties, studies of climate physics, discussion of the law of the sea and its impacts on *in-situ* marine observations, introduction into the international climate negotiations and approaching scientific questions through art.

All survey participants were divided into groups of five scholars which rotated between the five main disciplines (see Fig. 3.1):

1. Climate and Meteorology
2. Oceanography
3. Remote Sensing of Ocean and Atmosphere
4. Ocean and Climate Change Governance
5. Understanding the Ocean and Atmosphere Through Art



Fig. 3.1: Rotation scheme: all survey participants were divided into groups of five which will rotate between the five main disciplines

Each group rotation lasted 4 days and included an average of two (CTD-) stations per rotation. The last station was conducted by the students without active engagement of the teachers to prove their acquired knowledge. Along the transect stationary work as well as en-route sampling were carried out. The maps of the conducted stations are shown in Fig. 3.2.

## Work at sea

### *CTD Rosette sampling*

Investigations of the hydrographic regime included about 11 CTD casts measuring temperature, salinity and depth coupled with additional sensors to provide information on fluorescence, turbidity, oxygen etc. Water samples from depth will be recovered via Niskin bottles in a rosette frame and analysed for quantitative determination of "chlorophyll a" concentrations (Fig.3.2).

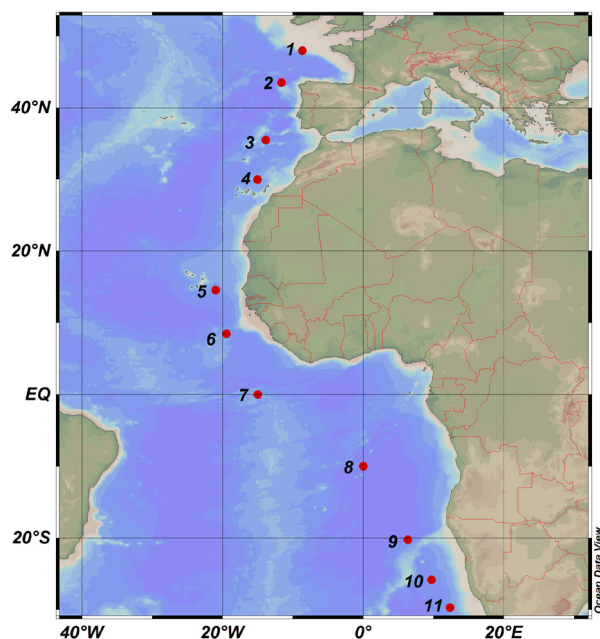


Fig. 3.2: Locations of CTD stations along the transect

### XBT Deployments

Physical environmental data were enhanced by regular deployment of Expendable Bathythermographs (XBTs) to measure the thermal structure of the upper 1.8 km of the water column. XBT probes were ‘fired’ during the second leg of the cruise when the vessel was underway at a speed of approximately 6 knots. In order to resolve fine scale shelf features such as fronts and mesoscale eddies XBT probes were generally deployed each day covering a distance between the stations of about ~25 km (Fig. 3.3). Additionally, an UnderwayCTD (Ocean science 10-400 UnderwayCTD) were used for underway profiling.

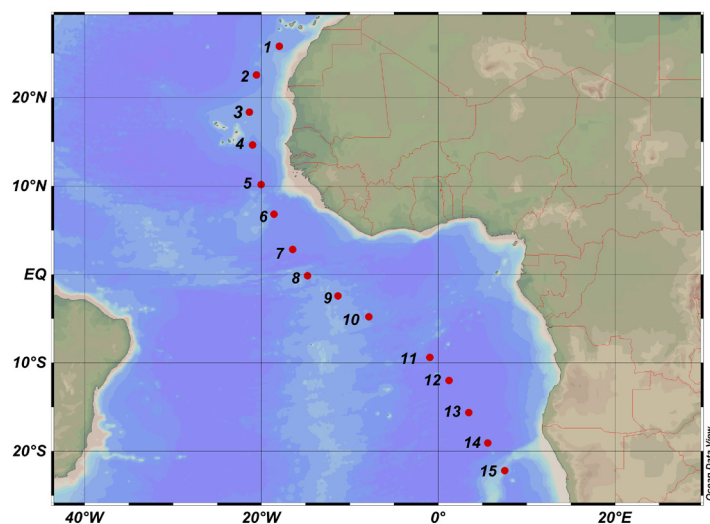


Fig. 3.3: Locations of XBT stations along the transect

### *Thermosalinograph DAS measurements & sampling*

Temperature and salinity are measured by means of a Thermosalinograph (TSG), a Ferry Box, an Underway Conductivity, Temperature and Depth (UCTD), and CTD (conductivity, temperature and depth) casts, which can sample at various depths down to the seafloor. Additionally, temperature is measured by an Expendable Bathythermographs (XBT) which measures the upper ocean (circa 1,800 metres). In addition, underway sub-surface (ca. 3 m) temperature, salinity and fluorescence data will be collected using the vessels thermosalinograph unit and underway data acquisition system (DAS).

### *Data analysis*

Simple T/S (CTD) and scatter plots (XBT) were worked up along the transect to give the students a good understanding of differing water mass characteristics and data handling. At the end of the cruise the students provided reports concerning the measured data (see Reports of the research projects on board). For increased spatial resolution of temperature records along the transect, measurements from both CTD and XBT stations were combined, linearly interpolating (in Ocean Data Viewer; ODV) between the individual profiles. For the purpose of identifying upwelling, only data for the upper 300 m of the water column are shown here, focussing on the variability of temperature, salinity, and oxygen concentrations in the surface ocean.

The CTD and XBT show a generally good correlation in the results, indicating that the results are robust. There is some symmetry north and south of the equator. Temperature shows symmetry, particularly in the top surface and at depth. This is likely due to the similar characteristics of the deep-water masses. The Antarctic Bottom Water is slightly denser than the North Atlantic Deep Water and therefore the water masses sit on top of each other, both north and south of the equator. The surface waters exhibit a slight symmetry. Similarly, the salinity at depth exhibits a general symmetry either side of the equator, however, the top 1,000 m is asymmetrical.

By using oceanographic and atmospheric data of the transect from the North to South Atlantic one station showed clear characteristics of upwelling. It is likely that this station has the influence of the Benguela upwelling system, which is known to occur during this area at this time. For the other stations, the collected data was inconclusive and insufficient to clearly define further upwelling systems. Results may be skewed due to the extrapolation of data in between stations. To investigate upwelling along this transect using CTD data a more appropriate distance of ~ 30 nautical miles between stations in and around the known upwelling region would be required. Post cruise analysis of biochemical data including nutrients is expected to lead to a more accurate analysis and identification of upwelling regions along the transect.

*In-situ* measured conductivity [ $S\ m^{-1}$ ] was converted into salinity as a function of temperature and pressure. Temperature and salinity data of the eastern Atlantic from *Polarstern* cruises PS73 (October 1985), PS81 (November 2012), PS95 (November 2015) were used for the estimation of heat content. Co-locating stations were selected to estimate long-term change.

Heat content of sea water is calculated as the vertical integration of temperature multiplied by the sea water density and specific heat capacity. Thus, heat contents ( $H$ ) of sea water along the North South Atlantic Transect (NoSoAT) is estimated using the formula: Where,  $\rho$  is the sea water density ( $kg/m^3$ ),  $C$  is the specific heat capacity (Joule/kg),  $T_0$  is the temperature ( $^{\circ}C$ ) profile,  $dh$  is the change of depth and,  $h_2$  and  $h_0$  indicate the lower and upper limit of the depth profile.

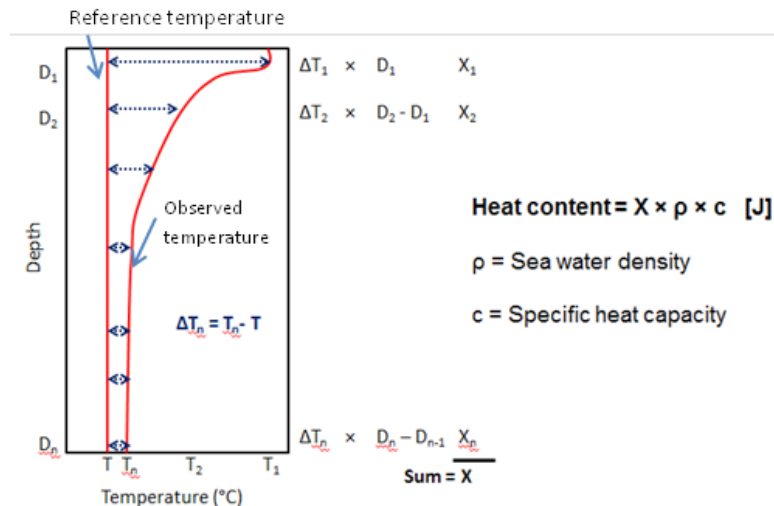


Fig. 3.4: Schematic representation of the ocean heat content estimation process

To estimate the heat content, a reference temperature ( $T = -2^{\circ}\text{C}$ ) was chosen to calculate the difference between observed temperature and reference temperature for each depth i.e.  $\Delta T_n = T - T_n$ , where  $n = \text{depth}$ . Using the temperature difference ( $\Delta T_n$ ), change in depth for that station was calculated by subtracting the previous depth from the current depth (i.e.  $D_n - D_{n-1}$ ). Temperature difference was then multiplied by the change in depth which gives a series of values (i.e.  $\Delta T_n \times (D_n - D_{n-1}) = X_n$ , see Fig. 3.4). The sum of this series of values  $\sum_{n=1}^N X_n = X$ , where  $n = 1, 2, \dots, N$  was then multiplied by the sea water density  $\rho$  and specific heat capacity  $C$  to estimate the oceanic heat content  $H$ . The data was visualised using Ocean Data View 4.

Estimations of heat content are represented in this section. Both long and short-term changes are presented and discussed. Along with the heat content, salinity changes are also presented from 2008 to 2012. Here, we first discuss the methodology behind heat content estimation and then discuss short term and long-term heat content change along with salinity.

### Education

Due to the multi-disciplinary concept of the programme, the excellent diverse teachers and the different technical and cultural backgrounds of the chosen scholars, the students gained knowledge in different fields of science beyond their “comfort zones” and gained massive intercultural competence. They experienced how to apply scientific procedures on board of a research vessel with different workings groups and interests (including all communication paths and ship intern procedures).

### Summary of outreach activities

To promote the idea that “Oceans have no boundaries” and that the new generation of scientists will have to solve the challenges of the upcoming future in marine environments together and communicate this to stakeholder groups, we conducted a set of different outreach activities. Every ten days the scholars written a blog, which was published, we set informative tweets during the programme. A mural was painted by all participants and the crew under the supervision of the artist in residence during the cruise Lionel Playford (Fig. 3.5).



Fig. 3.5: Participants in front of the mural painting

For the first time onboard of *Polarstern* “Ship to Shore” transmissions via Skype were conducted. This was used for interviews with the Deutsche Welle that featured the programme online, for discussions with school classes and for lecture from ship to Universities in Ireland and New Zealand. Together with the *Meteor* in Cape Town an open ship event took place during which the scholars presented the programme, the sampled data and the laboratories on board. Both NoSoAT programmes were highly

recognized (commocean, twitter, blogs etc. see links). The ship board training cruises NoSoAT 2015 and 2016 on *Polarstern* has shown the importance of this experience. This training provides the scholars with practical knowledge how data are collected and processed on research vessels including the communication with other scientific working groups and colleagues as well as with the crew while collecting real data on a fixed transect. This experience is most valuable for young scientists and their future work. The institutes benefit from participants which are - having fulfilled this training - familiar to work on research vessels. Additionally, the collected data can be included in long term observation programmes. To secure those benefits, it is important to develop a reliable and continuous programme on Ship Board Training. By creating a teacher pool and using the infrastructures and research vessel of institutes of a variety of ship board training modules could be coordinated via a platform. We hope that this NoSoAT programme will be established on an annual to a biannual regular basis. At the moment at least one publication on the data and methods of this training is in preparation.

### Preliminary (expected) results

#### *Long-term changes in heat content*

We observed long-term changes in heat content of 1985 in comparison with other years (i.e. 2012, 2015 and 2016; Fig. 3.6) in some stations for the upper 700 m. North of Las Palmas (Fig. 3.6) a difference in heat content between the year 1985 and 2016 was observed. From 1985 to 2016, in these 29 years, we observed a shift in the temperature profile from this area and thus, heat content has also changed. In 1985 heat content value was found  $3.51 \times 10^{10}$  [J/m<sup>2</sup>] while in 2016 was found as  $3.9 \times 10^{10}$  [J/m<sup>2</sup>]. At the south of Las Palmas (Fig. 3.6), we also observed significant change in heat content between the year of 1985 and 2012. In 1985 estimated heat content was found  $3.31 \times 10^{10}$  [J/m<sup>2</sup>] and in 2012 as  $4.23 \times 10^{10}$  [J/m<sup>2</sup>]. Below of this station (Fig. 3.2), heat content also changed in 2015 from 1985. In 2015 heat content is estimated as  $4.10 \times 10^{10}$  [J/m<sup>2</sup>] which is higher than 1985 ( $3.44 \times 10^{10}$  [J/m<sup>2</sup>]).

At the mouth of the Mediterranean outflow region, we did not observe any major shift in heat content among the years of 1985, 2012 and 2016 (Fig. 3.6) in the upper 700 m. In 1985 heat

content is estimated as  $3.5 \times 10^{10}$  [J/m<sup>2</sup>], and in 2012 and 2016 heat contents are estimated as  $3.7 \times 10^{10}$  [J/m<sup>2</sup>] and  $3.79 \times 10^{10}$  [J/m<sup>2</sup>] respectively (Fig. 3.7). We observed only little variation in temperature after 600 m depth which caused slight variation in heat content values for these stations.

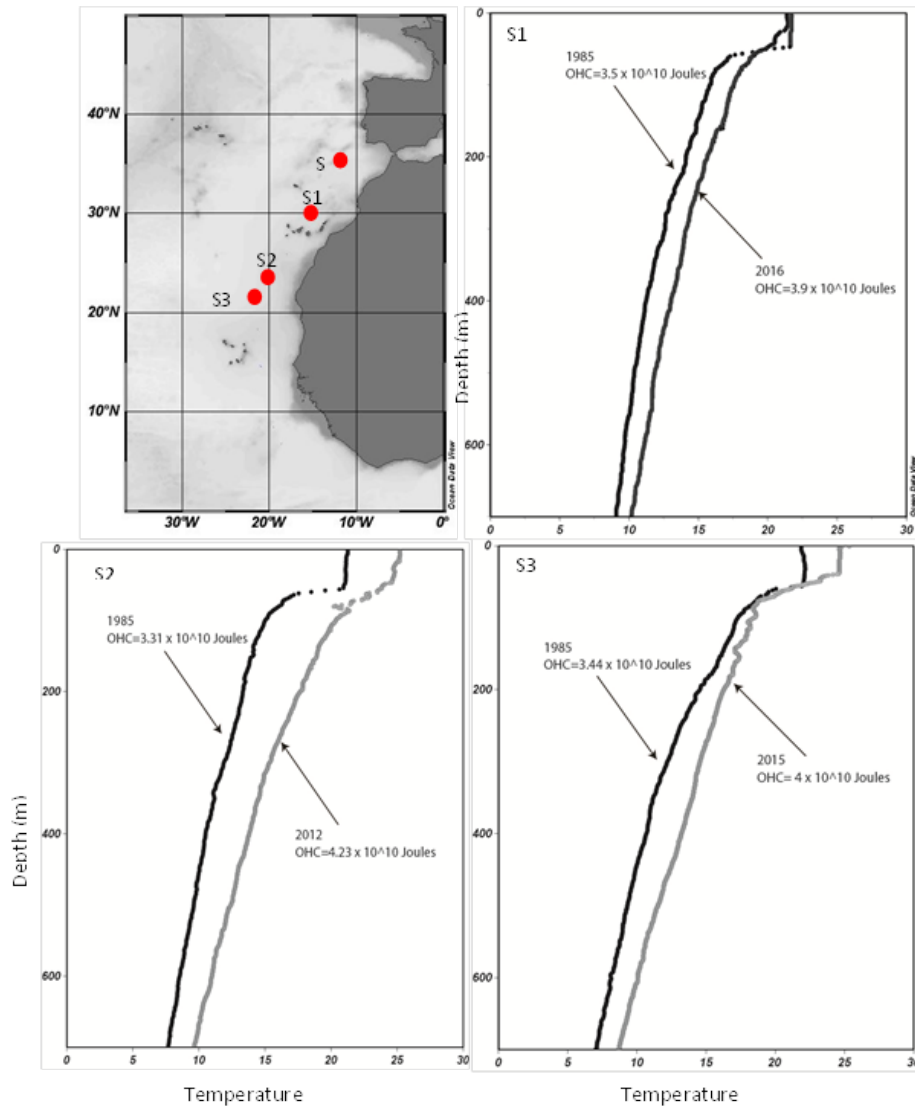


Fig. 3.6: Long-term positive change in heat content per m<sup>2</sup> of upper 700 m in the tropical Atlantic. Upper left panel map shows the location of the sampling stations (red dots) and right panel shows the shift in heat content between 1985 and 2016 at station S1. Lower left panel shows the heat content change between 1985 and 2012 at station S2, and right panel shows change between 1985 and 2015 at station S3.

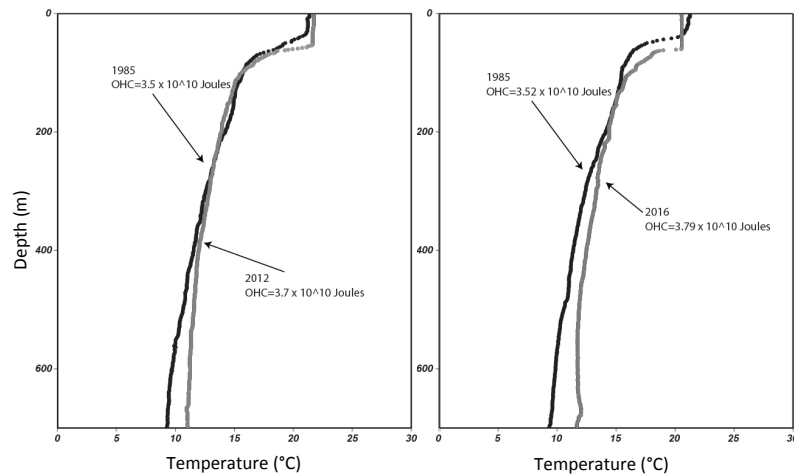


Fig. 3.7: Long-term change in heat content (per  $\text{m}^2$ ) at stations S in the year of 1985, 2012 and 2016

### Short term changes in heat content

It is important to understand that the ocean system does not act as one body. The upper ocean (>700 m depth) and the deeper ocean (<700 m depth) are distinct. Excess heat in the upper ocean constitutes two thirds of the total heat absorbed by the ocean; while the remaining is stored in the deeper ocean (Levitus et al., 2012). Within the upper layer, transport of heat to the atmosphere can result in a positive feedback loop. This is especially evident during upwelling events, such as El Niño in the equatorial Pacific. As ocean heat content increases due to climate change, this process will result in continued warming 'events' of the atmosphere.

Unlike the distinct changes seen in the long term ocean heat content described above, short term heat content comparisons are hard to quantify due to the short time scales involved. The data collected during the North South Atlantic Transect (NoSoAT) in 2015 and 2016 is shown and compared in this section from three homogeneous points along the transect.

There is no significant change in heat content between 2015 and 2016 in any of the three stations from southwest of Portugal (Fig. 3.8), the equator (Fig. 3.8) or south of the equator (Fig. 3.8). Heat content is estimated as  $7.59 \times 10^{10}$  [ $\text{J}/\text{m}^2$ ] and  $7.73 \times 10^{10}$  [ $\text{J}/\text{m}^2$ ] in 2015 and 2016 respectively at the southwest of Portugal for first 1,880 m depth. The only observed difference between the two years is that the higher temperatures of the Mediterranean outflow are more evident in 2016 than 2015. This effect will be discussed in greater detail in a later section. In the equator, heat content for 2015 and 2016 is found almost same ( $5.07 \times 10^{10}$  [ $\text{J}/\text{m}^2$ ] and  $5.1 \times 10^{10}$  [ $\text{J}/\text{m}^2$ ] respectively). This is because this area is more stable and has no advection of other water masses. Thus there is no change in heat content. In the south of the equator we also observed similar pattern of heat content like equator ( $4.9 \times 10^{10}$  [ $\text{J}/\text{m}^2$ ] and  $4.74 \times 10^{10}$  [ $\text{J}/\text{m}^2$ ] in 2015 and 2016 respectively). The lack of variation over such a short time scale was expected and highlights the need for greater synchronicity of data sets at similar if not homogeneous locational points along this transect.

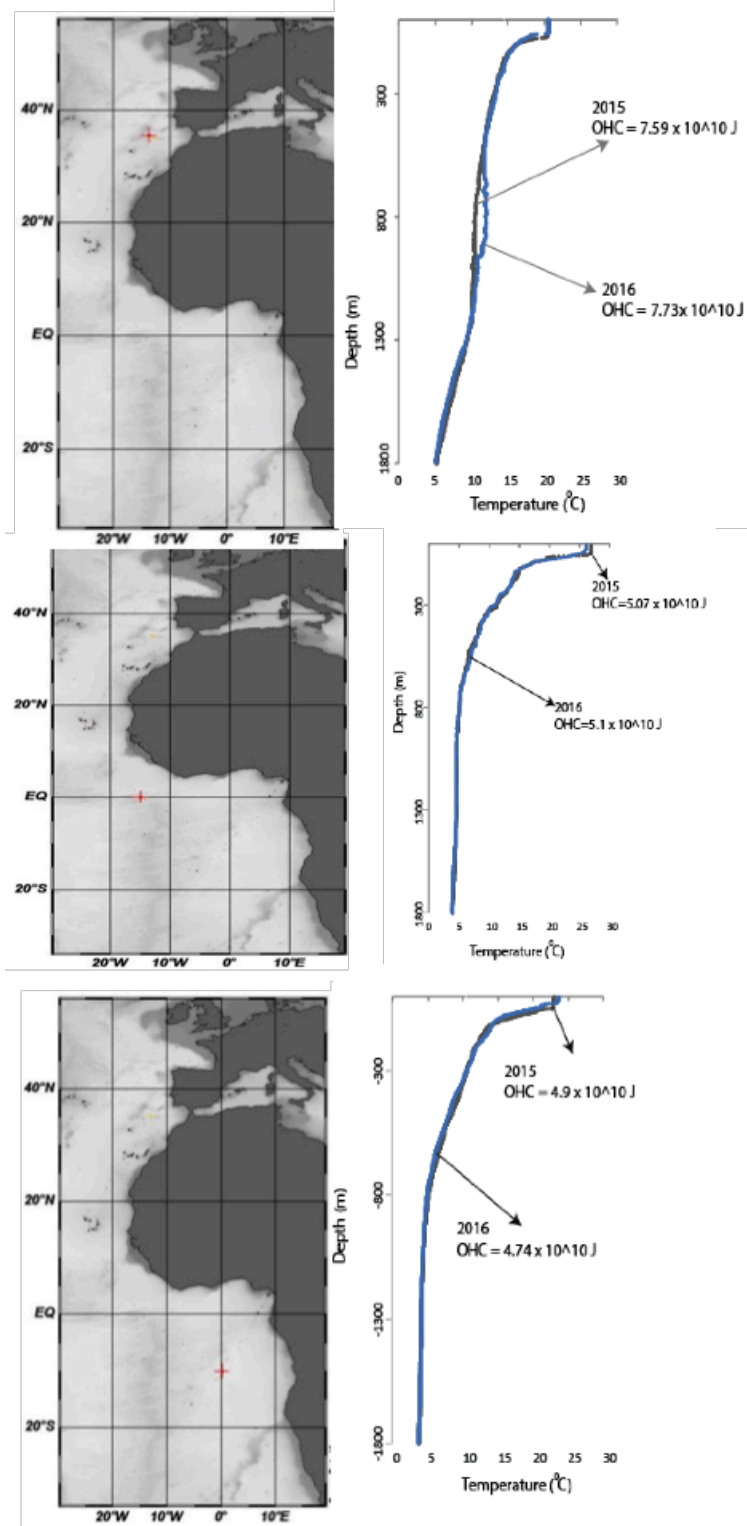


Fig. 3.8: Short term change in the top 1,800 m of ocean temperature profiles and heat content ( $m^2$ ) from three different stations along the transect highlighted by a red cross. The years 2015 and 2016 are compared on the plot.

### Short term changes in Salinity

Due to a lack of data on the long-term scale along this transect only a short-term change of salinities can be looked at from 2008-2016 (Fig. 3.9). Salinity is an essential characteristic of certain water masses discussed in great detail later in this report. Salinity, much like temperature, is dependent on a range of factors and can vary year on year in certain locations. However, a trend can be seen clearly in the set of transect data. High salinities can be seen in the upper most section from 20°S to 20°N at a depth above 300 m, other than in 2008 where there were abnormally low salinity values at 20°S at this depth. In all years, the salinities increase towards the northern end of the transect with a value of 35 psu being recorded at a maximum depth of ~1,600 m between 30-50°N. South of 20°N at a depth of between 1,500 m and 300 m there is a sharp change to less saline waters in all years with a 34.45 psu minimum salinity at ~17°S, 700 m depth in 2016. Below the changes seen above there are uniform salinity values from 2,500-4,000 m depth. 2016 is the first year of transect data that shows the beginning of less saline waters below 4,000 m south of 20°S. The reason for these changes in salinity along the transect in different years are discussed in great detail in a later section.

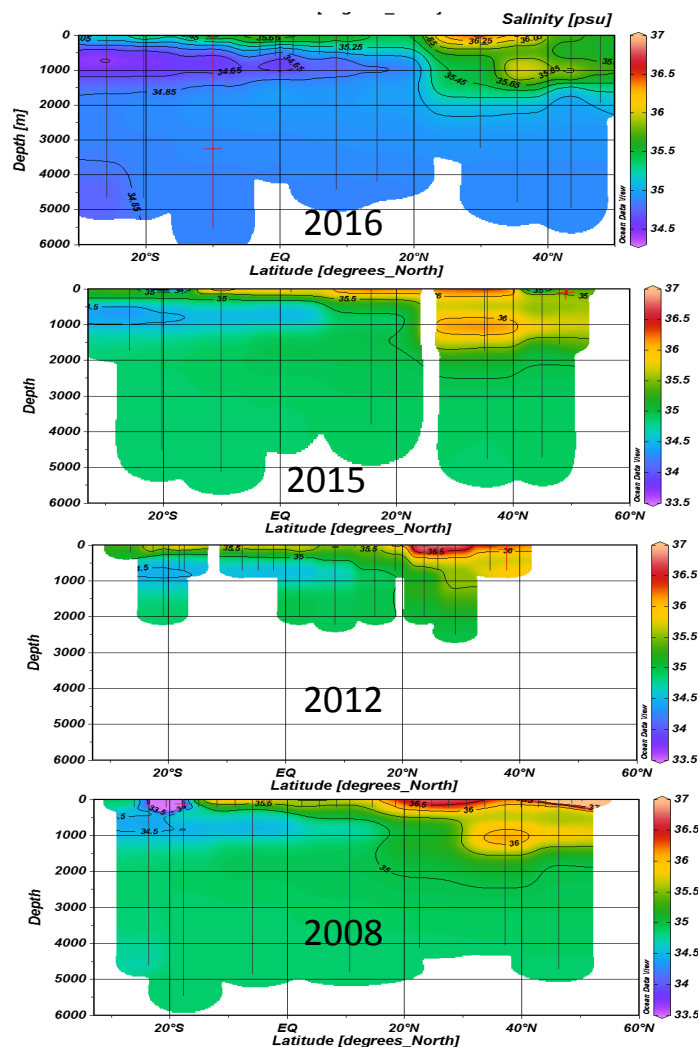


Fig. 3.9: Salinity plots along transect for the years 2008, 2012, 2015 and 2016. Note that the 2016 plot only extends to ~50°N while all other years extend to 60°N.

The evidence of human influence on climate is clear and “unequivocal” for a warming world with many changes in Earth systems since the 1950s that are “unprecedented” (IPCC, 2013). Over the last 16 years, the earth’s surface warming trend has slowed down, this is because ocean is storing the extra heat from the atmosphere. Ocean warming accounts for over 90 % of the warming in Earth’s climate system and ocean heat storage has increased substantially since 1993, hitting a record high in 2015 (Maher et al., 2014). Heat energy rises and falls every few years in response to natural patterns like El Niño and La Niña, but those ups and downs are superimposed on a long-term increase (Johnson et al., 2016). We observed a positive shift in heat content in our stations which is similar to other studies in Atlantic and Southern oceans (Chen and Tung, 2014). In the Indian Ocean, heat content has increased abruptly, which accounts for more than 70 % of the global ocean heat gain in the upper 700 m during the past decade (Lee et al., 2015). IPCC estimates of heating between 1971 and 2010 range from 43-105 TW (equivalent of average temperature increase of 0.005 – 0.01 °C) (Smith and Murphy, 2007) to 120-154 TW (equivalent of an average temperature increase of 0.01 – 0.02 °C) (Domingues et al., 2008). All these studies indicate a positive trend in heat uptake in both upper and bottom of the oceans.

In our present study, we found that there is a positive shift in heat content long-term which is similar to that of other studies mentioned above. This higher heat content indicates a warming ocean which causes thermal expansion of sea water and results in sea level rise. Rising sea threatens human structures near coastlines around the world. Weather patterns will be affected by the warmer oceans, for example causes more tropical storms which will end in huge economic losses.

#### *Water Masses Encountered on the North South Atlantic Transect*

The knowledge and identification of water masses is crucial to assess changes in the ocean interior, in key climate related properties such as heat content and salinity. Changes in the extension of water mass can greatly influence the heat content without overall warming or cooling of the water bodies. Therefore, studies into the characteristics and movement of water masses are critical to be able to show underlying long- and short-term trends, such as rising water temperature.

Overall, four main categories of water masses are distinguished: surface, central, intermediate and deep and bottom water. Surface waters are very variable. They make up the mixed layer and have a high seasonal and latitudinal dependency. Therefore, they are not more closely considered here.

Below the surface water lies central water, which is the water body in the upper 500 – 1,000 m with well-defined, almost linear T-S (potential temperature and salinity) characteristics (Tomczak, 1981). Going deeper, first intermediate waters are reached and then, below 2000 m deep and bottom waters.

The measured values for pressure [dbar], salinity, potential temperature  $\theta$  [°C], potential density anomaly  $\sigma_\theta$  [ $\text{kg m}^{-3}$ ] and oxygen concentration [ $\text{mg l}^{-1}$ ] were used to differentiate the water masses. These parameters lie in a characteristic range and are conservative, when no mixing occurs. The potential temperature  $\theta$  was used, as temperature T increases with increasing depth due to compression. Thereby the water mass can be traced independent of its depth. Possible other important characteristics are nutrients, such as silicate, nitrate and phosphate as well as chemical parameters like pH or trace element concentrations.

In the T-S plot (Fig. 3.10) water masses that have been observed during the cruise PS102-in 2016 are depicted. The water temperature ranges from 0.78 to 29.15 °C with a salinity range of 34.36 to 36.73. Six water masses can be differentiated due to their depth [m], salinity, potential temperature  $\theta$  [°C] and oxygen concentration [ $\text{mg l}^{-1}$ ] (cf. Tab. 3.1).

Along the transect, two different masses of central water have been encountered. In the northern part, North Atlantic Central Water (NACW) is found between 100 – 1,000 m depth and extends southward to 30 °N. It has a wide temperature and salinity range (Fig. 3.10). In the upper Atlantic Ocean, it is one of the two main water masses.

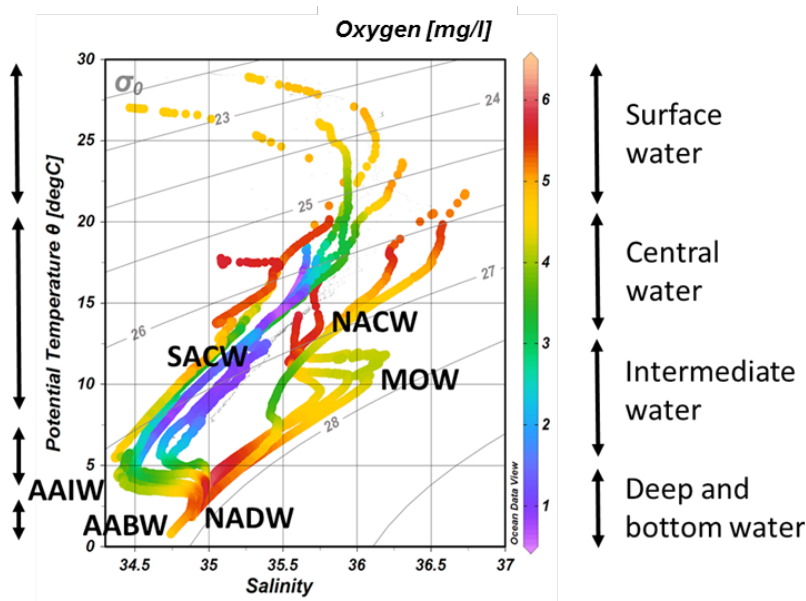


Fig. 3.10: T-S plot and oxygen concentration [ $\text{mg l}^{-1}$ ] of CTD and UCTD station data along the Atlantic North-South transect during the cruise PS102 on Polarstern in 2016. Six different water masses are indicated and divided into four categories (on the right).

The other water mass is South Atlantic Central Water (SACW), which can be traced from 14.55 °N to 10 °S in the same depth as NACW. In comparison to its northern counterpart, the SACW can be slightly colder and less saline, which leads to lower  $\sigma_0$ . A very distinct difference is the oxygen concentration of these central waters (Fig. 3.10). In SACW, it ranges from ~1 – 2  $\text{mg l}^{-1}$ , in NACW concentrations are higher, at around 3.5 – 5  $\text{mg l}^{-1}$ . This difference is caused by the ventilation age of SACW and can be used to distinguish the water masses in mixing zones. The lowest oxygen concentration of 0.53  $\text{mg l}^{-1}$  has been found at a depth of 62 m (14.553 °S, 20.985 °W). This local oxygen minimum was probably enhanced by bacterial and zooplankton respiration of primary production sinking down from the upper layer.

Off the European and North African coast in 1,000 m depth, the warm ( $\theta$ , ~9.4 – 11.8 °C) and saline (35.8 – 36.1) Mediterranean Outflow Water (MOW) has been found between 43.5 and 35.5 °N. At a similar depth, Antarctic Intermediate Water is observed south of 14.5 °N. There, it forms a fresh and cold tongue with a subsurface oxygen maximum at 1,000 m depth. The depth range broadens southward to 500 – 1,200 m at 25.8 °S (Fig. 3.10). This water mass is here characterised by temperatures of 3.4 to 5.5 °C and a salinity of 34.4 to 34.8. AAIW is separated from SACW by the increase of  $\sigma_0$  from 27.05 to 27.3  $\text{kg m}^{-3}$  as well as the steep increase in oxygen concentration. The density gradient between the two water masses decreases vertical mixing and oxygenation of the SACW from below.

Along the entire transect, North Atlantic Deep Water (NADW) can be found at depth of 2,000 to 5,500 m identifiable by the salinity maxima. Temperature and salinity vary only slightly over the entire depth ( $\theta$  = 1.8 – 4 °C, salinity 34.88) but change due to isopycnal mixing at fronts with MOW and AAIW. NADW is an essential part of the thermohaline circulation. It transports cold water southward over the equator causing a compensatory flow of warm water northward. This results in a net heat loss of the Southern Hemisphere (Rühlemann et al., 1999).

At the southernmost station of the transect (25.83 °S), Antarctic Bottom Water (AABW,  $\theta = 0.79 - 1.7$ , salinity 34.7 – 34.8) has been identified at depth below 3,800 m. This marks the extent of its northward distribution in the Eastern Atlantic resulting from the bathymetry.

**Tab. 3.1:** Position and depth range of water masses on North-South transect PS102 in 2016 and respective *in-situ* measured parameters.

Water mass	Latitude [°N]	Depth [m]	Pot. $\theta$ [°C]	Salinity	$\sigma_\theta$ [kg m <sup>-3</sup> ]
<b>NACW</b>	30.0 – 35.5	100 – 1,000	7.5 – 18.65	35.4 – 36.4	26.5 – 27.5
<b>NADW</b>	-25.8 – 43.5	2000 – 5500	1.8 – 4.0	34.88	27.89
<b>MOW</b>	35.5 – 43.5	750 – 1200	9.4 – 11.8	35.8 – 36.1	27.59 – 27.54
<b>AAIW</b>	-25.8 – 14.5	500 – 1200	3.4 – 5.5	34.4 – 34.8	27.3 – 27.46
<b>SACW</b>	-10 – 14.5	100 – 700	6 – 15	34.6 – 35.6	27.1 – 27.3
<b>AABW</b>	-25.8	>3800	0.79 – 1.7	34.7 – 34.8	27.85

In the previous section, changes in ocean heat content and salinity of the upper ocean from 1985 to 2016 have been analysed. It has been shown, that heat content has significantly increased over this period in most areas. However, it is not possible to draw any conclusions on water masses from the data set of 1985, since it is based solely on temperature values. Therefore, possible change in water mass distribution and extent cannot be compared to the calculated increase in heat content.

However, taking these estimations into account, effects on the water masses can be hypothesized. An increase of heat content in the upper ocean is caused by an increase in global temperature. As the warming will result in ice melting in the Arctic and subsequent freshening of arctic surface waters, the formation of NADW will be slowed (Rühlemann et al., 1999). Fresh water at the surface decreases the density and slows the sinking speed of the cold water, thereby slowing the entire water mass circulation. Through the compensatory coupling of heat transport across the equator, less flow of NADW results in a decrease of net heat export from the Southern to the Northern Hemisphere. This will cause further heating of the tropical Atlantic. Stronger thermal stratification, decreased mixing and primary production are the effects.

The higher thermal stratification will impact the central water masses, especially SACW. Weaker vertical mixing at the surface decreases the oxygenation of the lower water masses. Additionally, it decreases the formation of central water, which is subducted from the thermocline. In the case of SACW, the formation takes place in the Indian Ocean as well as off Brazil, where the Brazil and Falkland Current confluence (Stramma & England, 1999). Higher stratification slows the subduction and formation of the water masses. Similar to NADW, slower formation results in decreased flow and ventilation. The aging of SACW in the Eastern Atlantic will lead to lower oxygen concentrations and spreading of the oxygen minimum zones (OMZ) found below the thermocline south of the equator (Fig. 3.10). This phenomenon has been reported by Stramma et al. (2009), causing a record oxygen minimum of 40  $\mu\text{mol kg}^{-1}$  south of 11 °S in the Eastern Atlantic. In the affected surface and central waters, it correlated with an increase in temperature as well as salinity. However, it is suspected to be partly caused by seasonal variation of the North Equatorial Counter Current and changes in the AAIW depth.

The change in the depth of AAIW is caused by warming and a following decrease in potential density. This causes the water to rise and the water mass to shoal. It has been shown that AAIW has undergone significant warming since the mid-1970s with a maximum increase of 0.14 °C at

40 – 50 °S in the Atlantic Ocean (Schmidtko & Johnson, 2012). The increase in temperature is slowing down towards the equator but still noticeable. The shoaling and warming of the AAIW will have an impact on oxygenation of the subtropical thermocline and lower waters, as AAIW is an important oxygen supplier in this depth. When it rises and the density decreases, lower lying waters with higher density cannot get into exchange and are therefore less ventilated by AAIW. (Schmidtko & Johnson, 2012).

On the North-South transect six different water masses have been found: North and South Atlantic Central Water (NACW, SACW), Mediterranean Outflow Water (MOW) and Antarctic Intermediate Water (AAIW), North Atlantic Deep Water (NADW) and Antarctic Bottom Water (AABW). Change in heat or salt content in specific water masses could not be shown using the available data. However, in multiple studies (Schmidtko & Johnson, 2012) (Stramma et al., 2009), warming of water masses has been documented. Effects are shoaling, decrease in density, and deoxygenation of the water mass. This can greatly impact the ventilation of the surrounding water body and the formation rate of the water mass itself. Consequences are the expansion and formation of oxygen minimum zones and global changes in heat transport.

#### *Mediterranean Outflow Waters in the North Atlantic*

Water masses are identifiable due to a change in variables including heat and salinity. Heat diffuses faster than salinity in the ocean, this process can lead to local instabilities in the density structure which causes mixing within a layer (Kawase & Sarmiento, 1986). The Mediterranean Outflow Water (MOW) mixing into the North Atlantic is an example of this salt fingering. The MOW is a saline and warm water mass primarily residing in the intermediate depths of the eastern North Atlantic. This water mass is produced from the transformation of fresh and warm surface Atlantic waters into dense and salty Mediterranean water (Bozec et al., 2011), and has been cited as a possible contributor to the preconditioning of deep water mass formation in key areas of global overturning circulation such as the Labrador and Nordic Seas (Bozec et al., 2011; Kawase & Sarmiento, 1986; Rahmstorf, 1998).

Differences in instrument stations and frequency over the years create a variance in both spatial and data resolution. Consequently, minor changes in the temperature or salinity of the MOW in the last 8 years will not be visible in the data (2008-2016). However large thermohaline shifts can be monitored.

2008 and 2016 results show similar salinity distributions (see Fig. 3.9). 2015 data suggests the MOW has spread further south; however due to 2015 having one station less, this may be a result of poor interpolation and cannot be confirmed. 2012 salinity measurements do not have enough data points in the area to investigate the full extent of the MOW.

Temperature profiles taken during recent research (2008-2016) would suggest no significant warming has occurred. On the other hand, the heat content gain in the MOW from 1955 to 1993 surpasses the average gain in heat content of the North Atlantic basin over the latter half of the 20<sup>th</sup> century (Shaltout & Omstedt, 2015; Rahmstorf, 1998; Kawase & Sarmiento, 1986; Bozec et al., 2011; Potter & Lozier, 2004). This suggests the MOW is an important contributor to climatological changes at intermediate depths within the mid-latitude North Atlantic (Bozec et al., 2011; Kawase & Sarmiento, 1986).

1985 data does not reach the depths of the MOW; therefore, we look to past research papers for long term change in temperature and salinity. However, the top 700 m in 1985 suggest no warming has occurred in the upper North Atlantic in this area (see Fig. 3.11), this further suggests the MOW heat content gain surpasses the average gain in heat content of the North Atlantic basin over the last 30 years (Potter & Lozier, 2004).

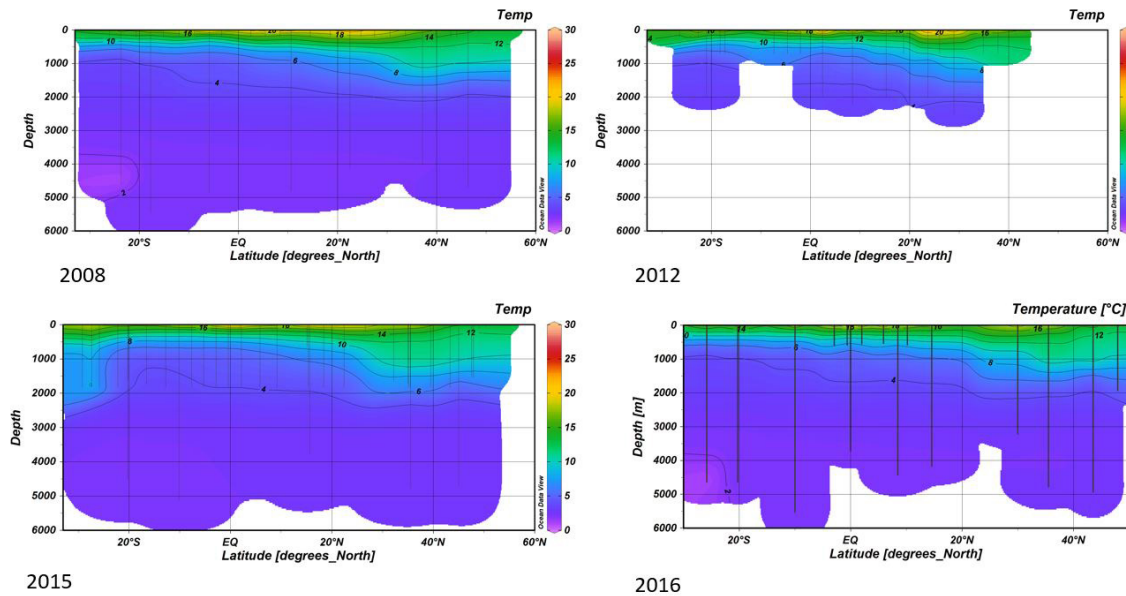


Fig. 3.11: Temperature distribution based on data as collected on *Polarstern* between 2008 and 2016

The data collected on *Polarstern* shows no significant change in heat and salinity over the last 8 years, however higher resolution data may show more minor variations. Data from 1985 also shows no significant change in the top 700 m of the water column at 35.101°N 12.501°W; however, in the literature review warming of the MOW is evident. This would suggest the MOW heat gain surpasses that of the North Atlantic (Potter & Lozier, 2004) (Bozec et al., 2011). The warming and salinification of Mediterranean surface waters are density-compensated (Potter & Lozier, 2004), hence increasingly warmer and saltier waters continue to sink at the same density and depth. If high latitude waters continue to freshen much of the convective activity, which sends heat to the deep ocean, may fall to mid latitudes (Rahmstorf, 1998). Therefore, the investigation of this water mass is key to researching the Atlantic Ocean’s role in climate change. Further, the resultant heat content gain suggests that the MOW has been an important source of warming at mid-depth in the North Atlantic (Potter & Lozier, 2004), and advocates monitoring of the MOW for further variability in the future. Cf. Figs 3.12, 3.13 (not cited in text).

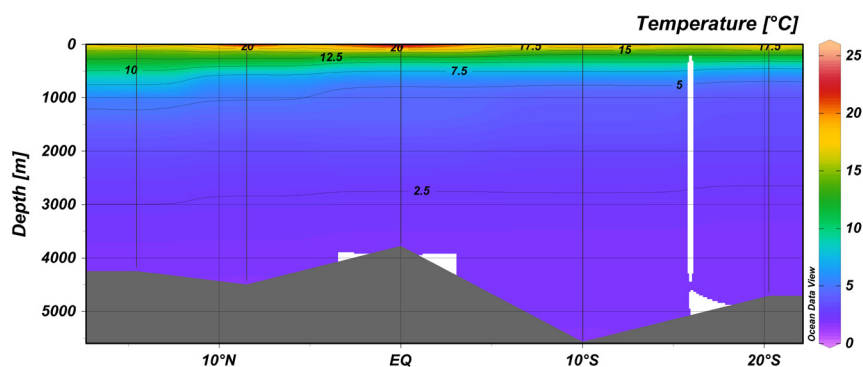


Fig. 3.12: Temperature distribution based on CTD profiles taken between 20°N and 20°S

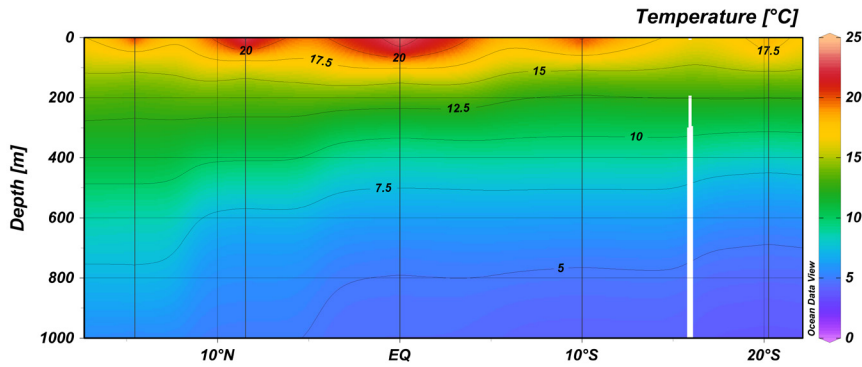


Fig. 3.13: Temperature distribution based on CTD profiles taken between 20°N and 20°S; top 1,000 m

Figure 3.14 displays the vertical salinity distribution along the transect. The distribution is one of generally low salinity. A wedge of saline water (35.5 psu) originating in the north is discernible at a depth of ~500 m at 15°N narrowing to ~200 m to the south of the equator. Asymmetry in salinity values can be observed below ~1,200 m to the south of the equator and ~1,000 m to the north of the equator. A wedge of low saline water (34.5 psu) is distinguishable at 1,000 m either side of the equator, widening to the south of the equator. Below this wedge, is an area of higher salinity (~35.25 psu) originating from the north to a depth of 3,000 m and spreading southward, eclipsing at ~20°S to a depth of 2,200 m. Below this depth either side of the equator is a somewhat homogenous salinity profile of 35 psu. Figure 3.15 highlights the high saline wedge of 35.5 psu originating from the north stretching throughout the transect. The low saline wedge of 34.5 psu at 1,000 m, is clearly distinguishable to 10°N from this Fig.3.15.

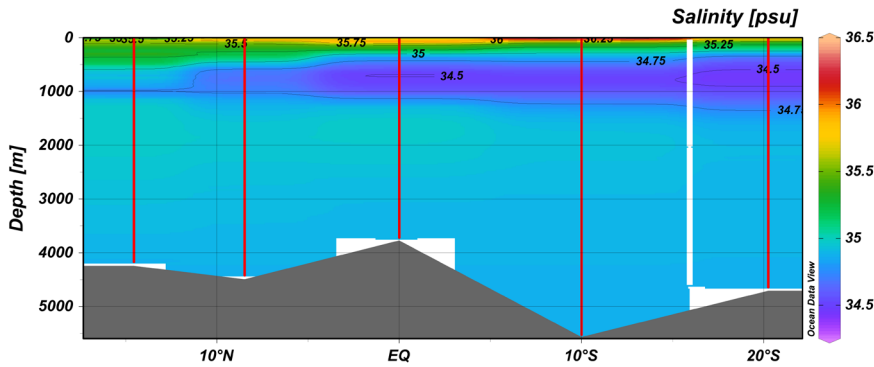


Fig. 3.14: Salinity distribution based on CTD profiles taken between 20°N and 20°S

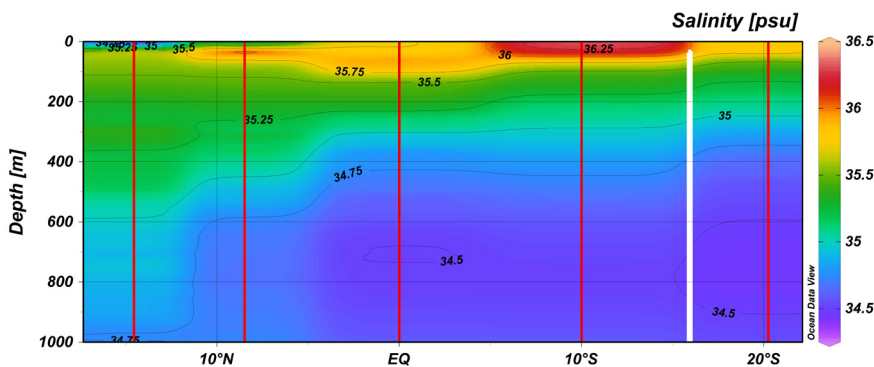


Fig. 3.15: Salinity distribution based on CTD profiles taken between 20°N and 20°S; top 1,000 m

It appears that the biggest influences measured on this transect are the MOW and the AAIW. The cold and low saline wedge at ~1,000 m to the south is interpreted as AAIW. It is inferred that the warm and saline wedge at ~200-400 m is the remnants of the MOW. The cool 7.5°C and less saline (35 psu) water originating at ~300 m 20°S is inferred as SACW, spreading out down to ~600 m at 15°N is interpreted as ENACW. The warmer MOW water is more buoyant and therefore sits above this water mass. The cold and more saline waters at a depth of below ~2,000 m are interpreted as NADW. The colder waters, with a relatively low salinity at depths of 4,000 m and below are an indication of AABW. The high saline and warm waters in the top 100 m are surface waters.

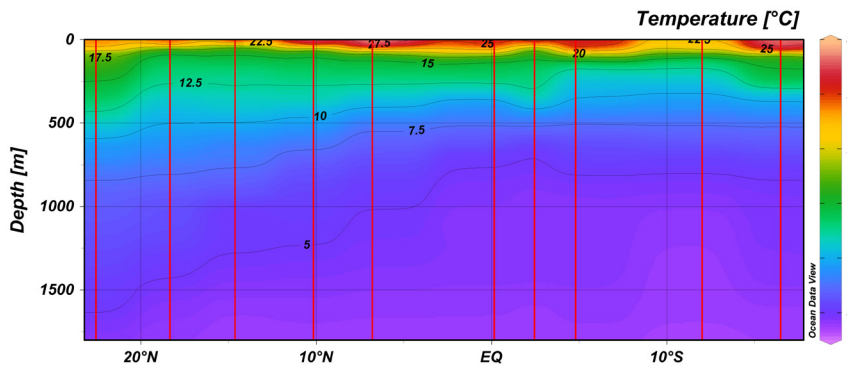
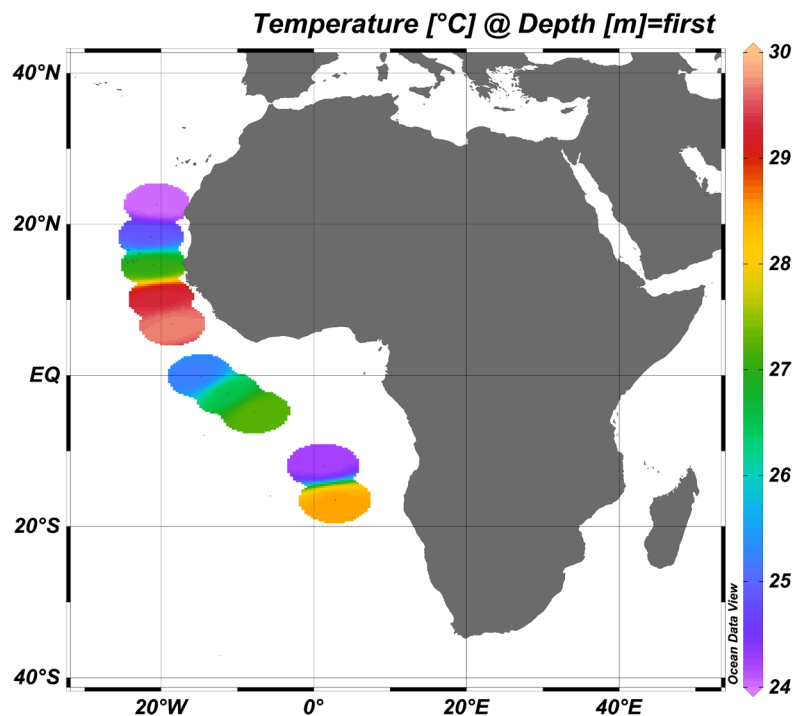


Fig. 3.16: Temperature distribution based on XBT profiles taken between 20°N and 20°S. Red lines indicate XBT stations.

Figure 3.16 displays the vertical temperature distribution provided by the XBT within the study area. At 20°N surface temperatures are significantly cooler than 20°S. The surface mixed layer extends deeper North of the equator to approximately 500 m. A strong cool signal originating from the south can be identified throughout the transect, however, it is more pronounced at and to the south of the equator. Figure 3.17 shows the surface water temperature recorded by the XBT. Maximum temperatures of 29.96°C were recorded at 6°81' N, 18°58' W. Coldest waters were recorded just north of 20°N.

Fig. 3.17:  
Surface water  
temperature  
recorded by the  
XBT



Similar to the CTD there is somewhat of a symmetry between 10°N and S, however, there is no strong symmetry of surface waters north and south of the equator recorded by the XBT. The maximum surface temperature located at ~7°N is interpreted as the location of the ITCZ. The cooler water mass at a depth of ~800 m north of the equator is interpreted as a mixing of ENACW and MOW waters. The warm tongue at 20°N is inferred as the remnants of MOW. At depth, below 1,000 m north and south of the equator show a slight symmetry, but is skewed towards the South. The significantly cooler waters at depth are interpreted as AAIW.

The CTD and XBT show a generally good correlation in the results, indicating that the results are robust. There is some symmetry north and south of the equator. Temperature shows symmetry, particularly in the top surface and at depth (Fig. 3.12). This is likely due to the similar characteristics of the deep-water masses. The AABW is slightly more dense than the NADW and therefore the water masses sit on top of each other, both north and south of the equator. The surface waters exhibit a slight symmetry (Fig. 3.17). Similarly, the salinity at depth exhibits a general symmetry either side of the equator, however, the top 1,000 m is asymmetrical (Fig. 3.14; Fig. 3.15).

### *Dissolved oxygen and pH*

#### *Surface data*

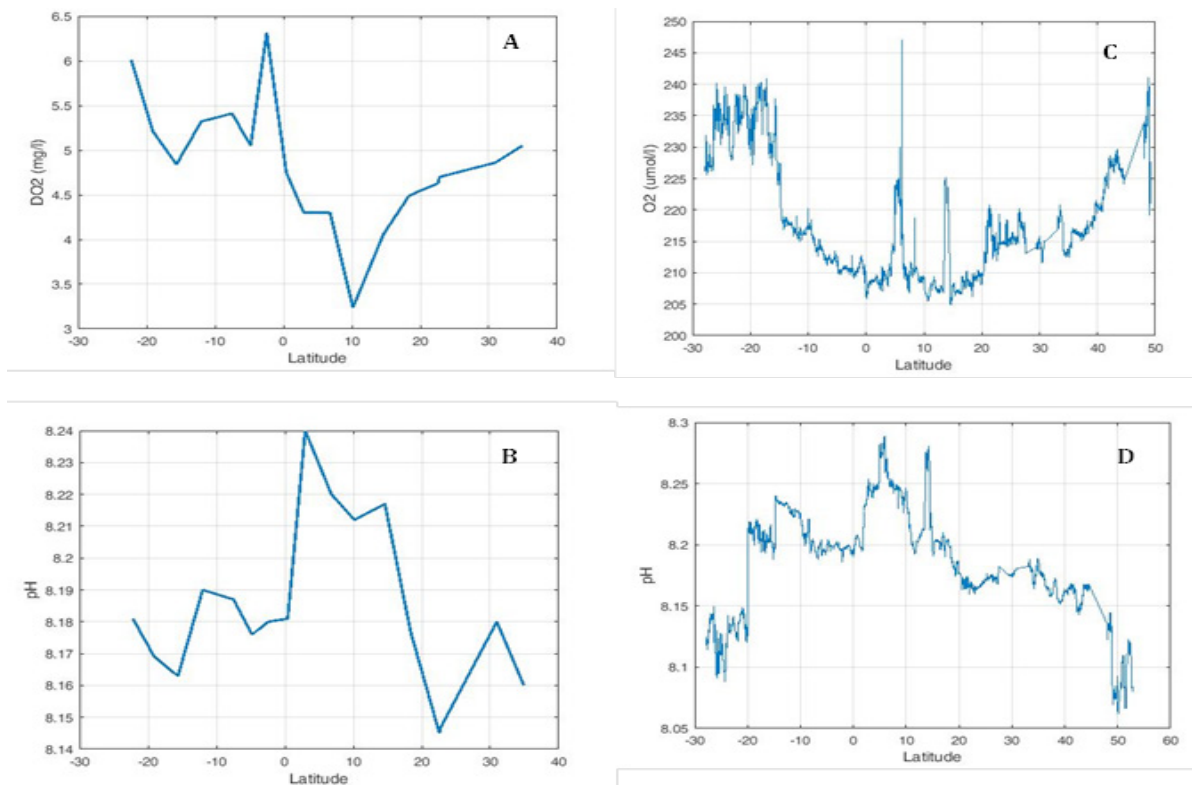


Fig. 3.18: A) and B) Surface DO<sub>2</sub> and pH from the bucket sampling. C) and D) O<sub>2</sub> concentration and pH from the underway ferry box measurements

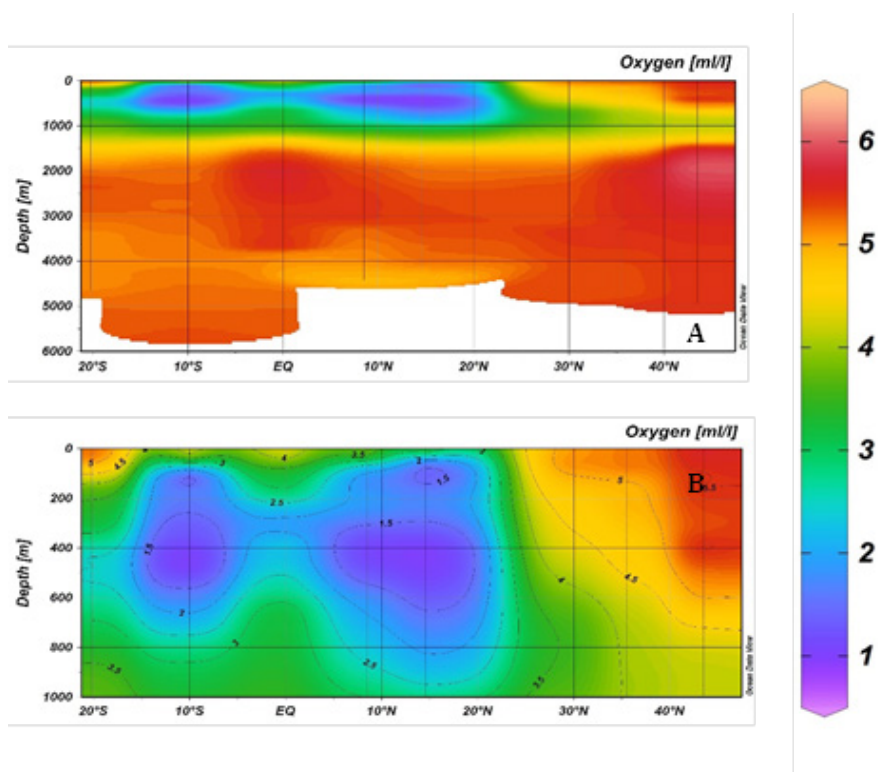


Fig. 3.19: Oxygen concentration ( $\text{mg}\cdot\text{L}^{-1}$ ) measured with the CTD sensor. A) Coverage of the entire depths-range. B) Close-up to the Minimum Oxygen Zone within the first 1,000 m in the water column.

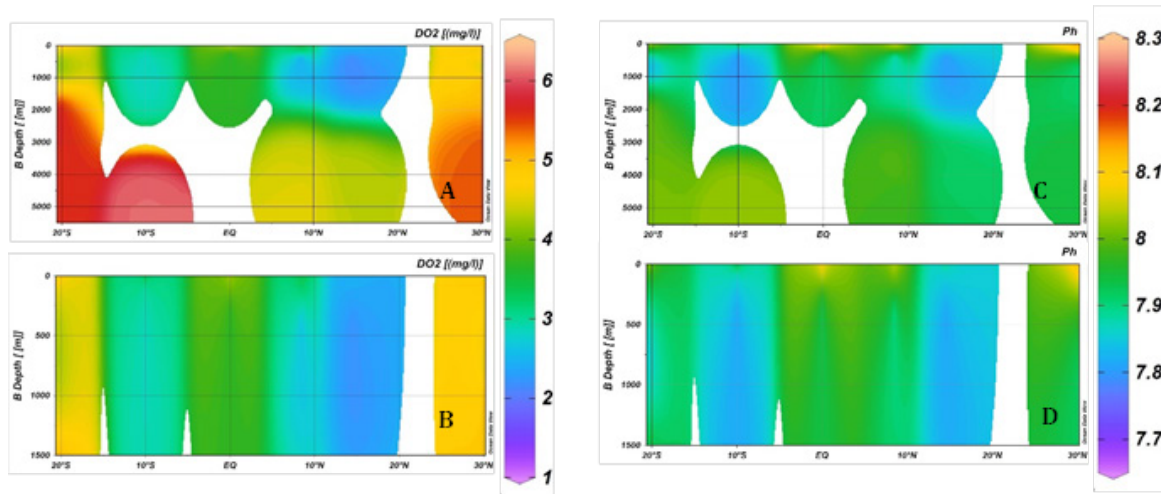


Fig. 3.20: Oxygen concentration ( $\text{mg}\cdot\text{L}^{-1}$ ) and pH from water samples. A) and B)  $\text{DO}_2$  and pH along the water column. C) and D)  $\text{DO}_2$  and pH in the first 1,500 m of the water column.

Two Oxygen Minimum Zones (OMZs) were found along the study transect. These features are well known since the 1920's, when the German vessel *Meteor* revealed their existence. Ever since, they were described as "OMZs in both hemispheres of the eastern tropical Atlantic at depths between 300 and 700 m, situated equatorward of the subtropical gyres and separated by an equatorial oxygen maximum".

Such characteristics are observed in our data set. Fig. 3.18 shows the oxygen concentration and pH on the surface. The equatorial O<sub>2</sub> maximum mentioned before, is found around 0 degrees in A) and C). Fig. 3.18 B) and D) peak values of pH are the ones to be expected, due to the respiration processes releasing CO<sub>2</sub> in these areas. The difference in latitude between the O<sub>2</sub> peaks between the bucket samples (~ 3° S) and the ferry box data (~6° N), might be due an error when registering coordinates, since pH peaks in B and D show the same behavior for both measurement sources. Aside this O<sub>2</sub> maximum, two oxygen surface minimums are observed with minor values for the one in the northern areas.

Fig. 3.19 and Fig. 3.20 show the OMZs along the water column. As observed before, above the equator a maximum of oxygen is found with the two OMZs on both sides. Both show a core of equal oxygen concentration (1.5 mg.L<sup>-1</sup>) which is not in accordance with other studies (Brandt, 2010, 2015) that have established a major oxygen depletion trend of the northern OMZs as the main difference between the northern and the southern Atlantic areas. However, their horizontal and vertical extension differs, with the observation of the extensional area of the northern OMZs closer to the surface. A possible explanation to the similar oxygen trend on both sides of the equator observed in this report, is the coastal influence along the study transect. The transect for previous studies were along an established meridional zone. This way, in their case the northern OMZ was measured close to the coast and the southern one, further away from the coastal influence. The transect for this specific study, on the other side, followed a closer-to the coast route, measuring both OMZ with the influence of the eastern upwelling zones. According to Helly & Levin (2004) OMZs are from the biogeochemical point of view located in eastern boundary upwelling areas with high productivity.

The symmetry of the data could be as well explained by the ocean currents' similar behavior aside the equator, with two eastward flows (North Equatorial Undercurrent between 4° and 10°N; South Equatorial Undercurrent at about 4.5°S) and the Equatorial Undercurrent at the equator supplying oxygen-rich water towards the eastern Atlantic. Such supply is the reason for the high oxygen values both north and south the Equator (Brandt et al., 2010; Stramma et al., 2008) from where O<sub>2</sub> starts decreasing again.

The equator does act as a mirror to a limited extent, specifically within the range 20°S-20°N. This symmetry seems to act based on the behavior of the ocean currents in this area and the Ekman processes acting the opposite way in both hemispheres. However, the variation in geographical distribution and oxygen depleted quantities outside this range varies based on the different atmospheric and oceanographic characteristics on each side of equator.

#### *Chlorophyll in-situ measurements*

Chlorophyll data was obtained through six CTD deployments, six BBE® probe deployments (200 m), and daily bucket sampling events (surface waters) analyzed using the BBE cuvette method. Data used was cross calibrated between instruments with regard to the fluorometer, BBE cuvette and BBE probe however emphasis was given on the equatorial and ITCZ symmetry.

The importance of the divergent water flows along the Atlantic equatorial margin for phytoplankton assemblages has long been known (Signorini et al., 1999), resulting in a shallowing of the thermocline and the injection of nutrient rich, deeper waters that drive primary production in oligotrophic waters. However, the ITCZ has been shown to shift towards the warmer hemisphere and when far enough from the equator a shift in the central upwelling zone responsible for nutrient and O<sub>2</sub> inputs can be seen (Schnieder et al., 2014; Levine et al., 2011). Here comparisons of chlorophyll concentrations were made using data from the *in-situ* fluorometer mounted to the rosette, BBE probe deployed, BBE lab measurements, RAMSES spectrometer and satellite data to try define a point of symmetry between the northern and southern hemispheres. Special consideration was given to the photic zone (upper 200 m) to investigate symmetry of the Atlantic equatorial zone specifically 20° north to 20° south (Fig. 3.21).

*In-situ Fluorometer (CTD/RO)*

The *in-situ* fluorometer provides a vertical distribution of chlorophyll concentrations through the water column through excitation and emittance of the chlorophyll molecules at specific light wavelengths. Sampling methodology was in accordance with standard oceanographic protocols (Strutton, 2016).

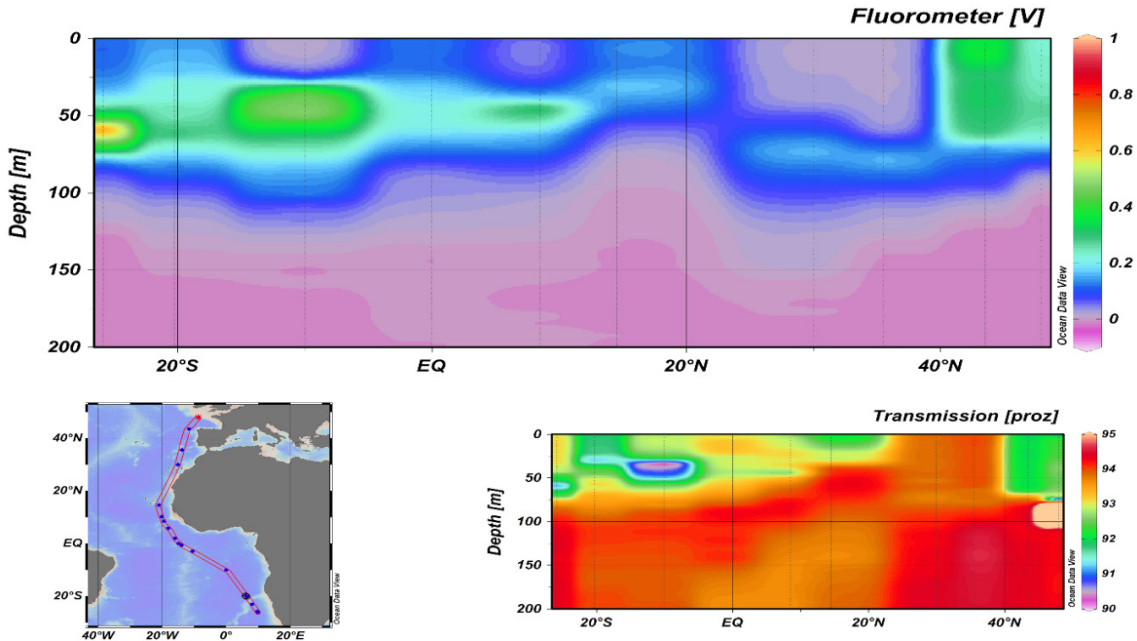


Fig. 3.21: Sectional plot showing the depth profile of fluorescence and transmission

All data were analyzed and sectional plots were generated in ODV. Transmission clearly shows a direct relationship with the fluorescence, both suggesting no clear relationship of symmetry between the equatorial line or in the region of the 6° to 10° north (ITCZ) for the top 200 m, but for the surface near surface layer some symmetry can be seen in very low concentrations. However, a clear chlorophyll maximum is shown to have a southern latitudinal distribution.

Fig. 3.22: Fluorometer vs. BBE probe scatter graph for all CTD deployments

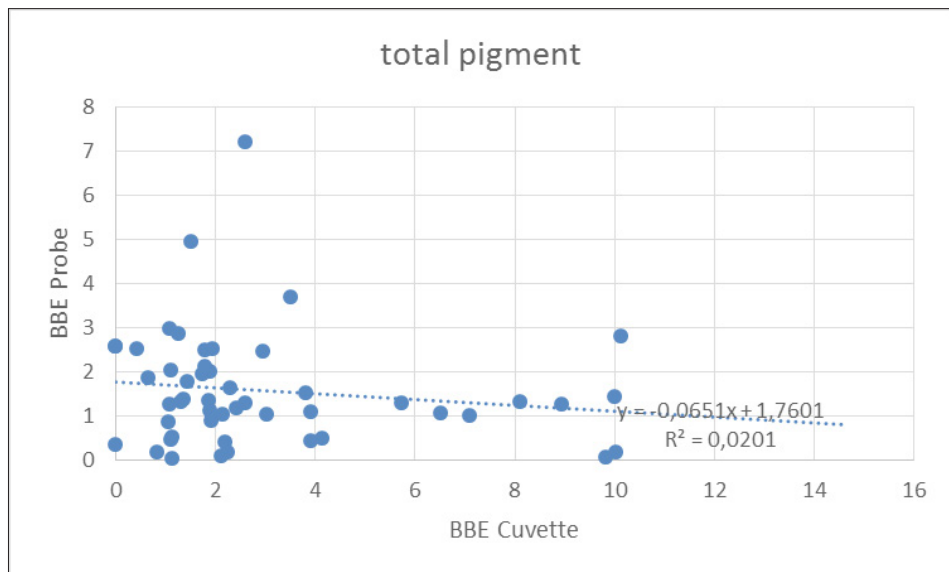


Fig. 3.22 displays a relatively strong correlation between the fluourometer measures and the BBE probe measures obtained from CTD deployments. Correlation would be stronger if the negative values of the fluoumeter had been removed.

BBE probe methods were in accordance with Zeng et al. (2015). Data was inputted into ODV to generate sectional plots for analysis.

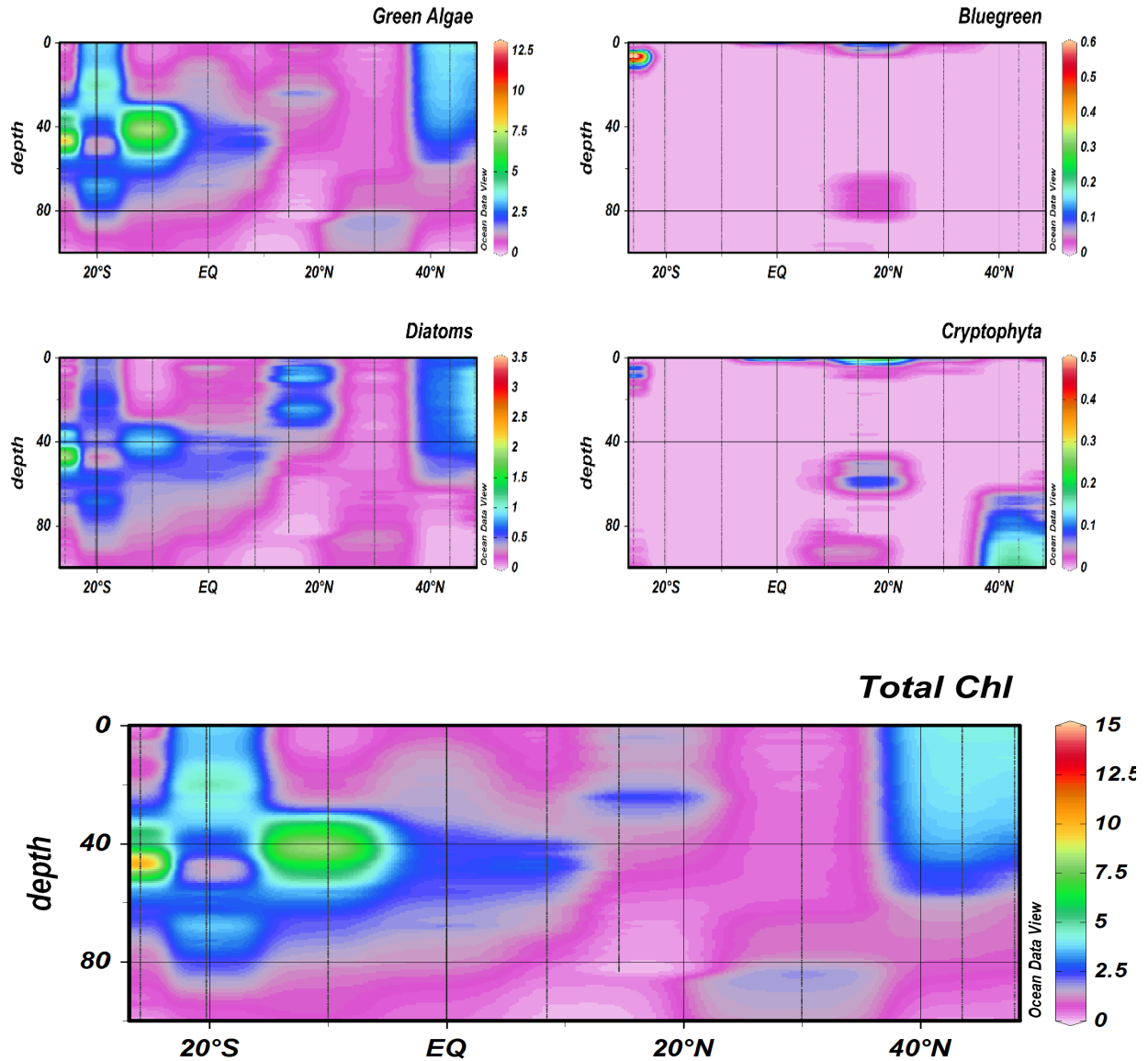


Fig. 3.23: Sectional ODV plots from the BBE probe deployed at all CTD stations for green algae, blue greens, Diatoms, cryptophyta and total chlorophyll

No clear axis of symmetry is displayed between any of the above parameters (Fig. 3.23), but instead a clear favouring of the southern latitudes is observed, with a chlorophyll maximum at 40-50 m. The above sections do however show a very similar relationship in the fluoumeter measurements. Fig. 3.24 shows that no correlation between the CTD fluoumeter and the BBE probe were observed.

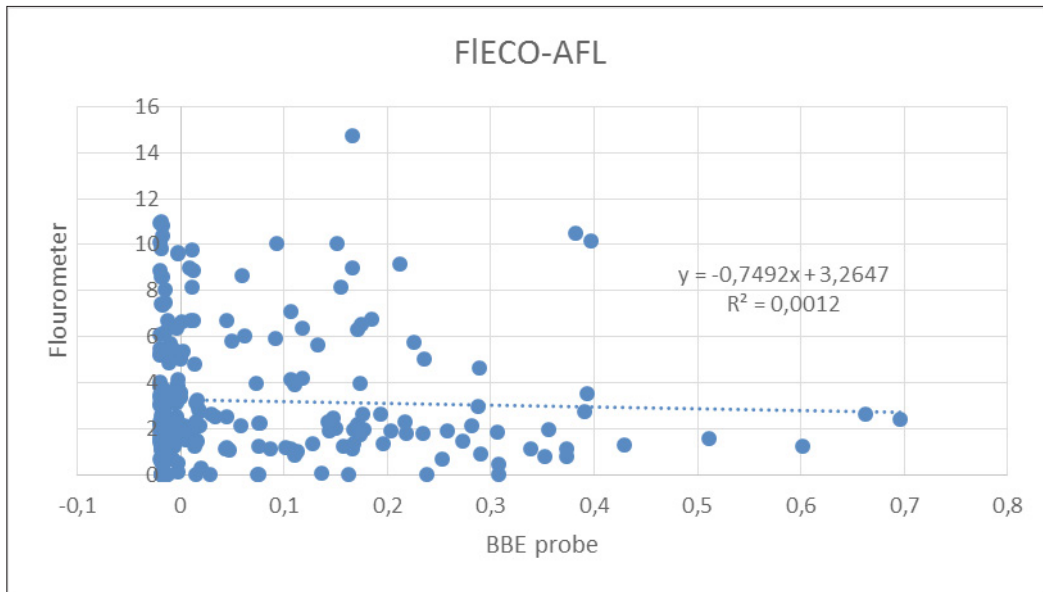


Fig. 3.24: Scatter graph of fluorimeter vs BBE probe measurements showing no correlation between the two systems

*BBE Cuvette*

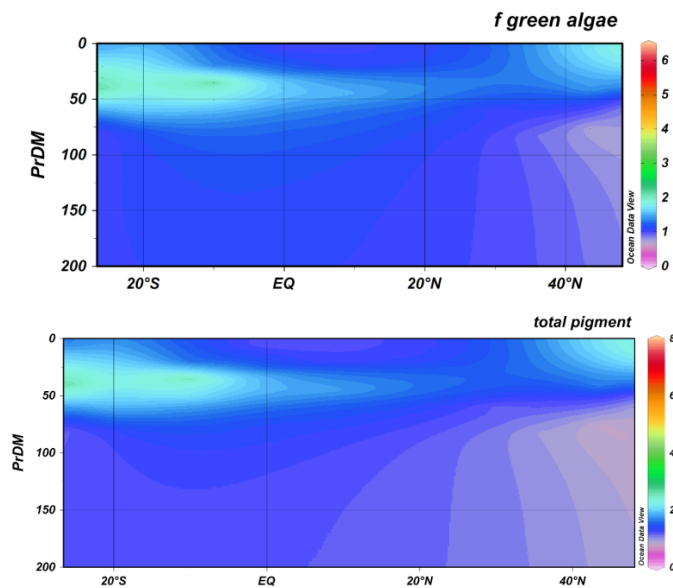


Fig. 3.25: ODV plot of BBE cuvette analysis for the whole transect

The above sections (Fig. 3.25) display the same chlorophyll maximum in the same regions as previous sectional plots, with a clearly higher chlorophyll max in the southern hemisphere and no symmetry across the equator or ITCZ. Fig. 3.26 shows no correlation between the BBE probe measurements and the BBE cuvette measures.

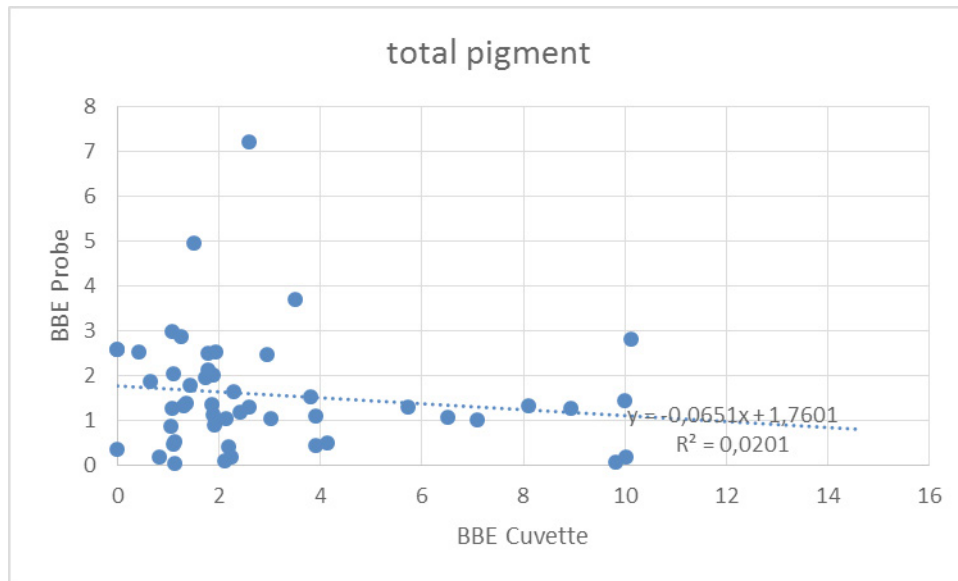


Fig. 3.26: Scatter graph of BBE probe versus BBE cuvette measurements

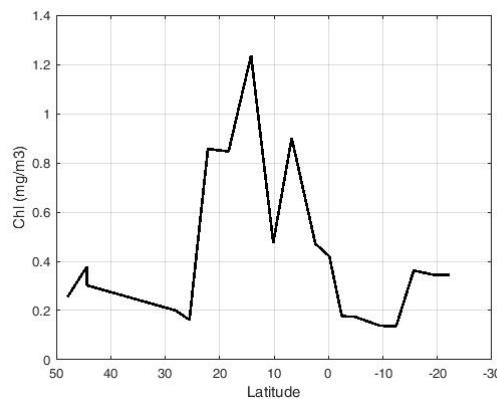


Fig. 3.27: Surface chlorophyll a concentration along the transect between 47° North and 23° South. Mean values of two calculated algorithms: OC4 and OC3S

Further on, our data show us an averaged surface chlorophyll concentration more than twice higher in the Northern Hemisphere ( $0.55 \pm 0.02 \text{ mg.m}^{-3}$ ) than in the southern hemisphere ( $0.26 \pm 0.06 \text{ mg.m}^{-3}$ ) along our transect. These results show us that our mirror-hypothesis is not verified for the remote sensing surface chlorophyll data. Surface chlorophyll a concentration along the transect between 47° North and 23° South are shown in Figure 3.27.

#### MODIS/VIRRS merged satellite data

If we compare the ground based remote sensing data from the Ramses spectrophotometer to synchronic satellite images on surface chlorophyll concentration, we obtain similar global low results below  $2 \text{ mg.m}^{-3}$  along our transect (Fig. 3.28).

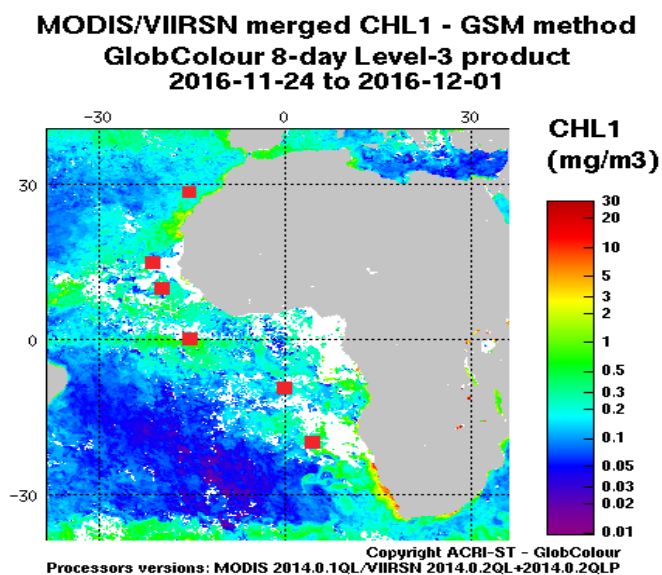


Fig. 3.28: MODIS/VIIRS merged CHL1 data. Global Colour Product between November 24 and December 1, 2016. Red squares symbolize the CTD stations

On a more global scale of the entire world ocean averaged on the month of November 2016, we can identify a clearer pattern: in the Pacific, we observe a surface chl max at the equator region ( $1 \text{ mg}\cdot\text{m}^{-3}$ ) compared to the very oligotrophic ocean ( $0,05 \text{ mg}\cdot\text{m}^{-3}$ ). In the Atlantic Ocean, the surface chl max is shifted north to  $10^\circ$  and the difference is more visible in the more oligotrophic Western Atlantic (Fig. 3.29).

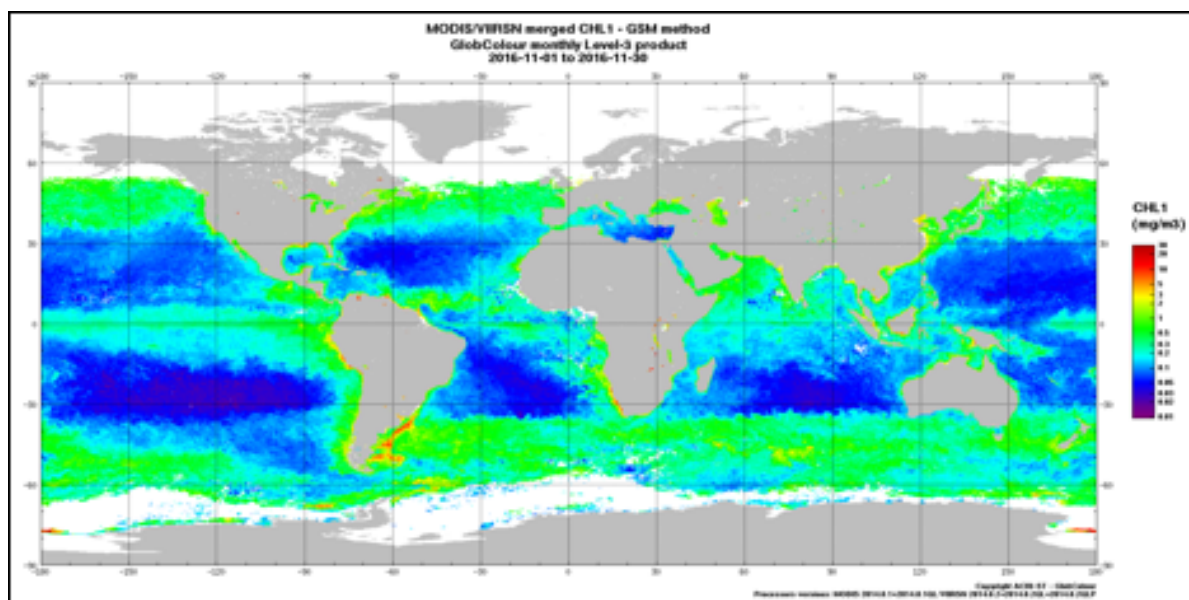


Fig. 3.29: MODIS/VIIRS merged CHL1 data. Global Colour Product between November 1 and 30, 2016

*MATMET*

*Atmosphere*

Thanks to remote sensing measurements, we were also able to determine different parameters of the atmosphere during the transect. The Microwave radiometer HATPRO (MWR) and the Radiosonde both measure air temperature and humidity. The MWR also estimates Cloud Bottom Height and Integrated Water Vapor in the atmosphere and the Radiosonde is able to determine wind speed and direction thanks to the attached GPS signal.

*Temperature*

Temperature and humidity are recorded continuously by the MWR. We observe an evenly stratified atmosphere up to 10 km with a temperature maximum of 30°C in the first kilometer of the troposphere between 15°N and the equator (Fig. 3.30a). The humidity also reaches its maximum of 15 g.m<sup>-3</sup> between 10°N and the equator (Fig. 3.30b).

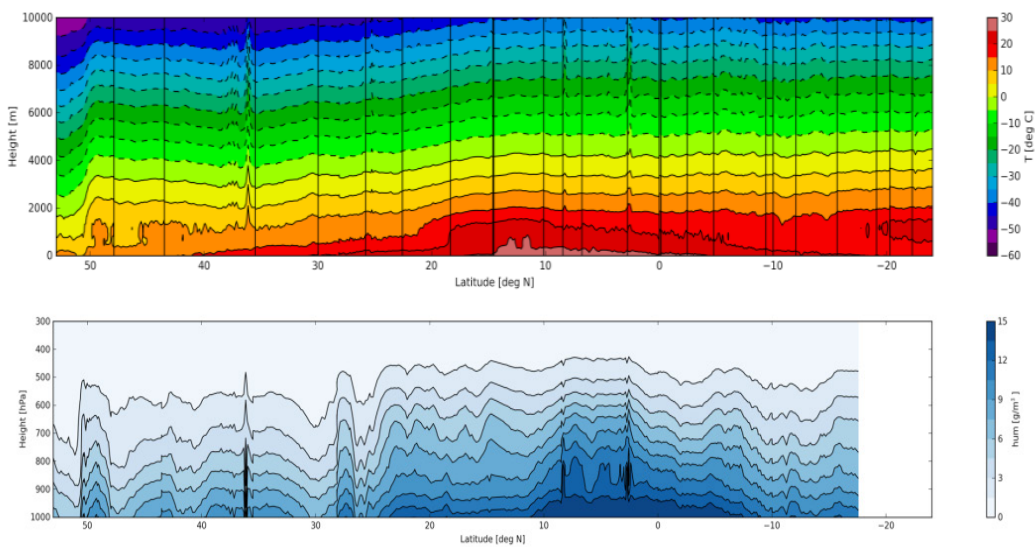


Fig. 3.30: transect of atmospheric profiles during PS102: a. (top) temperature and b. (bottom) humidity

These results show that the atmospheric temperature and humidity are symmetric between the northern and the southern hemisphere on our transect. Axis of symmetry is shifted slightly to the North and is situated around 10° North of the equator.



Fig. 3.31: Transect of the Integrated Water Vapor along the transect

We obtain similar results for the Integrated Water Vapor, showing that the mirror is not located on the equator but shifted between 10° and 5°N (Fig. 3.31).

Microbes are central to structuring and functioning of marine ecosystems. Given the remarkable diversity of the ocean microbiome, efforts to uncover geographical distribution of microbes remain a fundamental inquiry in ecology. Marine microbes are amenable to flow cytometric measurements because of its size and the presence of fluorophores specifically chlorophyll and phycoerythrin (Petersen et al., 2012). Here, we define marine microbes as both eukaryotic and prokaryotic microbes amenable to flow cytometric measurements. Water samples obtained using a bucket and CTD-Rosette were subjected to flow cytometry (Accuri Biometrics) to determine the abundance of total bacteria and other relevant taxa such as *Prochlorococcus*, *Synechococcus*, and *Chrysophytes*.

As expected total bacterial abundance is higher in the surface and coastal areas (Fig. 3.32). Distribution patterns of the microbes identified in the NoSoAT 2016 corroborates with previous studies (Fig. 3.32). The global distribution of *Synechococcus* and *Prochlorococcus* abundance is symmetric around the equator with a slight skew, while *Chrysophytes* distribution is difficult to determine (Fig. 3.32). In an Atlantic meridional transect, *Chrysophytes* was found to be widely distributed along the Atlantic basin characterized with total chlorophyll-a concentrations ( $>1\text{mg/m}^3$ ) found to be highest in the northern and southern temperate zones as well as in the Benguela and north-west African upwelling regions (Kirkham et al., 2011; Gibb et al., 2000; Aiken et al., 2009). Similarly, a previous study showed that *Synechococcus* peaked at the northern and southern temperate as well as in the upwelling regions while *Prochlorococcus* peaked at the oligotrophic gyres and equatorial region. (Kirkham et al., 2011). *Prochlorococcus* is highly adapted to oligotrophic water because of its small size (Dufresne et al., 2003). *Synechococcus* and *Prochlorococcus* are the most abundant cyanobacteria in the global ocean central to the ocean's primary productivity and carbon cycle (Biller, Berube, Lindell, & Chisholm, 2015; Scanlan & West, 2002). *Prochlorococcus* can be found up to a depth of 150 m with geographical extent of  $40^\circ\text{N}$  and  $40^\circ\text{S}$  whereas *Synechococcus* has a wider extent up to polar regions and high nutrient waters but limited depth distribution compared to that of *Prochlorococcus* (Flombaum et al., 2013).

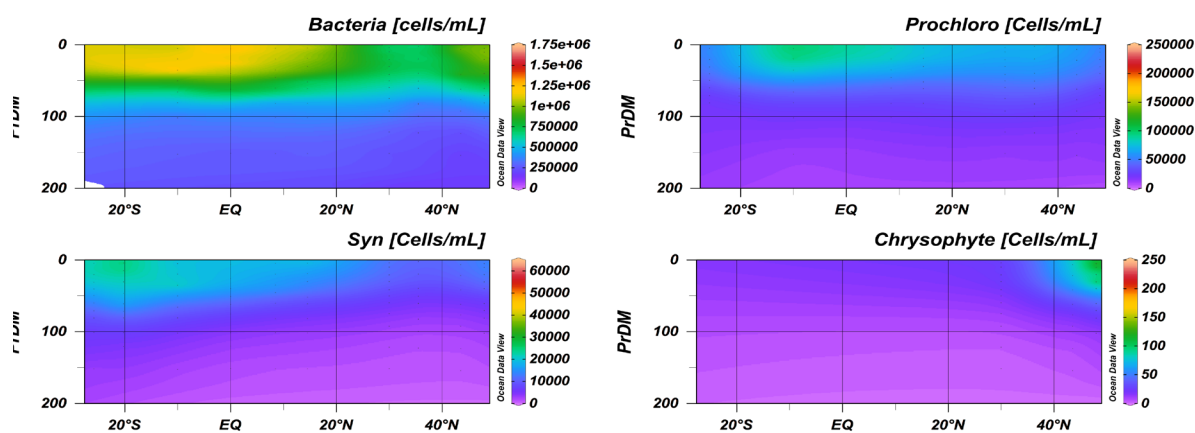


Fig. 3.32: Section plot of the abundance of total bacteria, *Synechococcus*, *Prochlorococcus* and *Chrysophytes* in the Atlantic

#### Impact of Climate Change to Axis of Symmetry of Cyanobacteria

Climate change projection is proven to be difficult because of the complexity of interactions, feedback loops and regional variations. This is especially true with regards to the biosphere. One of the modeling efforts to predict future climate scenarios resulted in a warmer upper

ocean with reduced pH and nutrient concentration, and enhanced iron (Boyd et al., 2014). In addition, future upper ocean is predicted to have an enhanced vertical density stratification (Sarmiento et al., 2004). Decrease in surface nitrate is attributed to the enhanced stratification and reduced upward nutrient supply (Boyd et al., 2014). These changes may or may not result in the shift of axis of symmetry of the properties of the water column. Reduced surface nitrate concentrations may increase the geographical extent of *Prochlorococcus* (Boyd et al., 2014) but not the axis of symmetry. Based on a global model, *Prochlorococcus* and *Synechococcus* axis of symmetry will most likely be unchanged instead an increase of global abundance is expected (Fig. 3.33) (Flombaum et al., 2013).

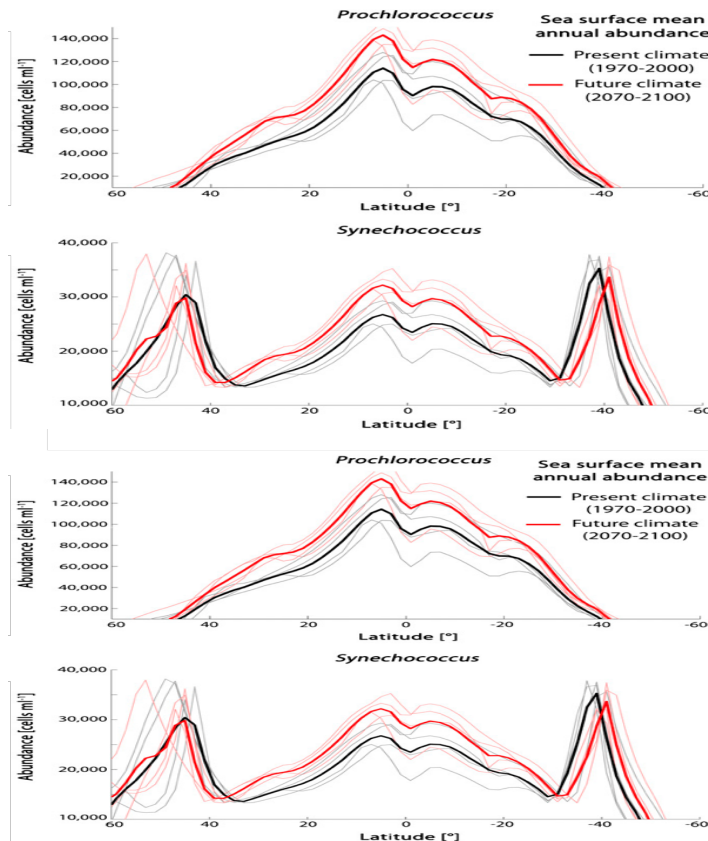


Fig. 3.33: Present and future global abundance of *Prochlorococcus* and *Synechococcus* (from Flombaum et al., 2013)

In general, we observed considerable symmetry in dissolved oxygen, pH, temperature, integrated water vapor, *Synechococcus* and *Prochlorococcus* but with some skewness. Other parameters such as chlorophyll and salinity show asymmetry. Atmospheric temperature, humidity and integrated water vapor are skewed to the north. All of these environmental factors are highly variable subject to influences of different spatial and temporal processes. Local processes, even on a small scale, may have significant consequences on physiochemical conditions of the water column, subsequently affecting the biological communities therein. However, long term monitoring on a finer scale is needed to understand the Equatorial Atlantic ocean processes.

#### *Large Scale Global Circulation and their Implications for Climate Change: a West African Monsoon Case Study*

A worthy feature of the WAM circulation is that the coastal areas within the core convective WAM region experience considerably amount of rainfall during the post-monsoon season although large swaths of the WAM is dominated by winds originating from the northern high latitudes (Fig. 3.34). Enhanced post-monsoon precipitation over some parts of WAM suggests that increased SST anomalies over the equatorial Atlantic exert significant influence during the drier season in line with our CTD SST records and precipitation observations.

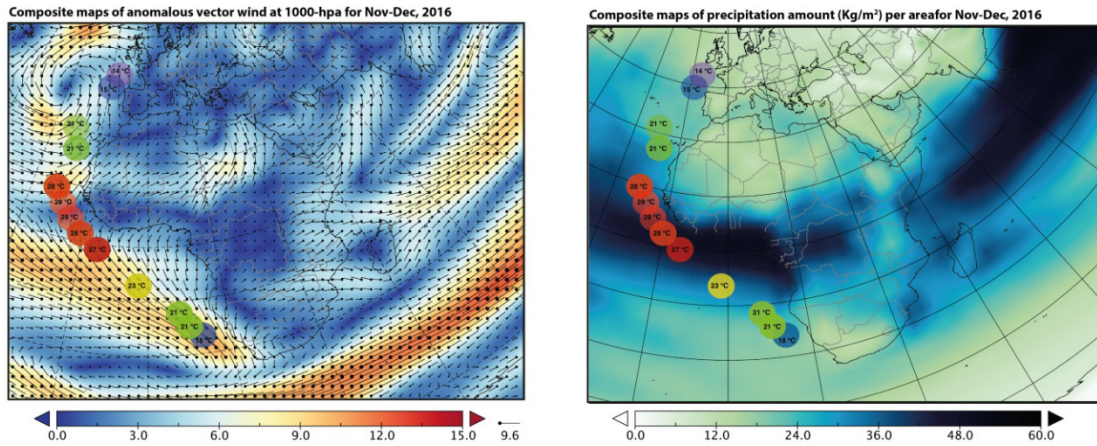
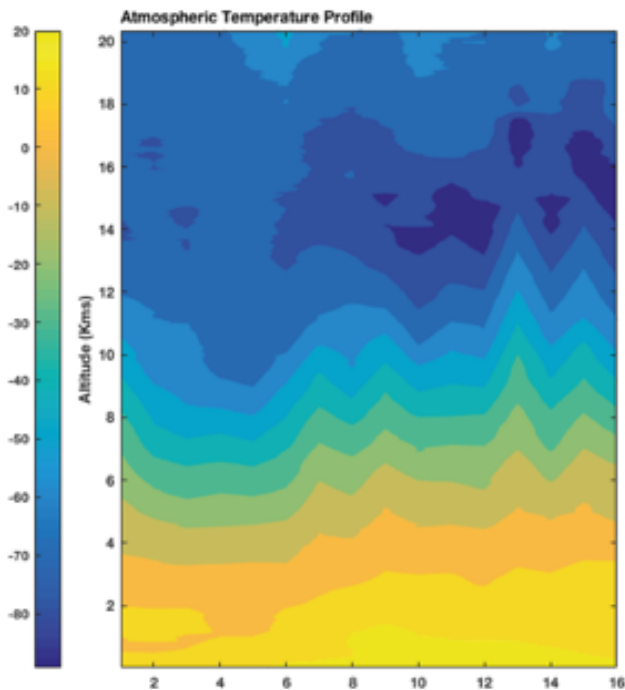


Fig. 3.34: Post summer composite mean for November to December, 2016; a) (left) Wind vector fields for November-December 2016 period. Also shown are discrete measurements of SST from CTD performed on a North-South transect in the Atlantic Ocean. SST values are estimated from measurements from the upper 10 m of the ocean; b) (right) Precipitation amount per area for November-December 2016 period. Circles denote same features as in a).

The impact of warmer SST anomalies on coastal rainfall over parts of the WAM region is also well documented (e.g. Hirst & Hastenrath, 1983; Nicholson & Entekhabi, 1987). Abnormally heavy rains have also been reported for the post-monsoon season in the coastal parts of Gabon in line with the development of a warm anomaly over the equatorial Atlantic (Buisson, 1985; Philander, 1986). The mode of variability, however, is dependent on the mean position of the ITCZ, typically situated south of the equator during the post-monsoon season and can also be identified looking at latitudinal changes in the atmospheric temperature profiles

Fig. 3.35: Radiosound measurements of Atmospheric temperature taken over the same North-South transect as in Fig.10. Initial date of measurement refers to day 1 (15th of November, 2016) and continues to day 16 (30th of November, 2016). The mean location of the Inter-Tropical Convergence Zone (ITCZ) can be identified by looking at the sharp changes in the tropopause height (day 10).



Despite incoherencies in interpretations, rainfall variation over the WAM region can be explained in terms of shifts in the mean position of the ITCZ and is also clearly observed in the atmospheric temperature latitudinal profiles (Fig. 3.35). SST over the North-South Atlantic transect range from  $\sim 30^\circ\text{C}$  to  $24^\circ\text{C}$ . Coldest SSTs are observed outside the English Channel and average around  $25.8^\circ\text{C}$ . This is  $\sim 3^\circ\text{C}$  lower than the maximum SSTs observed along

the equatorial Atlantic. Comparisons with the previous records of SST from a N-S transect interpolated in to the same latitude (PS95) show a similar SST cooling in the range of  $\sim 3$  °C and indicate little variations (paired-samples t-test,  $p < 0.01$ ). This is despite the fact that 2015 was one of the strongest El Niño years on record. However, whether this has a direct impact on the WAM is a matter of pure speculation at this stage. SST values reached as high as  $\sim 30$  °C over the equatorial Atlantic and gradually cooled to  $\sim 18$  °C over the mid-latitudes over the Southern Hemisphere. However, precise latitudinal differences in SST between the Northern and South Hemispheres remain difficult to resolve due to the inherent noise introduced in the discrete records through interpolation.

Dynamical interactions between the different water masses of the ocean offer critical information on the processes of ocean heat storage and transfer and potentially implicating mixed and surface layer temperature changes. Modern day upper ocean variability over the North and South Atlantic is characterized by seasonal variations of the mixed and thermocline layers and is driven by warming and to some extent freshening of the upper ocean, most likely due to the north-south migration of the ITCZ. This is also in line with observed SST changes and indicates a persistent diffusion of heat to the thermocline over large parts of the Atlantic and is strongest over the equator, decoupled from the deeper ocean temperature changes (Fig. 3.36). However, it is also likely that the transport of heat in regions with strong upwelling is driven by upward diffusion of heat.

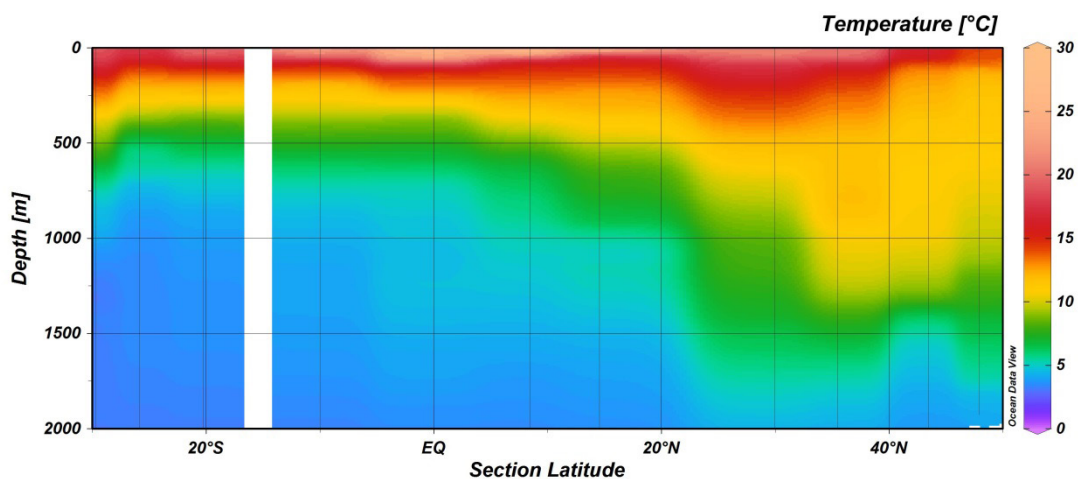


Fig. 3.36: Temperature depths profile section along the North-South Atlantic transect

Climate change and anthropogenic forcing of the Earth's system through input of  $\text{CO}_2$ , other toxic gases and pollution is perhaps one of the greatest challenges to the long-term viability of humans on this planet. *Polarstern* as part of an international fleet of ocean going research vessels, together with land based institutions, play their part in measuring the human impact on our climate. One of the tasks of *Polarstern*, is to monitor for trends that might be related to climate change. One of these changes over time is ocean temperature and can be clearly seen where *Polarstern* took expendable Bathymetry Thermograph (XBT) measurements at approximately the same position in 1985 and 2012. These readings were both taken just off the northwest African shelf in October. The temperature profiles of the upper 700 m are similar but with a marked offset between years, where 2012 is over  $1^\circ\text{C}$  warmer. If a one degree centigrade rise was seen across the Atlantic within 27 years that would indicate a huge change in energy balance equivalent to many degrees of heating in the atmosphere due to the ocean's heat capacity.

#### *Distribution and effects of Oxygen Minimum Zones on a transect from the Northern to Southern Atlantic Ocean*

The Figure 37 summarizes the DO concentration in the upper 1,500 m on the North South transect for the cruise PS81 (ANT-XXIX/1, 2012). North and South of the equator, two OMZs can be seen, which are defined in literature by values below 20  $\mu\text{mol/l}$  (Gilly et al., 2013). The minimum value observed by the CTD were 8.65  $\mu\text{mol/l}$  in a depth of 368.4 m in the core zone north of the equator. Both OMZs have their core regions situated from 20°N to approximately 18°S and consist of two vertically extended regions of about 500 m depth and one smaller patch at the equator with less than 20 m vertical extent. Therefore, the oxygen concentration varies from less than 10  $\mu\text{mol/l}$  to more than 200  $\mu\text{mol/l}$  within 1,000 m depth range, which can be seen in the steep colour gradient ranging from red to purple.

The ridges of the minimum zones extend just below 1,000 m and occupy the horizontal expansion across another 5°, respectively reaching from 25°N to 25°S.

The cruise PS95 (2015; Fig. 37) shows in general higher oxygen concentrations in the upper 1500 m than the PS81 (ANT-XXIX/1, 2012). The two core regions, described before, show DO concentrations above 47  $\mu\text{mol/l}$  and are therefore Oxygen Limited Zones (OLZ), which are defined between 20 and 90  $\mu\text{mol/l}$  (Gilly et al., 2013). The extension of the core region reaches from 20°N to 20°S with a slow oxycline from within the core (47  $\mu\text{mol/l}$ ) to the surrounding area (more than 230  $\mu\text{mol/l}$ ). The area of the oxygenated waters with concentrations above 200  $\mu\text{mol/l}$  is concentrated in the surface waters going down to 600 m in the Northern and Southern most extent of the transect.

This year's cruise (PS102, 2016; Fig. 37) shows the lowest DO concentration of 21  $\mu\text{mol/l}$ , resulting in 2016's OMZ regions being defined as OLZs, which is close to the threshold of being defined as OMZ. The core region (less than 45  $\mu\text{mol/l}$ ) vertically goes down to 750 m. Even down to 1,000 m, DO concentrations do not exceed 90  $\mu\text{mol/l}$ . Colour changes are therefore less rapid, ranging from red to blue in a smooth transition. The horizontal extension exceeds 40°N, whereas the southern extension ends due to sampling limits at 25°S. Additional to the two core regions North and South of the Equator, Fig. 37 shows decreased DO values below the connecting water mass as well as in the surrounding areas. None of the plotted areas for 2015 and 2016 have DO concentrations in their water mass above 200  $\mu\text{mol/l}$ .

There is a strong difference in oxygen concentrations between the 2015 (El Niño year) and 2012/2016 (non-El Niño) years along the North to South transect in the Atlantic. According to the classification of the oxygen reduced zones, 2012 can be classified as a OMZ, while both 2015 and 2016 are classified as OLZs. During 2015 and 2016 the lowest oxygen concentrations were around 50  $\mu\text{mol/l}$ . During 2012 the DO concentrations in the cores of the OMZ reached below 20  $\mu\text{mol/l}$ .

The DO dropped between 2015 and 2016 by 50 % in the cores of the OLZ areas from 90 to 45  $\mu\text{mol/l}$  intensifying the OMZ in one year. The OLZ also expanded from 2015 to 2016, where the OLZ increased in depth and horizontal distribution. The shallow extent of the OLZ in 2015 is smaller and deeper than during 2012 and 2016. There is a clear expansion of the OLZ from 2015 to 2016 into shallower waters as well as deeper. The horizontal extent has also spread out with the surrounding waters of the OLZ decreasing from 200  $\mu\text{mol/l}$  to 175  $\mu\text{mol/l}$  from 2015 to 2016.

The differences seen between the two normal years (2012 and 2016) show that the extent of the oxygen reduced region has shoaled at the surface and increased its latitudinal extent from 23°N to 30°N. The 2012 OMZ has a lower DO concentration, which falls to as low as 20  $\mu\text{mol/l}$  with a strong concentration gradient, where as in 2016 the lowest DO concentration

is 45  $\mu\text{mol/l}$  and the gradient is less pronounced. The surrounding waters of the Atlantic has decreased in DO concentration by 60  $\mu\text{mol/l}$  from 2012 to 2016 particularly in the North surface waters between 40° and 20°N. The surface concentration has also decreased from 2012 to 2016. There is a small OLZ in the equatorial region (between 5° North and South) in 2012 with only a weak DO decrease in the same area in 2016.

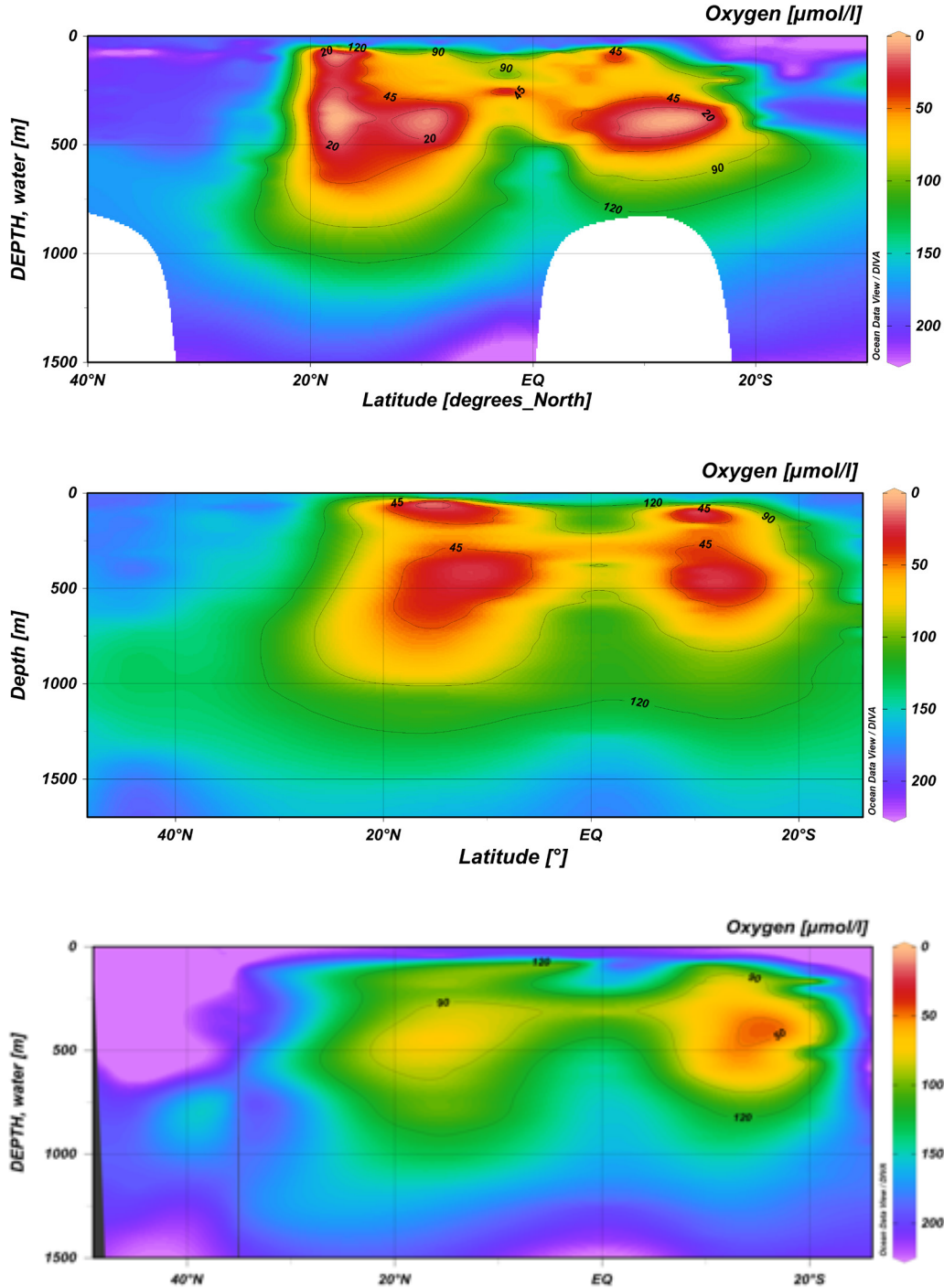


Fig. 3.37: Sections of the dissolved oxygen concentration along the North South Atlantic Transect. a) 2012 (top), b) 2015 (middle) and c) 2016 (bottom)

In the Angola Dome region OLZ (centered around 12°S) is more intense (50  $\mu\text{mol/l}$  DO) in the El Niño year (2015) than the Guinea Dome region OLZ (centered around 16°N; 90  $\mu\text{mol/l}$  DO). During normal years, the Guinea Dome region oxygen reduced zone is more intensive with the lowest concentration reaching 20  $\mu\text{mol/l}$  with a deeper vertical extent than the Angola Dome region OLZ, which extends from 50 to 1,200 m and 75 to 1,000 m depth respectively. The change in DO concentration between El Niño and normal years is more pronounced in the Guinea Dome region than the Angola Dome region.

Within the histograms showing the concentrations of DO versus the count of points with certain concentrations there are clear differences between the three years. Fig. 3.38 a) of 2012 DO concentration distributions shows clear bimodal distribution with a larger spread of DO concentrations over the latitudinal gradient. The 2016 histogram (Fig. 3.38 c)) shows a more uni-modal distribution of concentrations with less higher concentration levels than seen in 2012. 2015 shows a larger count of high concentrations with very few low concentrations (Fig. 3,38 b).

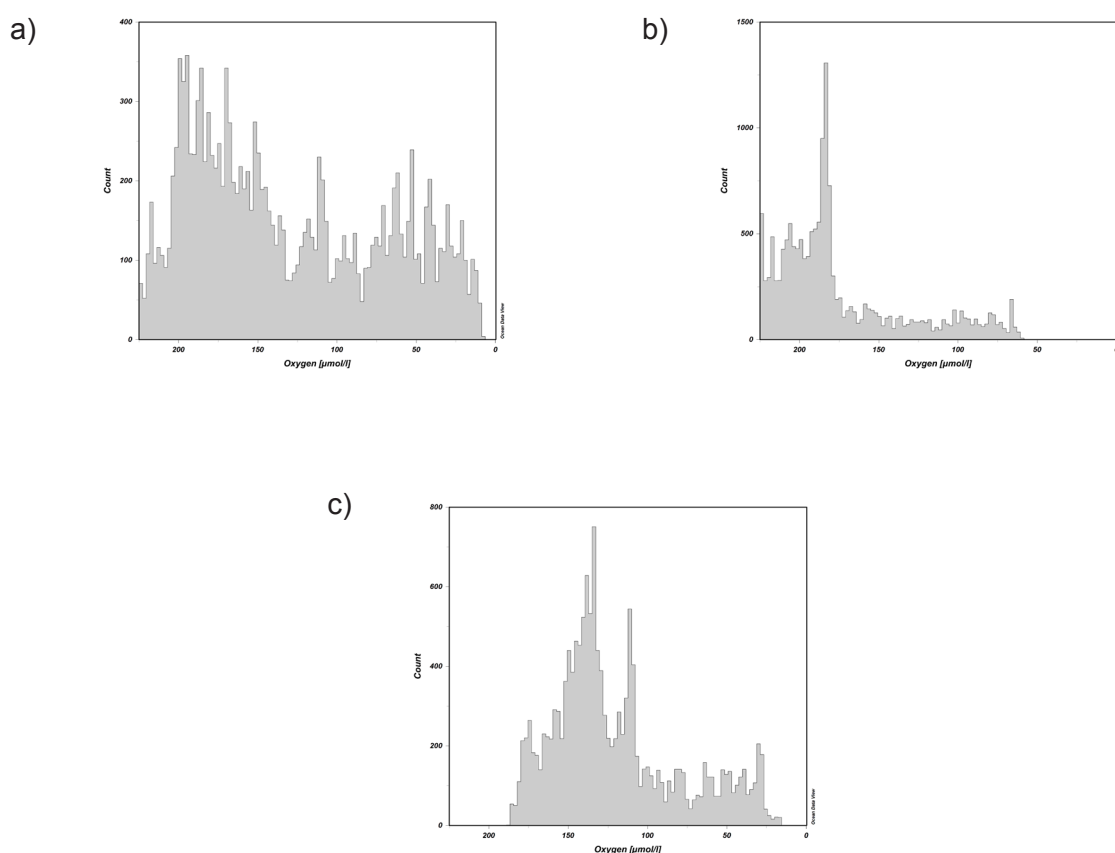


Fig. 3.38: Histograms depicting the DO concentration distribution along the North South Eastern Atlantic transect in the years a) 2012, b) 2015 and c) 2016

Our results showed an inter-annual variability. The OMZs showed an expansion in the extent horizontally and vertically from 2012 to 2016. Although the El Niño year contributed to the ventilation of the OMZs, it can be predicted the general concentration of DO will decrease within the next couple of years. The effects of deoxygenation of the ocean are not an isolated issue and should be considered in conjunction with other major issues such as the ocean acidification and temperature increase. There needs to be a better understanding that oxygen reduced zones do not just effect a select number of species but can alter entire ecosystems. Chemically, OMZs and OLZs are an important factor regarding the carbon and nitrogen cycle.

Future research needs to investigate the following questions to obtain a better understanding of OMZs and their dynamics.

*Identifying upwelling areas along the transect between Bremerhaven and Cape Town based on oceanographic and atmospheric data*

### *CTD, XBT, and In-situ Meteorological Measurements*

Measurements of temperature, salinity, oxygen concentrations, and fluorescence along the transect from Bremerhaven to Cape Town showed great variability both with latitude and depth.

As expected, water temperature was generally highest at the surface and ranged in magnitude between ca. 14 °C and 28 °C (Fig. 3.39 a; cf. Fig. 3.42). The vertical extent of the warm surface water was greatest between ca. 35°N to 25°N and at around 3°N where 15 °C warm water reached depths of ca. 300 m and 180 m, respectively. In contrast, the northernmost CTD casts at ca. 48°N and 43°N revealed a mostly homogenous upper water column regarding temperature, with temperatures ranging between ca. 15 °C and 13 °C. A penetration of colder water towards shallower depths when compared to previous measurements was evident at CTD station 10.

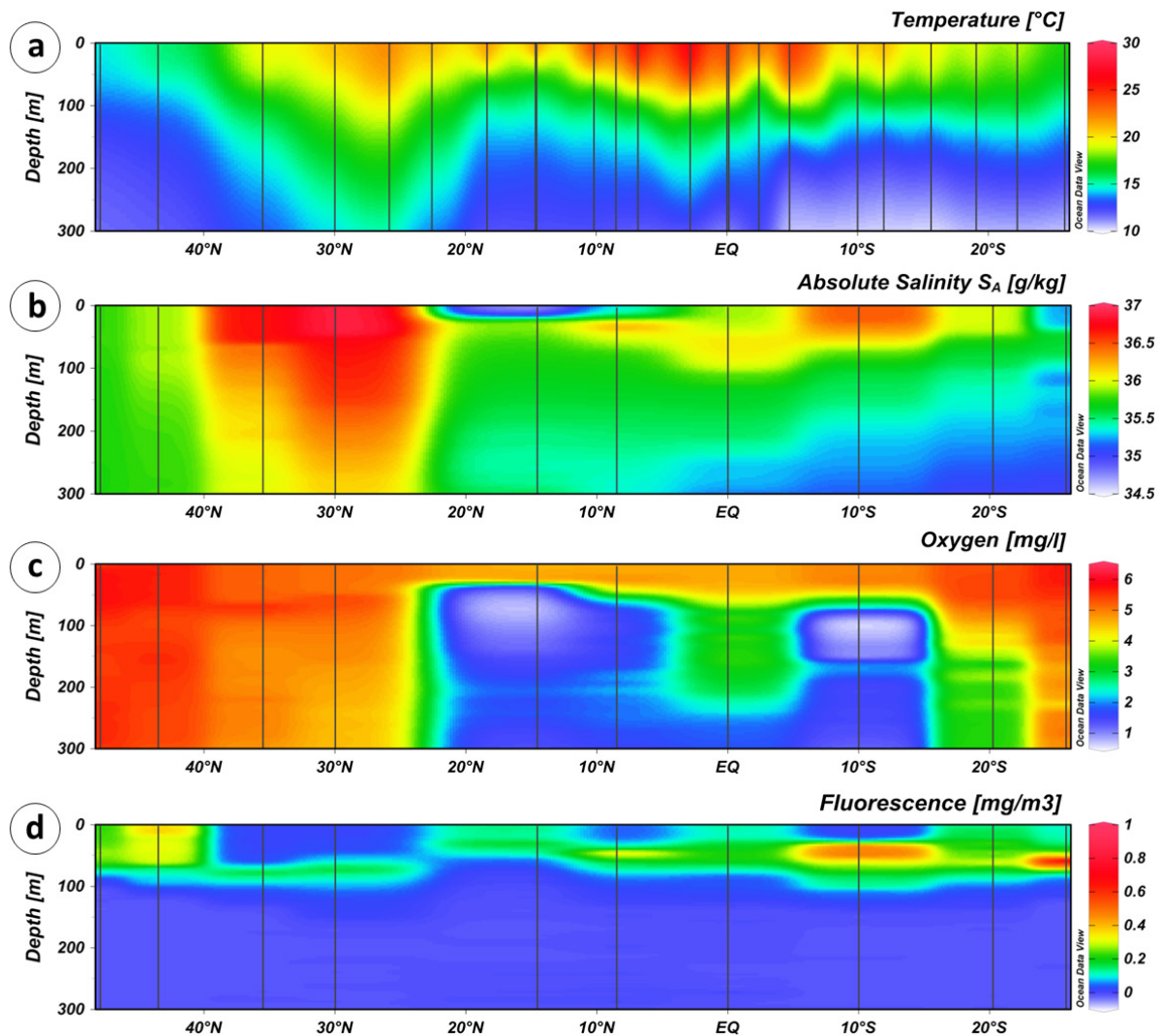


Fig. 3.39: Temperature (a), absolute salinity (b), oxygen (c), and fluorescence (c) measurements based on CTD data. Temperature records also include XBT data. Vertical lines indicate stations

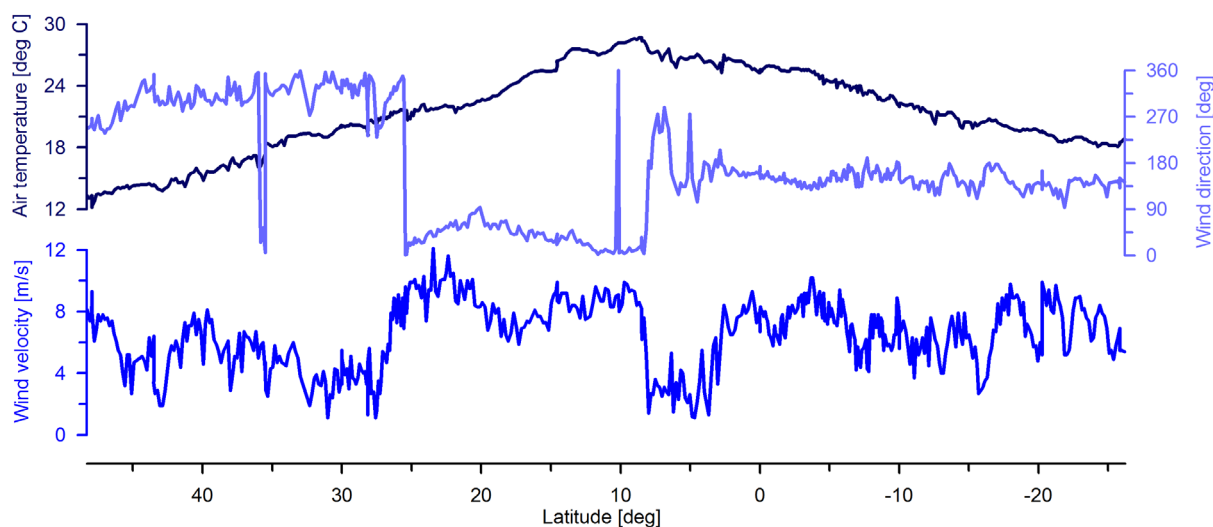


Fig. 3.40: Hourly air temperature, wind direction, and wind velocity records from the vessel's meteorological station

From ca. 48°N to 40°N, salinity was relatively consistent in the upper 300 m (ca. 35.7 g/kg) and did not show a significant stratification (Fig. 3.39 b). Between ca. 35°N to 25°N, a saline layer (36.5 – 37.0 g/kg) was evident in the CTD data, which correlated with elevated water temperatures and a deeper penetration of this warm surface layer. At CTD station 10, several lenses of less saline water were evident throughout the water column.

The oxygen concentrations depicted two pronounced oxygen minimum zones on both sides of the equator at ca. 50 m depth (Fig. 3.39 c). These zones extended to more than 300 m depth and were overlain by waters of moderate oxygen concentrations (ca. 4 mg/l). At the equator, a deep vertical gradient in oxygen concentrations was evident with diminishing oxygen around 240 m depth. Higher oxygen concentrations were found towards higher latitudes in both hemispheres.

Chlorophyll contents, herein reflected in total fluorescence measurements, varied considerably along the transect and showed several distinct layers and masses of water with high chlorophyll levels (Fig. 3.39 d). Between ca. 40°N and 27°N, fluorescence was effectively absent at the surface and only low values were observed between ca. 70 – 100 m depth in a weak chlorophyll maximum layer. Prominent chlorophyll maximum layers occurred at ca. 10° north and south of the equator overlying the respective oxygen minimum zones previously described. Another strong maximum of chlorophyll concentrations was found at CTD station 10 at ca. 80 m depth with values reaching as high as 0.8 mg/m<sup>3</sup>.

Hourly resolved observations by the vessel's meteorological station revealed dominant south-easterly winds ranging in velocity from ca. 1 to 12 m/s (Fig. 3.40). Following a period of relatively weak north-westerly winds, a significant increase in the wind velocity occurred at ca. 26°N. These stronger winds of ca. 8 m/s on average prevailed on the rest of the transect with the exception of weaker winds between 8°N to 2°N. From about 8°N, winds were consistently of south-easterly direction.

Air temperature (in intervals of 1 hour) along the transect depicted a steady warming of the lower atmosphere from higher to low latitudes, reaching a maximum of ca. 28 °C around 8°N before decreasing consistently again on the course of travelling south. Importantly, the region of peak air temperatures corresponded with maximal sea surface temperatures which were also recorded over several degrees of latitude north of the equator while warm waters reached less far away from the equator in the southern hemisphere.

Two stations along the transect showed some indication of potential upwelling. Of these, CTD station 10 provided the strongest signatures in terms of temperature, salinity, oxygen, and fluorescence that suggested the upward transport of deeper water. CTD measurements at this location depicted colder and fresher water rising close to the sea surface, and furthermore showed a deep mixed layer with regards to oxygen concentrations. The pronounced chlorophyll maximum suggested high nutrient levels for enhanced primary productivity, which is another typical characteristic of upwelling water masses (Louw et al., 2016). Moreover, the dominant wind direction over the course of the cruise was SE to SSE, and winds on the transect in the southern hemisphere were entirely of this nature. Importantly, these prevailing SE winds of 4 – 9 m/s observed in the southern hemisphere provide a critical prerequisite for upwelling since resulting Ekman transport should effectively carry water seaward from the African continental shelf and thus promote the pumping of deeper water towards the sea surface. Based on these observations while also considering the location of CTD station 10 at ca. 25°N, it is reasonable to suggest that these signatures may be associated with the Benguela Upwelling System (Louw et al., 2016).

While equatorial upwelling has often been described (e.g. Subramaniam et al., 2013), CTD and XBT data could not unambiguously show evidence of upwelling at the equator during this cruise (CTD station 7). Although there were indications of a deeper mixed layer with regards to temperature, salinity, oxygen, and fluorescence, the origin of the signals were unclear. One reason for this was the low spatial resolution of CTD data north and south of the equator, which did not allow for a more detailed study of the physical and biochemical parameters in the equatorial water column and nearby locations.

Another interesting region regarding CTD and XBT data was the transect between ca. 40°N and 27°N, however, this water mass with elevated temperatures and salinities should be associated with the Mediterranean Outflow Water and should not be confused with upwelling or related processes (e.g. Price et al., 1993). Similarly, the shallow layer of low salinity water north of the equator corresponded to the approximate location of the Intertropical Convergence Zone (ITCZ), and was therefore likely a result of elevated precipitation in this region.

Thus, oceanographic measurements at only two stations provided some indication of upwelling. A major challenge, and simultaneously a great source of uncertainty, in attempting to identify upwelling along the cruise transect was the low spatial resolution of CTD casts and associated water samples and analyses.

#### *Mixed Layer Depth and Ekman Pumping*

The mixed layer depth (MLD) was estimated using vertical profiles of temperature of the CTD stations. The method to estimate the MLD was the maximum gradient of temperature. Using these estimations, vertical profiles of temperature and their respective MLD were made (Fig. 3.41; cf. Fig. 3.43).

Because the surface MLD is directly estimate on individual profiles (with data at observed levels) this value represents the depth over which surface fluxes have been recently mixed and integrated. The profiles show stratification and they are not totally homogenous with depth. There is a high variability in the vertical profiles of temperature related with the fact that the CTD stations were made along a transect, where physical processes change from one CTD station to the other. The MLD represents the starting point of the thermocline (when the temperature decreases with depth) and Bourlès et al. (2002) found that thermocline shoaling is related with the equatorial upwelling and to enhanced vertical mixing. This fact shows a relationship between the mixed layer depth with the upwelling areas. In this case, the St. 10 show the deepest value of the MLD and this station is located in the Benguela upwelling area.

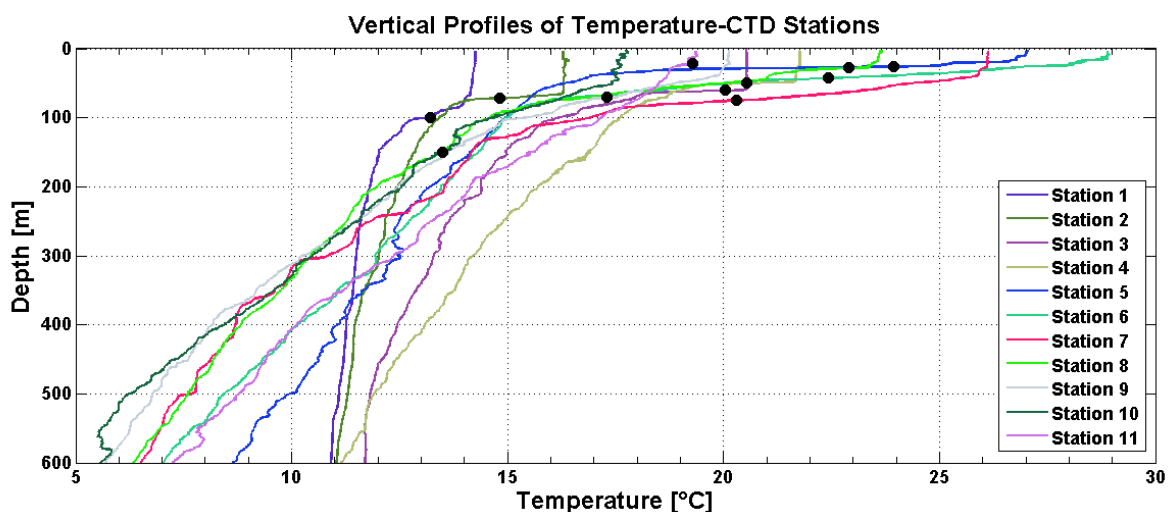


Fig. 3.41: Vertical profiles of temperature. The colour lines represent the vertical profiles of temperature for each CTD station and the black dots show the MLD using the temperature maximum gradient criterion.

There are several reasons to try to relate the MLD with the upwelling areas. Ekman pumping also produces planetary (Kelvin) waves that changes the depth of the thermocline (Zelle et al. 2004) and this results in a change in sea surface temperature. Besides, when the thermocline is shallow, the upwelling waters are usually rich in the dissolved nutrients (e.g., nitrogen and phosphate compounds) required for phytoplankton growth. In this case, it is not possible to identify the change of the sea surface temperature but the St. 7 and the St. 10 show deep values of the MLD and also high concentrations of chlorophyll around 80 m (Fig. 3.41).

It is important to note that there is a long distance between CTD stations on the currently research cruise. For this reason, the MLD for XBT profile was estimated too (Fig. 3.42; cf. Fig. 3.43). The applied methodology for XBT is the same that the previously mentioned.

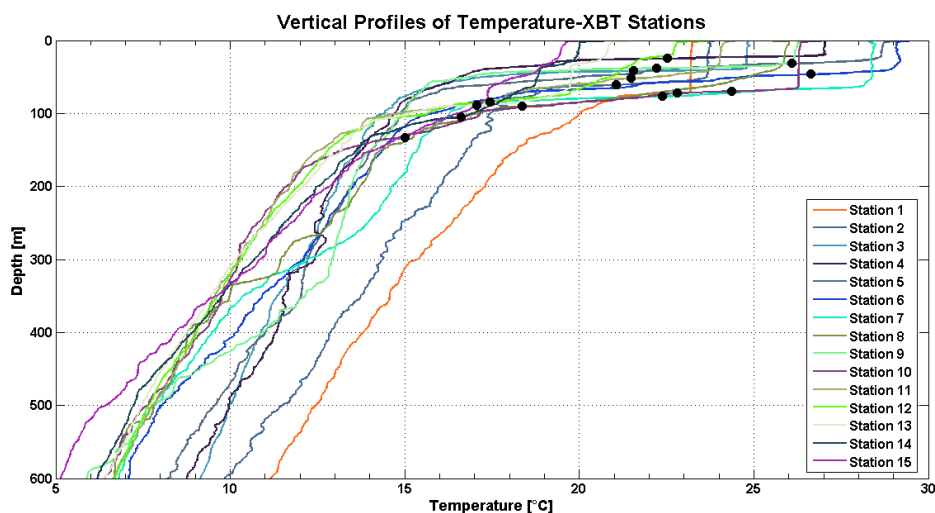


Fig. 3.42: Vertical profiles of temperature. The color lines represent the vertical profiles of temperature for each XBT station and the black dots show the MLD using the temperature maximum gradient criterion.

The XBT data has a better resolution than the CTD because it has one profile per day. However, the XBT data began on leg 2 of the transect. The last XBT station (located in the vicinity of Benguela upwelling) shows the deepest values of MLD as the same for the CTD data. This

station also shows a high concentration of fluorescence and more mixture rather than the other stations.

The MLD values for CTD and XBT stations vs. latitude were also made for a better understanding of the situation (Fig. 3.43). The bigger differences are between 10-20°S and between 25-30°N, being the biggest around the 30 m. However, there are not so many CTD stations to efficiently compare these two sets of data but it can infer that the behavior of the both curves are similar. In the beginning of the research cruise the MLD was deeper but as the ship was moving to the south the MLD was shallower until 10°N. After that, the MLD curve has a relative maximum located on the Equator with a value of 80 m. Besides, the curve has a more marked maximum around 27°S, in the vicinity of Benguela upwelling area. Is important to note that the last station shows a shallow MLD, so probably the upwelling areas cannot be identified beyond that latitude.

Using the information summarized up to now it can be inferred that Station 7 and 10 from CTD data and Station 15 of XBT data could have upwelling characteristics. Three profiles were made in other graphics to further investigate upwelling at these stations (Fig. 3.44).

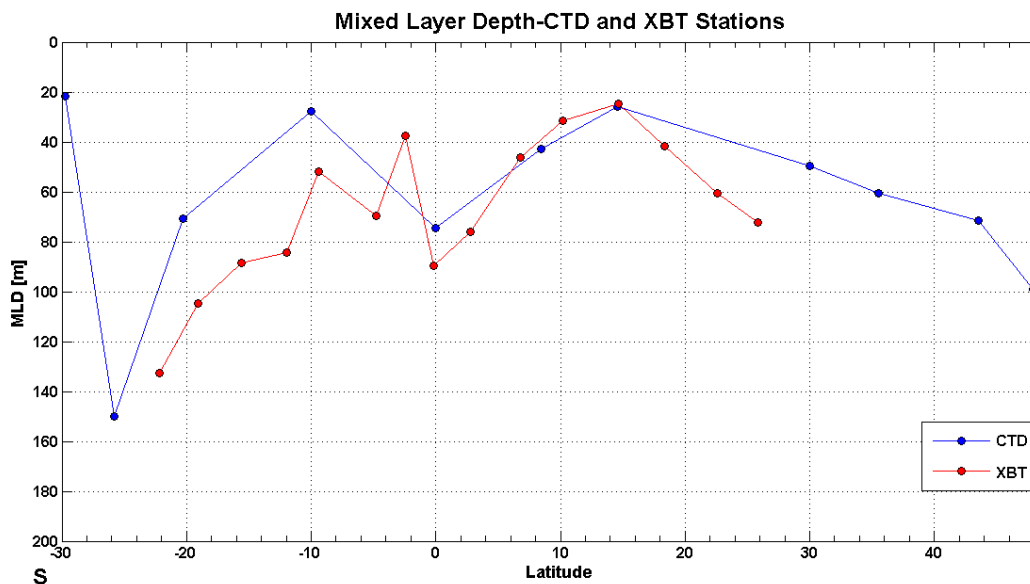


Fig. 3.43: Mixed Layer Depth vs. Latitude. The blue line (red line) represents the change of the MLD with the latitude for CTD (XBT) stations. The dots show the MLD values effectively estimated using the temperature maximum gradient criterion.

The figure 3.43 shows weak vertical gradients in a deep MLD for the three stations. This could be a feature of upwelling areas since weak vertical gradients are associated with well mixed surface waters, i.e. a common feature of temperature observations from upwelling regions (Lentz, 1992). Lentz (1992) also show that the surface mixed-layer events are related with strong wind periods. These three profiles don't have a clearly stratification so the upper surface-layer could be mixed by the entrance of upwelling waters below the thermocline.

Using data from reanalysis the Ekman pumping (velocity) or velocity of Ekman was calculated for the year 2007 (Fig. 3.45). Because the wind data from the cruise was not enough to estimate this parameter the last year of available reanalysis data was incorporated.

Although 2007 is not the current year, the Fig. 3.45 shows a magnitude for upwelling velocity for the positions of the CTD stations for this transect. In the position of the Station 10 there is a strong upwelling that matches with the previous analysis. At the other positions, it can be

inferred something about the upwelling regimes but the magnitudes of the vertical velocities are not relevant because in upwelling areas the vertical velocities are higher than 50 m/year (Talley et al., 2011) Stations located between 5° North and 5° South have been excluded as Ekman pumping does not apply there.

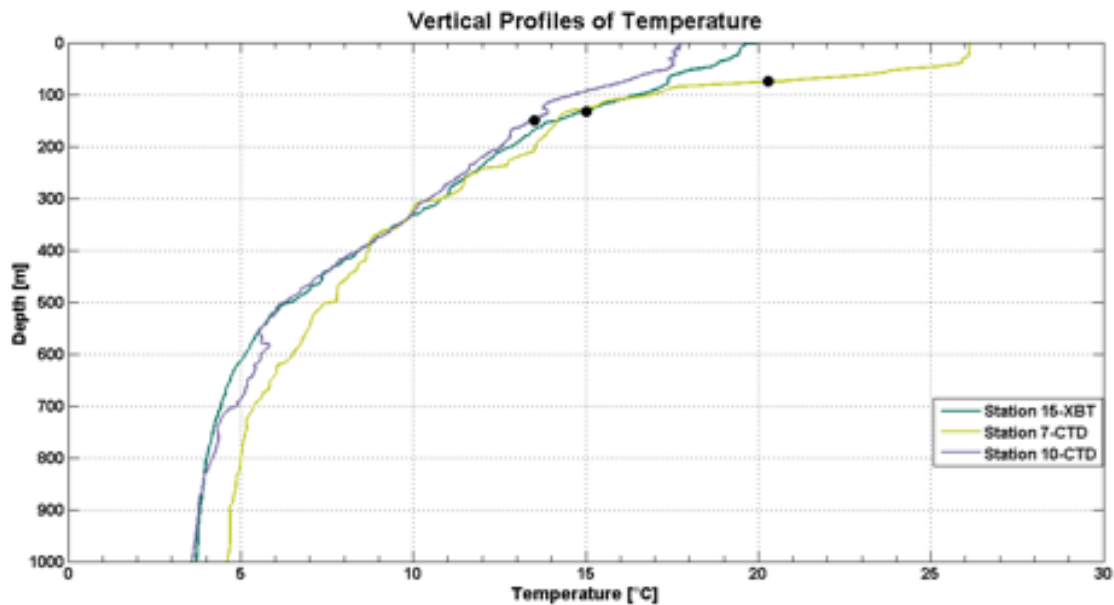


Fig. 3.44: Vertical profiles of temperature. The color lines show the vertical profile of temperature for one station of XBT data (Station 15) and for two stations of CTD data (Station 7 and Station 10).

The BBE measurements of chlorophyll-a on station 1 (Fig. 3.46) showed up to 5.33  $\mu\text{g/l}$  overall concentration within the first 10 meters depth, rapidly decreasing at around 50 meters. There, a stationary phase with about 1.00  $\mu\text{g/l}$  appeared until approximately 85 m. After that, a slow decrease in chlorophyll-a values was observed down to 0.11  $\mu\text{g/l}$  until 130 m. When distinguishing between chlorophyte (green algae) and diatom chlorophyll-a, similar pattern was observed, with a range up to 5.33  $\mu\text{g/l}$  in green algae and 3.18  $\mu\text{g/l}$  in diatoms, respectively. The high primary production in this area can be explained by the shallow, anthropogenic influenced British channel, rather than coastal upwelling.

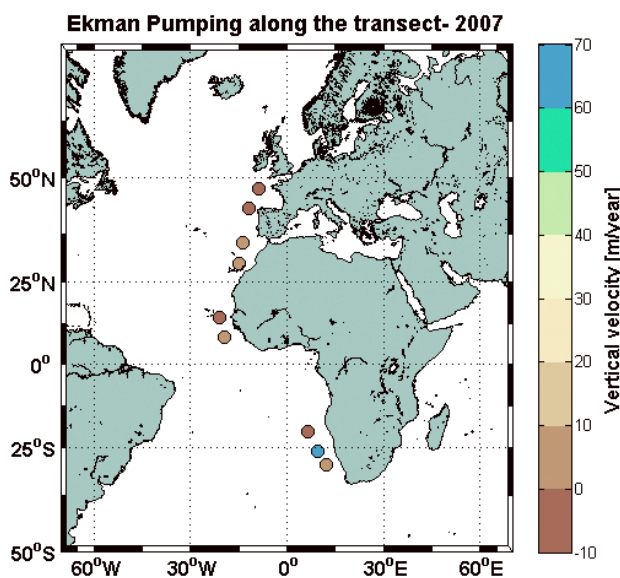
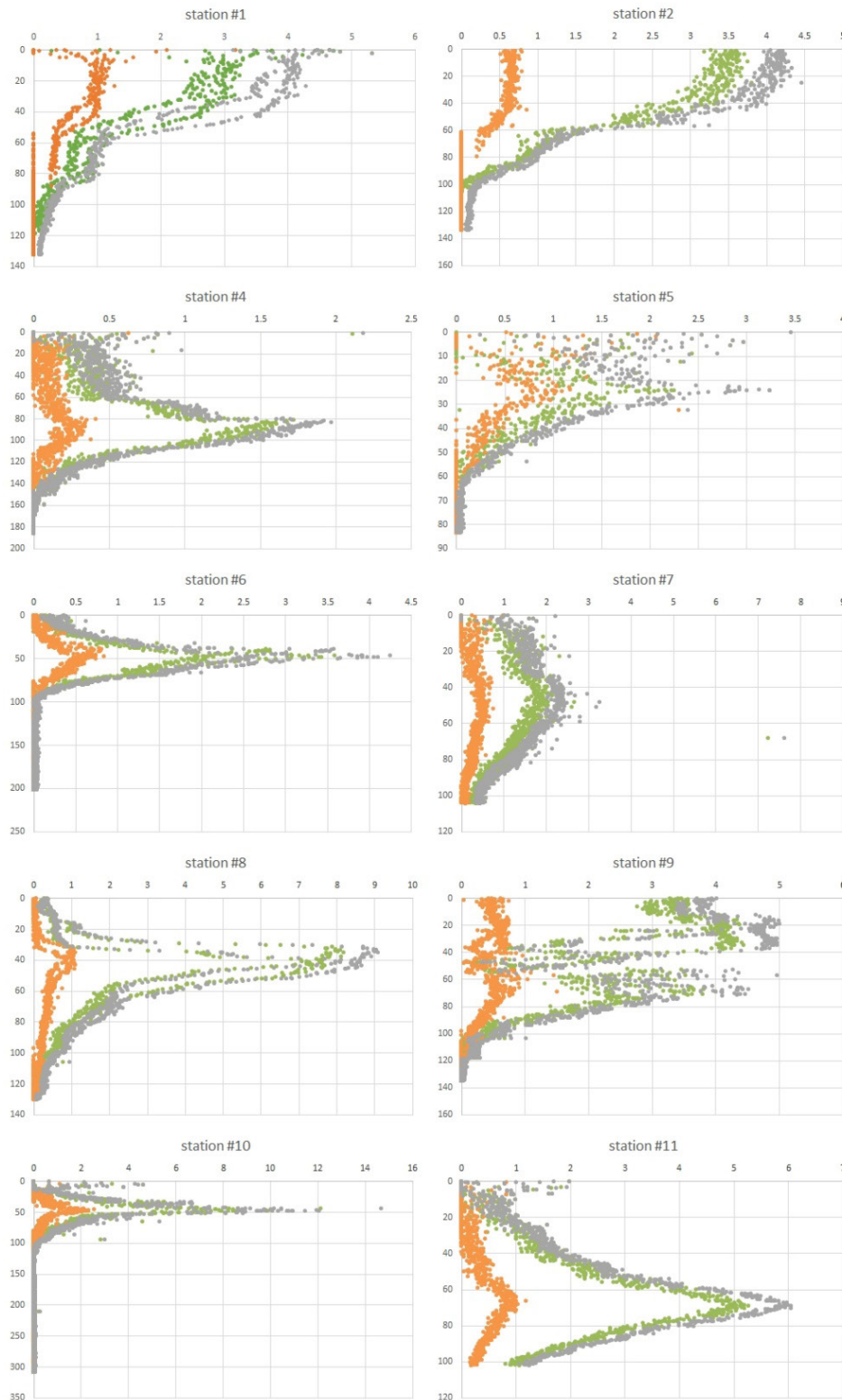


Fig. 3.45 Ekman pumping along the coordinates of the CTD stations. Ekman pumping was calculated using the year 2007 of reanalysis data. The color dots show the magnitude of the vertical velocity of upwelling (positive values) or downwelling (negative values).



*Fig. 3.46: Vertical profile of chlorophyll-a concentrations for each station (except station #3) green: green algae, orange: diatoms, grey: total*

At the station 2 a clear difference in values between green algae and diatom chlorophyll-a was noticed. While green algae values were close to the pattern of total measured chlorophyll, the maximum of diatom signals remained around 0.60 µg/l within the first 40 m under the surface. The green algae maximum was detected at 25.02 m with 3.81 µg/l, the overall maximum at the same depth with 4.46 µg/l. Also station 4 did not provide high signals in chlorophyll-a in the water. Maximum values were 2.18 µg/l (total) and 2.11 µg/l (green algae) at 1.22 m and 0.63 at 0.92 m (diatoms).

A high dispersion of fluorescence signals was found within the upper 30 meters of the water column in station 5. Total chlorophyll-a signal density reached up to 3.46  $\mu\text{g/l}$  in 0.14 m. However, a clear peak of overall, as well as in diatom (0.94  $\mu\text{g/l}$ ) and green algae (2.00  $\mu\text{g/l}$ ) signals was observed at around 25 m depth. After rapidly decreasing between 40-50 m, the values stagnated after 60 m on minimum values. Looking at the RAMSES measurements however, high chlorophyll values can be observed. This may be due to the fact that the phytoplankton is only abundant in the surface layer, and hence, is captured by the surface reflection measurements

The maximum value of total chlorophyll-a was detected at a depth of 46.3 m station 6 with 4.25  $\mu\text{g/l}$ . Again, green algae and diatom signals follow that pattern with densities of 3.59  $\mu\text{g/l}$  and 0.66  $\mu\text{g/l}$  at that depth, respectively. At station 7 no clear peak in chlorophyll-a could be determined. Total signal densities varied from 0.00-2.55  $\mu\text{g/l}$  within the first 30 m of surface water and slightly increased to up to 3.27  $\mu\text{g/l}$  between 30-70 m. Diatom values were considerably homogenous, reaching its maximum at 52 m with 0.75  $\mu\text{g/l}$ . Density for green algae chlorophyll-a was highest at 48 m (2.67  $\mu\text{g/l}$ ). Even though equatorial upwelling was expected to occur on this station, chlorophyll data from BBE as well as RAMSES do not show exceptionally high primary productivity.

A high chlorophyll-a peak was found in station 8 with 9.09  $\mu\text{g/l}$  at 35 m depth. Green algae signals nearly overlapped with those signals with a peak at same depth and a concentration of 8.18  $\mu\text{g/l}$ . The diatom maximum was considerably lower with 1.11  $\mu\text{g/l}$  at 43 m depth. High productivity at station 8 (9  $\mu\text{g/L}$  total fluorescence) is evident when compared to the previous stations. Upwelling could be suggested as a reason for this when looking at productivity alone as these results are anomalous for such open ocean locations. Yet, when combining these results with physical parameters measured through the water column such as temperature and salinity the evidence for upwelling is not supported. One possible theory for such high productivity at station 8 could be remnants of the Congo freshwater river plume. The Congo plume has an annual mean daily discharge of 39,866  $\text{m}^3 \text{s}^{-1}$ . It is second only to the Amazon river plume in both volume and quantity of terrestrial organic carbon exported. It can extend between 400 – 1,000 km west, west/southwest (direction of station 8) or northwest driven by wind stress and large scale ocean circulation (Hopkins et al 2013). This is a hypothesis that merits further investigation.

The water column within the first 80 m at station 9 shows a large variety of chlorophyll concentrations, especially in green algae and total values. The highest values for green algae is 4.44  $\mu\text{g/l}$  at approximately 35 m depth and 5.01  $\mu\text{g/l}$  at 19 m. Signals of diatoms ranged mostly between 0-1  $\mu\text{g/l}$ .

Compared to all other stations, the highest values were discovered at station 10. A steep peak of all 3 signal types lied close to 50 m depth. Maximum chlorophyll concentrations were 2.88  $\mu\text{g/l}$  (diatoms), 12.11  $\mu\text{g/l}$  (green algae) and 14.68  $\mu\text{g/l}$  (total). This high concentration of diatoms, together with high other phytoplankton concentrations, hint to upwelling in this area (Wasmund et al., 2014). Also a deep mixed layer depth (Fig. 3.34), fluorescence measurement of the CTD (Fig. 3.39 d), cold and well mixed surface water (Fig. 3.39 a) strengthen this assumption. Data from the same transect of 2007 shows high Ekman pumping in this area too (Fig. 3.45). Contrastingly, the remote sensing data from RAMSES measurements (Fig. 3.48) does not show high chlorophyll values. This may be due to the fact that RAMSES only measures surface reflection, whereas the chlorophyll maximum of this station was at 50 m depth. This station was conducted on 8 December 2016, which applies to the early austral summer peak in the Benguela upwelling (Louw et al. 2016).

At station 11 the concentration was lower again, with chlorophyll maxima between 60 and 80 m depth for both, green algae and diatoms. Expected influence of Benguela upwelling, or even Agulhas currents, was not detected here.

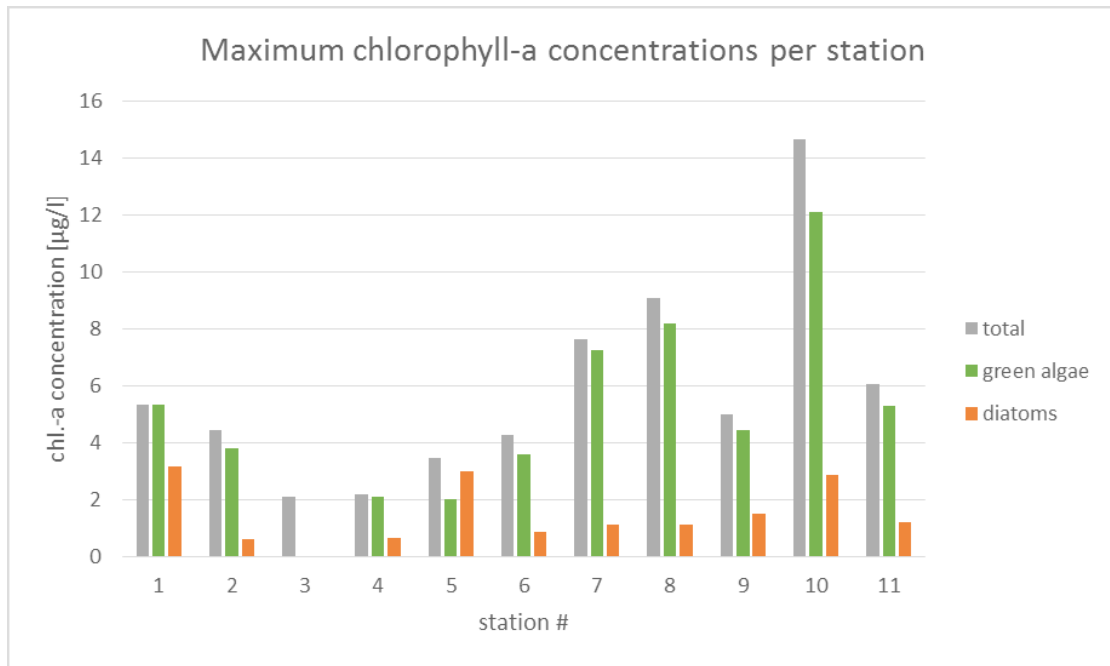


Fig. 3.47 Maximum chlorophyll-a concentrations based on BBE measurements

Comparing maximum values of chlorophyll-a concentrations at different stations through BBE measurements (Fig. 3.47), the highest total and green algae values were observed at station 10, followed by station 8 and 7. However, the values of station 7 were skewed by 2 outliers with approx. 7 µg/l, whereas other signals did not exceed 3.5 µg/l (cf. Fig. 3.49). Signals for diatom chlorophyll were the highest at stations 1, 5 and 10. Diatoms are an indicator of freshly upwelled water (Wasmund et al. 2014). However, values of diatom chlorophyll were considerably low hence do not provide strong evidence on upwelling on this transect.

Out of the 11 stations, one (#10) appears to be influenced by an upwelling system. For the other stations, chlorophyll data was insufficient to identify further upwelling areas on this transect.

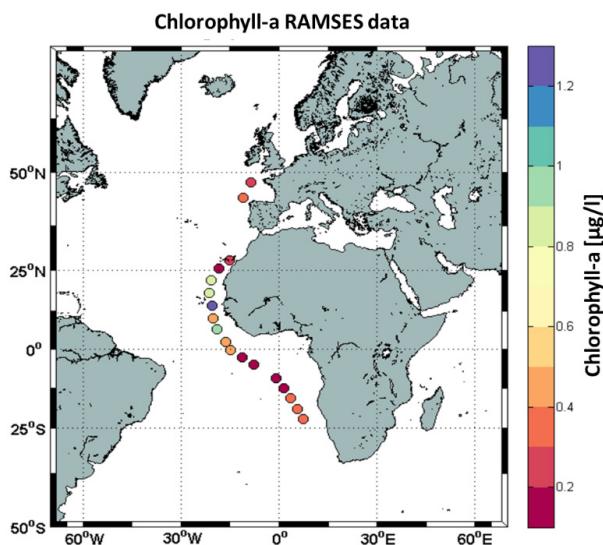


Fig. 3.48: Chlorophyll-a values based on ocean surface reflection, calculated with two algorithms (OC3 and OC4-S). Source of data: [http://oceancolor.gsfc.nasa.gov/cms/atbd/chlor\\_a](http://oceancolor.gsfc.nasa.gov/cms/atbd/chlor_a)

The photoautotrophic picoplankton *Synechococcus* is ubiquitously distributed through oceanic regions, from the poles to temperate and tropical regions although it is generally more abundant in nutrient rich surface waters. Originally thought to be a low light adapted species variations in chlorophyll pigment abundance allows the occupation of alternative niches at different depths within the water column and the occurrence of both low light and high light adapted ecotypes in the same regions.

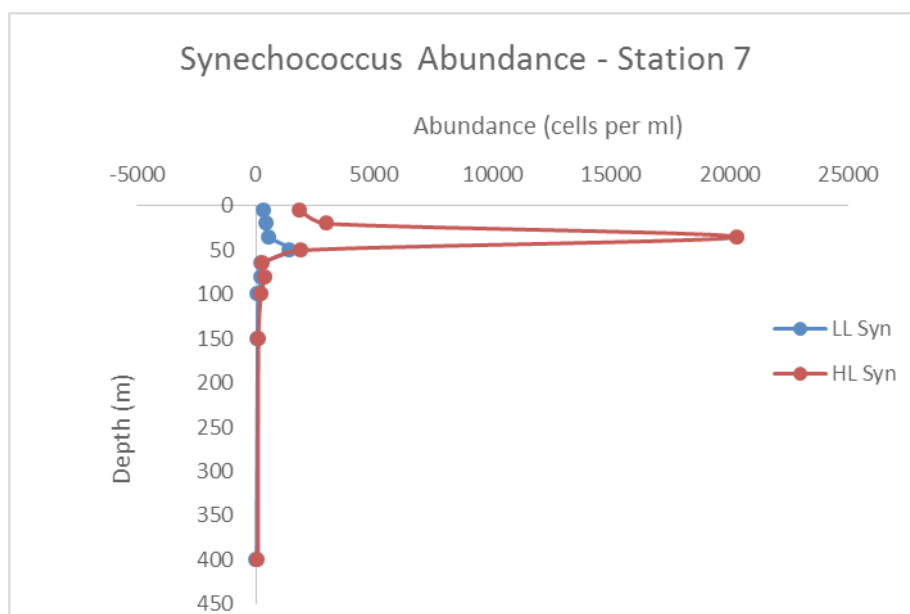


Fig. 3.49: *Synechococcus* abundance station 7. HL Syn (blue) = High light adapted *Synechococcus* ecotypes. LL Syn (orange) = low light adapted *Synechococcus* ecotype. High light adapted *Synechococcus* ecotypes are at maximum abundance (20,500 cells per ml) at 35 m. Abundance rapidly decreases with depth to values close to zero at 60 m. Low light adapted *Synechococcus* ecotypes are at a maximum abundance (1,250 cells per ml) at 50 m.

The occurrence of both high and low light adapted ecotypes, with differential chlorophyll pigmentation in surface waters (50-35 m) indicates that these waters may have originated at depth and can be taken as an indication of upwelling.

The cyanobacterium *Prochlorococcus* inhabits nutrient poor equatorial regions and has adapted differential chlorophyll a to chlorophyll b ratios in order to inhabit various depths within the water column. *P. marinus* strains which occupy greater depths have increased chlorophyll pigmentation in order to efficiently utilise light, while surface adapted strains have less chlorophyll pigmentation (Peterson et al., 2012). Preliminary results indicated an occurrence of both high and low light adapted *Prochlorococcus* in surface waters at station 7. Further analysis of this data is required post cruise.

Advances in the use of flow cytometry have led to novel ways for identifying upwelling regions. The cyanobacteria *Prochlorococcus* was first discovered by flow cytometry in the 1980's and since then its role and importance in the global carbon cycle has been well studied (Peterson et al., 2012). Many pico and nano plankton, as well as bacteria have proved to be hard to identify using conventional microscopy methods. The use of flow cytometry has led to the advancement of marine microbiology allowing the identification and characterisation of very small microbes. The identification of various *Prochlorococcus* and *Synechococcus* ecotypes in surface waters supported by additional empirical evidence such as physical and chemical characteristics of the water column can aid in the identification of upwelling regions.

## Data management

All data processing will be carried out at the AWI. It is foreseen to upload the quality checked data to the Pangaea database. However, this data processing and upload procedure might take a few months.

## References

- Abraham J P, Baringer M, Bindoff N L, Boyer T, Cheng L J, Church J A, Conroy J L, Domingues C M, Fasullo J T, Gilson J, Goni G, Good S A, Gorman J M, Gouretski V, Ishii M, Johnson G C, Kizu S, Lyman J M, Macdonald A M, Minkowycz W J, Moffitt S E, Palmer M D, Piola A R, Reseghetti F, Schuckmann K, Trenberth K E, Velicogna I, Willis JK (2013) A review of global ocean temperature observations: Implications for ocean heat content estimates and climate change. *Reviews of Geophysics*, 52 (3), 450-483.
- Aiken J, Pradhan Y, Barlow R, Lavender S, Poulton A, Holligan P, Hardman-Mountford N (2009) Phytoplankton pigments and functional types in the Atlantic Ocean: a decadal assessment, 1995-2005. *Deep Sea Research Part II Top Stud Oceanogr*, 56, 899-917.
- Ajit S, Claire M, William J, Natalie M (2013) Equatorial upwelling enhances nitrogen fixation in the Atlantic Ocean. *Geophysical Research Letters*, 40, 1766–1771.
- Arhan M, Mercier H, Bourles B, Gouriou Y (1998) Hydrographic sections across the Atlantic at 7°30'N and 4°30' S. *Deep-Sea Research I*, 45: 829–872.
- Ashok K, Guan Z, Yamagata T (2001) Impact of the Indian Ocean Dipole on the Relationship between the Indian Monsoon Rainfall and ENSO. *Geophysical Research Letters*, 28(23), 4499-4502.
- Athie G, Marin F (2008) Cross-equatorial structure and temporal modulation of intraseasonal variability at the surface of the Tropical Atlantic Ocean. *J Geophys. Res.*, 113, C08020, doi:10.1029/2007JC004332.
- Bader J, Latif M (2003) The impact of decadal-scale Indian Ocean sea surface temperature anomalies on Sahelian rainfall and the North Atlantic Oscillation. *Geophysical Research Letters*, 30, 2169.
- Bailey R, Gronell A, Phillips H, Tanner E, Meyers G (2011) XBT Cookbook: Quality Control Cookbook for XBT Data. Tasmania: Australian Oceanographic Data Centre.
- Bakun A, Weeks SJ (2004) Greenhouse gas buildup, sardines, submarine eruptions, and the possibility of abrupt degradation of intense marine upwelling ecosystems. *Ecol Lett.*;7, 1015–23.
- Bakun A (1990) Global Climate Change and Intensification of Coastal Ocean Upwelling. *Science, New Series*, 247(4939), 198-201.
- Beyerlin U, Marauhn T (2011) *International Environmental Law*. Oxford: Hart Publishing, 466 pp.
- Biller S J, Berube P M, Lindell D, Chisholm S W (2015) Prochlorococcus: the structure and function of collective diversity. *Nat Rev Microbiol*, 13(1), 13-27.
- Bollmann M, Bosch T, Colijn F, Ebinghaus R, Froese R, Güssow K, Khalilian S, Krastel S, Körtzinger A, Langenbuch M, Latif M, Matthiessen B, Melzner F, Oschlies A, Petersen S, Proelß A, Quaas M, Reichenbach J, Requate T, Reusch T, Rosenstiel P, Schmidt J O, Schrottko K, Sichelschmidt H, Siebert U, Soltwedel R, Sommer, K Stattegger, H Sterr, R Sturm, T Treude, A Vafeidis, C v. Bernem, J Beusekom U, Voss R, Visbeck M, Wahl M, Wallmann K, Weinberger F (2010) World ocean review. Maribus in cooperation with IOI
- Bopp L, Quere CL, Heimann M, Manning AC (2002) Climate-Induced Oceanic Oxygen Fluxes : Implications for the Contemporary Carbon Budget. *Global Biogeochemical Cycles*, 16(2), 1022, 10.1029/2001GB001445.
- Bourle`s B, D'Orgeville M, Eldin G, Gouriou Y, Chuchla R, DuPenhoat Y, Arnault S (2002) On the evolution of the thermocline and subthermocline eastward currents in the Equatorial Atlantic. *Geophys. Res. Lett.*, 29(16), 1785, doi:10.1029/2002GL015098.

- Bowie AR, Whitworth DJ, Achterberg EP, Mantoura RFC, Worsfold PJ (2002) Biogeochemistry of Fe and other trace elements (Al, Co, Ni) in the upper Atlantic Ocean. *Deep-Sea Res. Part I-Oceanogr. Res. Pap.*, 49, 605–636.
- Boyd A J (1987) The oceanography of the Namibian shelf. Ph.D thesis, University of Cape Town, 190 pp.
- Boyd PW, Lennartz ST, Glover DM, Doney SC (2014) Biological ramifications of climate-change mediated oceanic multi-stressors. *Nature Climate Change*, 5, 71–79, doi:10.1038/nclimate2441.
- Bozec A, Lozier S M, Chassignet E P & Halliwell GR (2011) On the variability of the Mediterranean Outflow Water in the North Atlantic from 1948 to 2006. *Journal of Geophysical Research*, 116(C09033), 1-18.
- Brandt P, Caniaux G, Bourles B, Lazar A, Dengler M, Fink A, Hormann V, Giordani H, Marin F (2011) Equatorial upper-ocean dynamics and their interaction with the West African monsoon. *Atmospheric Science Letters*, 12, 24–30.
- Brandt P, Bange HW, Banyte D, Dengler M, Didwischus S-H, Fisher T, Greatback RJ, Hahn J, Kanzow T, Karstensen J, Kortzinger A, Krahn G, Schmidt S, Stramma L, Tanhua T, Visbeck M (2015) On the role of circulation and mixing in the ventilation of oxygen minimum zones with a focus on the eastern tropical North Atlantic. *Biogeosciences*, 12, 489-515.
- Brandt P, Hormann V, Körtzinger A, Visbeck M, Krahn G, Stramma L, Rick, C (2010) Changes in the Ventilation of the Oxygen Minimum Zone of the Tropical North Atlantic. *Journal of Physical Oceanography*, 40(8), 1784-1801, doi: 10.1175/2010jpo4301.1.
- Brinton E (1979) Parameters relating to the distribution of planktonic organisms, especially euphausiids in the eastern tropical Pacific. *Progress in Oceanography*, 8(3), 125-168.
- Broecker W S, Peng T-H (1982) *Tracers in the Sea*, Lamont- Doherty Earth Obs., Palisades, NY.
- Bullister J, Rhein M, Mauritzen C (2013) Deep Water Formation. In: *Ocean Circulation and Climate - Observing and Modelling the Global Ocean*, second edition, Hrsg.: G Siedler, J Church, J Gould and S Griffies, Academic Press.
- Chang P, Fang Y, Saravanan R, Ji L, Seidel H (2006) The cause of the fragile relationship between the Pacific El Nino and the Atlantic Nino. *National Biotechnology. Nature*, 443,324-328.
- Chase TN, Pielke Sr, RA, Avissar R, Goswami BN, Vinayachandran PN, Yamagata T (1999) A dipole mode in the tropical Indian Ocean. *Nature*, 401, 360.
- Chavez FP, Messié MA (2009) Comparison of eastern boundary upwelling ecosystems. *Progress in oceanography*, 83:80-95.
- Chen X, Tung K-K (2014) Varying planetary heat sink led to global-warming slowdown and acceleration. *Science* 345, 897–903.
- Childress JJ (1995) Are there physiological and biochemical adaptations of metabolism in deep-sea animals? *Trends in ecological evolution*, 10, 30-36.
- Childress JJ, and Seibel BA (1998) Life at stable low oxygen levels: Adaptations of animals to oceanic oxygen minimum layers. *The Journal of Experimental Biology* 201: 1223–32.
- Coëtlogon G D, Janicot S, Lazar A (2010) Intraseasonal variability of the ocean-atmosphere coupling in the Gulf of Guinea during boreal spring and summer. *Quarterly Journal of the Royal Meteorological Society*, 136, 426–441.
- Craig RK (2012) Marine Biodiversity, Climate Change, and Governance of the Oceans. *Diversity* 4, 224-238, doi:10.3390/d4020224.
- Crowder L, Norse E (2008) Essential ecological insights for marine ecosystem-based management and marine spatial planning. *Marine Policy*, 32(5), 772–778.

- D J Scanlan, West N J (2002) Molecular ecology of the marine cyanobacterial genera *Prochlorococcus* and *Synechococcus*. *Microbiology Ecology* 40, 1-12.
- Deuser W, Ross EH, Mlodzinska Z J (1978) Evidence for and rate of de-nitrification in the Arabian Sea. *Deep-Sea Research*, 25, 431-445.
- Diaz RJ Rosenberg R (2008) Spreading dead zones and consequences for marine ecosystems, *Science*, 321, 926-929.
- Ding H, Keenlyside NS, Latif M (2011) Impact of the Equatorial Atlantic on the El Nino Southern Oscillation. *Climate Dynamics*, 38(9), 1965–1972.
- Domingues CM, Church JA, White NJ, Gleckler PJ, Wijffels SE, Barker PM, Dunn J (2008) Improved estimates of upper-ocean warming and multidecadal sea-level rise. *Nature*, 453, 1090–1093.
- Ekau W, Auel H, Portner HO, Gilbert D (2010) Impacts of Hypoxia on the structure and processes in pelagic communities (zooplankton, macro-invertebrates and fish). *Bio geosciences*, 7, 1669-99.
- Emery WJ (2003) Water Types and Water Masses, *Ocean Circulation*, 1556-1567.
- Fennel W (1999) Theory of the Benguela Upwelling System. *Journal of Physical Oceanography*, 29, 177-190.
- Fischer T, Banyte D, Brandt P, Dengler M, Krahnemann G, Tanhua T and Visbeck M (2013) Diapycnal oxygen supply to the tropical North Atlantic oxygen minimum zone. *Biogeosciences*, 10, 5079-5093.
- Flombaum P, Gallengos JL, Gordillo RA, Rincon J, Zabala LI, Jiao N, Karl DM WKW, Lomas MW, Veneziano D, Vera CS, Vrugt J A, Martiny A C (2013) Present and future global distributions of the marine cyanobacteria *Prochlorococcus* and *Synechococcus*. *Proc Natl Acad Sci USA*, 9824-9829.
- Folland C K, Palmer T N, Parker D E (1986) Sahel rainfall and worldwide sea temperature. *Nature*, 320, 602–607.
- Foster, T D Carmack, E C (1975) Frontal zone mixing and Antarctic Bottom water formation on the southern Weddell Sea, *Deep Sea Research and Oceanographic Abstracts*, 23(4), 301-317.
- Garsoli, S L, Gordon A L (1996) Origins and variability of the Benguela Current. *J Geophys. Res.*, 101, 987–906.
- Gibb SW, Barlow RG, Cummings DG, Rees NW, Trees CC and Holligan P (2000) Surface phytoplankton pigment distributions in the Atlantic Ocean: an assessment of basin scale variability between 50oN and 50oS *Prog Oceanogr.* 45. 339-368
- Gilly WF, Beman JM, Litvin YS, Robison BH (2013) Oceanographic and Biological Effects of Shoaling of the Oxygen Minimum Zone. *Annual Review of Marine Science*, 5:393-420.
- Gruber N (2011) Warming up, turning sour, and losing breath: Ocean Biogeochemistry under global change. *Philos. tran. R Soc. Lond. A*, 369, 1980-96.
- Gründlich ML (1983) On the course of the Agulhas Current. *South African Geographical Journal*, 65, 49-57.
- Hansell DA, Peltzer E T (1998) Spatial and temporal variation of total organic carbon in the Arabian Sea. *Deep-Sea Research II*, 45, 2171-2193.
- Hastenrath S (1984) Interannual variability and annual cycle: Mechanisms of circulation and climate in the Tropical Atlantic sector. *Monthly Weather Review*, 112, 1097–1107.
- Helly J, Levin L (2004) Global distribution of naturally occurring marine hypoxia on continental margins. *Deep-Sea Research I*, 51, 1159-1168.
- Herr D, Galland G (2009) *The Ocean and Climate Change. Tools and Guidelines for Action*. IUNG (International Union for Conservation of Nature Gland) 2009 Report.

- Hoerling M, Hurrell J, Eischeid J, Phillips A (2006) Detection and Attribution of Twentieth-Century Northern and Southern African Rainfall Change. *Journal of Climate*, 19(16), 3989-4008.
- Hollowed A B, Barange M, Beamish R, Brander K, Cochrane K, Drinkwater K, Foreman M, Hare J, Holt J, Ito S-I, Kim S, King J, Loeng H, MacKenzie B, Mueter F, Okey T, Peck M A, Radchenko V, Rice J, Schirripa M, Yatsu A, Yamanaka Y (2013) Projected impacts of climate change on marine fish and fisheries. – *ICES Journal of Marine Science*, 2013, doi:10.1093/icesjms/fst081.
- Hurrell JW (1995) Decadal trends in the North Atlantic Oscillation: regional temperatures and precipitation. *Science*, 269, 676-679.
- Interpol Environmental Security Sub-Directorate (ENS) (2014) Study on fisheries crime in the West African coastal region, p 66.
- Hopkins J, Lucas M, Dufau C, Sutton M, Stum J, Lauret O, Channelliere C (2013) Detection and variability of the Congo River plume from satellite derived sea surface temperature, salinity, ocean colour and sea level. *Remote Sensing of Environment*, 139, 365–385.
- JJ Cullen MacIntyre JG (1998) Behavior, physiology and the niche of depth-regulating phytoplankton. *Physiological Ecology of Harmful Algal Blooms*. G41, 1-21.
- James F P, Molly O, Baringer N, Roff G L, Gregory C J, Isabel A, Gregorio P, Alian C, Maureen A K, Thomas B S (1993) Mediterranean Outflow Mixing Dynamics. *Science*, 259(5099), 1277-1282. doi: 10.1126/science.259.5099.1277.
- Janicot S, Trzaska S, Pocard I (2001) Summer Sahel-ENSO teleconnection and decadal time scale SST variations. *Climate Dynamics*, 18, 303–320.
- Johnson GC, J M Lyman, T Boyer, C M Domingues, M Ishii, R Killick, D Monselesan, Wijffels S E (2016) Ocean Heat Content Bulletin of the American Meteorological Society (BAMS), 97(8), S66-S70.
- Johnson G C, Gruber N (2007) Decadal water mass variations along 20°W in the Northeastern Atlantic Ocean. *Prog. Oceanogr.*, 73, 277–295.
- KE Trenberth, WG Large Olson JG (1990) The Mean Annual Cycle in Global Ocean. *Journal of Physical Oceanography*, 20, 1742 - 1760.
- Karstensen J et al. (2015) Open Ocean Dead Zones in the Tropical North Atlantic Ocean. *Biogeosciences*, 12, 2597–2605.
- Karstensen J, Stramma L, Visbeck M (2008) Oxygen minimum zones in the eastern tropical Atlantic and Pacific oceans. *Progress in Oceanography*, 77, 331–350.
- Kawase M, Sarmiento J L (1986) Circulation and Nutrients in middepth Atlantic Waters. *Journal of Geophysical Research*, 91(C8), 9749-9770.
- Keeling RF, Körtzinger A, Gruber N (2010) Ocean deoxygenation in a warming world. *Annual Review of Marine Science*, 2, 199-229.
- Keenlyside NS, Ding H, Latif M (2013) Potential of equatorial Atlantic variability to enhance El Niño prediction. *Geophysical Research Letters* 40(10), 2278–83.
- Kennett JP, Stott LD (1991) Abrupt deep sea warming, Palaeoceanography changes and benthic extinctions at the end of the Palaeocene. *Nature*, 377, 510-514.
- Kirchner K, M Rhein, S Hüttl-Kabus, and C W Boning (2009) On the spreading of South Atlantic Water into the northern hemisphere. *J Geophys.*, 114, C05019, doi:10.1029/2008JC005165.
- Kirkham AR, Jardillier LE, Tiganescu A, Pearman J, Zubkov MV, Scanlan DJ (2011) Basin-scale distribution patterns of photosynthetic picoeukaryotes along an Atlantic Meridional Transect. *Environmental Microbiology*, 13, 975-990.
- Knowles R (1996) De-nitrification: microbiology and ecology. *Life Support and Biosphere Science*, 3: 31–34.

- Krishnamurthy V, Goswami B (2000) Indian monsoon-ENSO relationship on interdecadal timescale. *Journal of Climate*, 13(3), 579-595.
- Lalli CM, Parsons TR (1997) *Biological oceanography, an introduction*. 2<sup>nd</sup> Edition. The open book.
- Lamb PJ (1983) West African water variations between recent contrasting Subsaharan droughts. *Tellus*, 35, 198–212.
- Large W F, Pond S (1981) Open Ocean Momentum Flux Measurements in Moderate to Strong Winds. *Journal of Physical Oceanography*, 11(3), 324-336.
- Le Pichon X, Huchon P (1984) Geoid, Pangea and convection. *Earth and Planetary Science Letters*, 67, 123-125.
- Lee S, Park W, Baringer MO, Gordon AL, Huber, Band Liu Y (2015) Pacific origin of the abrupt increase in Indian Ocean heat content during the warming hiatus. *Nature Geo Science*, 2438.
- Lemke P Olbers D (2014) *On the Physics of the Climate System: Ice Age or Greenhouse Climate?.* Lectures on Climate Physics. Bremerhaven: Alfred-Wegener-Institut, University of Bremen.
- Lentz SJ (1992) The surface boundary layer in coastal upwelling regions. *Journal of Physical Oceanography*, 22(12), 1517-1539.
- Levin J, Schneider T (2011) Response of the Hadley circulation to climate change in an aquaplanet GCM coupled to a simple representation of ocean heat transport. *J. Atmos. Sci.* 68, 769–783.
- Levitus S, Antonov JI, Boyer TP, Baranova OK, Garcia HE, Locarnini RA, Mishonov AV, Reagan JR, Seidov D, Yarosh ES, Zweng MM (2012) World ocean heat content and thermosteric sea level change (0–2000 m), 1955–2010. *Geophysical Research Letters* 39: L10603, doi:10.1029/2012GL051106.
- Losada T, Rodriguez-Fonseca B, Mohino E, Bader J, Janicot S, Mechoso CR (2012) Impact of Tropical SST Anomalies on West African Rainfall. *Geophysical Research Letters*, 39, L12705. doi:10.1029/2012GL052423.
- Louw DC, van der Plas A K, Mohrholz V, Wasmund N, Junker T, Eggert A (2016) Seasonal and interannual phytoplankton dynamics and forcing mechanisms in the Northern Benguela upwelling system. *Journal of Marine Systems*, 157, 124 – 134.
- Lu J, Vecchi GA, Reichler T (2007) Expansion of the Hadley cell under global warming. *Geophys Res Lett.* , 34, L06805.
- Lynne D Talley (2002) *The Earth system: physical and chemical dimensions of global environmental change.* Ocean Circulation, John Wiley & Sons, Ltd, Chichester Vol. 1, pp 557–579.
- Maher N, Sen Gupta A, England M H (2014) Drivers of decadal hiatus periods in the 20th and 21st centuries. *Geophys. Res. Lett.*, 41, 5978–5986.
- Mani N J, E Suhas, Goswami BN (2009) Can global warming make Indian monsoon weather less predictable? *Geophysical Research Letters*, 36(8), 2-6.
- Manning AC, Keeling RF (2006) Global oceanic and land biotic carbon sinks from the Scripps atmospheric oxygen flask sampling network. *Tellus Ser. B*, 58, 95-116.
- Marsh R, Megann AP (2002) Tracing water masses with particle trajectories in an isopycnic-coordinate model of the global ocean, *Ocean Modeling*, 4, 27-53.
- Marshall J, Donohoe A, Ferreira D, McGee D (2014) The ocean's role in setting the mean position of the Inter-Tropical Convergence Zone. *Climate Dynamics*. 42, 1967-1979.
- Matear RJ, Hirst AC (2003) Long-Term Changes in Dissolved Oxygen Concentrations in the Ocean Caused by Protracted Global Warming. *Global Biogeochemical Cycles*, 17(4), 1125, doi: 10.1029/2002GB001997.

- McGill DA (1973) Light and nutrients in the Indian Ocean. In: The Biology of the Indian Ocean, Zeitzschel B, Gerlach SA (eds.), Springer-Verlag, 53-102.
- Mercier H, Arhan M, Lutjeharms, JRE (2003) Upper-layer circulation in the eastern Equatorial and South Atlantic Ocean in January–March 1995. *Deep-Sea Research*, 50, 863–887.
- Mittelstaedt E (1983) The Upwelling Area Off Northwest Africa – A Description of the Phenomena Related to Coastal Upwelling. *Prog. Oceanog.*, 12, 307-331.
- Mohino E, Rodriguez-Fonseca B, Mechoso CR, Gervois SP Ruti, Chauvin F (2011) Impacts of the Tropical Pacific / Indian Oceans on the Seasonal Cycle of the West African Monsoon', *Journal of Climate dynamics*, 42, 3878–3892.
- Mohrholtz V, Schmidt M, Lutjeharms JRE (2001) The hydrography and dynamics of the Angola-Benguela Frontal Zone and environment in April 1999. *South African Journal of Science*, 97, 199–208.
- Mohtadi M, Prange M, Steinke S (2016) Palaeoclimatic insights into forcing and response of monsoon rainfall. *Nature*, 533, 191.
- Montzka SA, Fraser PJ, Butler JH, Connell PS, Daniel JS, and Derwent RG (2003) Controlled substances and other source gases. In *Scientific assessment of ozone depletion: 2002, Global ozone research and monitoring project*, Geneva: World Meteorological Organization. Report 47, 1.1–1.83.
- Munk W H (1950) On the wind-driven ocean circulation. *Journal of Meteorology*, 2, 79 – 93.
- Naqvi S, Manghnani V, Prosperie L and Gundersen J S (1999) The oxygen minimum zone in the Arabian Sea during 1995. *Deep-Sea Research Part II-Topical Studies in Oceanography*, 46(8-9), 1903-1931.
- Naqvi S, Bange H W, Gibb SW, Goyet C , Hatton A D and Upstill-Goddard RC (2005) Biogeochemical ocean-atmosphere transfers in the Arabian Sea. *Progress in Oceanography*, 65, 116–144.
- Naqvi SW, Qasim SZ (1983) Inorganic nitrogen and nitrate reduction in the Arabian Sea. *Indian Journal of Marine Sciences*, 12, 21-26.
- Neff U, Burns S, Mangini A, Mudelsee M, Fleitmann D, Matter A (2001) Strong coherence between solar variability and the monsoon in Oman between 9 and 6 kyr ago, *Nature*, 411, 290-293.
- Nicholson SE (1981) The nature of rainfall fluctuations in subtropical West Africa. *Monthly Weather Review*, 108, 473–487.
- Nicholson SE, Webster PJ (2007) A physical basis for the interannual variability of rainfall in the Sahel. *Quarterly Journal of the Royal Meteorological Society*, 133, 2065–2084.
- Nolan G, Gillooly M, Whelan K (2010) Irish Ocean Climate and Ecosystem Status Report (2009). Marine Institute.
- Ocean Instruments (2016) Conductivity, Temperature, Depth (CTD) Sensors [online]. Available at: <http://www.whoi.edu/instruments/viewInstrument.do?id=1003>.
- Okajima H, Xie SP, Numaguti A (2003) Interhemispheric Coherence of Tropical Climate Variability: Effect of the Climatological ITCZ. *Journal of the Meteorological Society of Japan*, 81. 1371-1386.
- Olson R F (1981) Differential photo inhibition of marine nitrifying bacteria: a possible mechanism for the formation of the primary nitrite maximum. *Journal of Marine Research*, 39, 227-238.
- Ono T (2010) Oxygen decline in the continental slope waters off-Japan and its potential influence on ground-fishes. In *Pisces 2010. North Pacific ecosystems today and challenges in understanding and forecasting change*. p.1. Sid, Can, North Pacific Marine Scientific Organisation (Abstr).
- Oschlies A, Schulz KG, Riebesell R, Schmittner A (2008) Simulated 21st Century's Increase in Oceanic Suboxia by CO<sub>2</sub>-Enhanced Biotic Carbon Export. *Global Biogeochemical Cycles*, 22, GB4008, doi:10.1029/2007GB003147.

- Paulmier A, Ruiz-Pino D (2008) Oxygen minimum Zone (OMZ's) in the modern ocean. *Progress in Oceanography*, 80, issues 3-4, 113–128.
- Petersen TW, Harrison CB, Horner DD, and den Engh GV (2012) Flow cytometric characterization of marine microbes. *Methods*, 57, 350-358.
- Petersen WT, Harrison CB, Horner DN, van den Engh G (2012) Flow cytometric characterization of marine microbes. *Methods*, 57, 350–358.
- Peterson RG, Stramma L (1991) Upper-level circulation in the South Atlantic Ocean. *Prog. Oceanog.*, 26, 1-73.
- Peyrillé P, Lafore J-P, Redelsperger J-L (2007) An idealized two-dimensional framework to study the West African monsoon. Part I: validation and key controlling factors. *Journal of the Atmospheric Sciences*, 64, 2765–2782.
- Potter R A, Lozier M S (2004) On the warming and salinification of the Mediterranean outflow waters in the North Atlantic. *Geophysical Research Letters*, 31(L01202), pp. 1-4.
- Prather M, Ehhalt D, Dentener F, Derwent R, Dlugokencky E, Holland E (2001) Atmospheric chemistry and greenhouse gases. In J T Houghton, Y Ding, D J Griggs, M Noguer, P J Van der Linden, X Dai, K Maskell, & C A Johnson (Eds.), *Climate Change 2001: The scientific basis. Contribution of working group I to the third assessment report of the intergovernmental panel on climate change*. Cambridge: Cambridge University Press, 239–287.
- Purcell JE, Uye S, Lo WT (2007) Anthropogenic causes of jelly fish blooms and their direct consequences for humans: A review. *Marine ecology progress series*, 350, 153-174.
- Rahmstorf S (2006) Thermohaline Ocean Circulation. In: *Encyclopedia of Quaternary Sciences*, Edited by S A Elias. Elsevier, Amsterdam 2006.
- Rahmstorf S (1998) Influence of Mediterranean Outflow on Climate. *EOS*, 79, 24.
- Reid J L (1994) On the total geostrophic circulation of the North Atlantic Ocean: Flow patterns, tracers, and transports. *Prog. Oceanog.*, 33, 1-92. *Res.*, 114, C05019, doi:10.1029/2008JC005165.
- Richardson P L (2007) Agulhas leakage into the Atlantic estimated with subsurface floats and surface drifters. *Deep-Sea Research I* 54, 1361-1389.
- Rodriguez-Fonseca et al., (2011) Interannual and decadal SST-forced responses of the West African Monsoon and decadal SST-forced responses of the West African Monsoon. *Atmospheric science letter*, 12, 67-74.
- Rowell BDP, et al., (1994) Variability of summer rainfall over tropical north Africa (1906-92). *Observations and modeling*, 34, 669–704.
- Saji NH, Yamagata T (2003) Possible impacts of Indian Ocean Dipole mode events on global climate. *Climate Research*, 25, 151-169.
- Sarafanov A, Sokov A, Demidov A (2000) Water mass characteristics in the equatorial North Atlantic: A section nominally along 6.5° N *Journal of Geophysical Research*, (112), C12023, doi:10.1029/2007JC004222.
- Sarmiento et al., (2004) Response of ocean ecosystems to climate warming. *Global Biogeochem. Cycles*, 18, GB3003.
- Scanlan D J, West N J (2002) Molecular ecology of the marine cyanobacterial genera *Prochlorococcus* and *Synechococcus*. *FEMS Microbiol. Ecol.*, 40(1), 1-12.
- Schemainda R, Nehring D, Schulz S (1975) Untersuchungen zum Produktionspotentil der nordwestafrikanischen Wasserauftriebsregion 1970-1973. *Geodätische und Geophysikalische Veröffentlichungen*, R IV, H 16, 85 pp.

- Schmidtko S, Johnson G C (2012) Multidecadal Warming and Shoaling of Antarctic Intermediate Water. *American Meteorological Society*, 25, 207-225.
- Schneider T, Bischoff T, Haug GH (2014) Migrations and dynamics of the intertropical convergence zone. *Nature*, 513, 45-53.
- Sen Gupta R, Rajagopal M, Qasim S Z (1976) Relationships between dissolved oxygen and nutrients in the north-western Indian Ocean. *Indian Journal of Marine Sciences*, 5, 201-211.
- Shaltout M, Omstedt A (2015) Modelling the water and heat balances of the Mediterranean Sea using a two-basin model and available meteorological, hydrological, and ocean data. *Oceanologia*, 57, 116-131.
- Shannon L V, Nelson G (1996) The Benguela: Large-scale features and process and system variability. *The South Atlantic: Present and Past Circulation*, Wefer, Berger, Siedler and Webb. Springer Verlag, 162-210.
- Shannon L V (1985) The Benguela Ecosystem, Part I: Evolution of the Benguela, physical features and processes. *Oceanogr. Mar. Biol.*, 23, 105-182.
- Shannon LV, Boyd AJ, Brundrit GB, Taunton-Clark J (1986) On the existence of an El Nino-type phenomenon in the Benguela System. *Journal of Marine Research*. 44, 495-520.
- Small L F (1997) Basic concepts in oceanography. *Strategies and Methodologies for Applied Marine Radioactivity Studies*, 7.
- Smith DM, Murphy JM (2007) An objective ocean temperature and salinity analysis using covariances from a global climate model. *J Geophys. Res. Oceans*, 112(C2), 2156-2202.
- Somasundar K, Rajendran A M, Kumar D R, Sen Gupta SR (1990) Carbon and nitrogen budgets of the Arabian Sea. *Marine Chemistry*, 30, 363-377.
- Stenseth NC, Ottersen G, Hurrell JW, Mysterud A, Lima M, Chan K-S, Yoccoz NJ, Adlandsvik, B (2003) Studying climate effects on ecology through the use of climate indices: the North Atlantic Oscillation, El Nino Southern Oscillation and beyond. *The Royal Society's physical sciences research journal*, 270, 2087-2096.
- Stewart H (2008) *Introduction To Physical Oceanography*, Texas: Department of Oceanography Texas A & M University.
- Stocker TF, Qin D, Plattner GK et al. (2013) Technical summary. In: *Climate Change 2013: The Physical Science Basis. Contribution of Working Group I to the Fifth Assessment Report of the Intergovernmental Panel on Climate Change*. Cambridge: Cambridge University Press, pp. 33-115.
- Stramma L, England M (1999) On the water masses and mean circulation of the South Atlantic Ocean. *Journal of Geophysical Research: Oceans*, 104(C9), 20863-20883, doi: 10.1029/1999JC900139.
- Stramma L, Gregory C, Johnson, Sprintall J, Mohrholz V (2008) Expanding Oxygen-Minimum Zones in the Tropical Oceans. *Science*, 320, 655-658.
- Stramma L, Hüttl S, Schafstall J (2005) Water masses and currents in the upper tropical Northeast Atlantic off northwest Africa. *Journal of Geophysical Research*, 110: C12006, doi:10.1029/2005JC002939.
- Stramma L, Johnson G C, Sprintall J, Mohrholz V (2008) Expanding Oxygen-Minimum Zones in the Tropical Oceans. *Science*, 320(5876), 655-658, doi: 10.1126/science.1153847.
- Stramma L, Oeschlies A, Schmidtko S (2012) Mismatch between observed and modelled trends in dissolved upper-ocean oxygen over the last 50yr, *Biogeosciences*, 9, 4045-4057.
- Stramma L, Schmidtko S, Levin LA, Johnson GC (2010) Ocean oxygen minima expansions and their biological impacts, *Deep-Sea Res I*, 57, 587-595.

- Stramma L, Schmidtko S, Levin L A, Johnson G C (2010) Ocean oxygen minima expansions and their biological impacts. *Deep Sea Research Part I: Oceanographic Research Papers*, 57(4), 587-595. doi: 10.1016/j.dsr.2010.01.005
- Stramma L, Visbeck M, Brandt P, Tanhua T and Wallace DWR (2009) Deoxygenation on the oxygen minimum zone of the eastern tropical North Atlantic, *Geophys. Res. Lett.*, 36, L20607.
- Suga T, Talley L D (1995) Antarctic Intermediate Water circulation in the tropical and subtropical South Atlantic. *Journal of Geophysical Research*, 100(7), 3,441-13,453.
- Summerhayes CP, Emeis KC, Angel MV, Smith RL, Zeitzschel B, (Eds.) (1995) *Upwelling in the Ocean Modern Processes and Ancient Records*, John Wiley and Sons, Chichester, 418 pp.
- Sutton RT, Hodson DLR (2016) Atlantic Ocean Forcing of North American and European Summer Climate. *Science*, 305, 115.
- Suzuki T (2011) Seasonal variation of the ITCZ and its characteristics over central Africa. *Theor Appl Climatol*, 103, 39–60.
- Talley L D, Pickard G L, Emery W J & Swift J H (2011) *Descriptive Physical Ocean: An Introduction* (6th ed.), Elsevier, Oxford, UK.
- Thorncroft CD, Hanh N, Zhang CD, Peyrillé P (2011) Annual cycle of the West African monsoon: regional circulations and associated water vapour transport. *Journal of the Royal Meteorological Society*. 137, 129–147.
- Thurman HV, Trujillo AP (2003) *Introductory oceanography*, 10th edition. Pearson Prentice Hall.
- Tomczak M, Godfrey J S (1994) *Regional Oceanography: An Introduction*, Adjacent seas of the Atlantic Ocean, Australia: Elsevier.
- Trouet V, Esper J, Graham NE, Baker A, Scourse JD, Frank DC (2009) Persistent positive North Atlantic Oscillation mode dominated the Medieval Climate Anomaly. *Science*, 324, 78–80.
- Trzaska S, Moron V, Fontaine B (1996) Global atmospheric response to specific linear combinations of the main SST modes. Part I: numerical experiments and preliminary results To cite this version: Global atmospheric response to specific linear combinations of the main SST modes. Part I : numerical experiments and preliminary results. *Geophysicae*, 14, 10, 1066–1077.
- Tyson RV, Pearson RH (1991) *In modern and ancient continental shelf Anoxia*. London: The Geological Society: 1-24.
- Uitz J, Claustre H, Morel A, Hooker SB (2006) Vertical distribution of phytoplankton communities in open ocean: An assessment based on surface chlorophyll. *J Geophys. Res.*, 111, doi:10.1029/2005JC003207.
- UNEP (2015) *Climate change and human rights*. UNON Publishing Services Section, Nairobi . 43 pp.
- Vaquer-Sunyer R, Duarte CM (2008) Threshold of hypoxia for marine biodiversity. *Proc. Natl Acad. Sci. USA*, 105, 15452-15457.
- Varela R, Álvarez I, Santos F, deCastro M, Gómez-Gesteira M (2015) Has upwelling strengthened along worldwide coasts over 1982-2010? *Nature*, 5(10016), 1-15.
- Vellinga M, Arribas A, Graham R (2012) Seasonal forecasts for regional onset of the West African Monsoon. *Journal Climate Dynamics*, 40, 3047–3070.
- Visbeck MH, Hurrell JW, Polvani L, Cullen HM (2001) The North Atlantic Oscillation: past, present, and future. *Proceedings of the National Academy of Sciences*, 98(23), 12876-12877.
- Von Schuckmann K, Palmer MD, Trenberth KE, Cazenave A, Chambers D, Champollion N, Hansen J, Josey SA, Loeb N, Mathieu P-P, et al. (2016) An imperative to monitor Earth's energy imbalance. *Nature Climate Change*, 6, 138-144.

- Von Schuckmann K, Brandt P, Eden C (2008) Generation of tropical instability waves in the Atlantic Ocean. *J Geophys. Res.*, 113, C08034, doi:10.1029/2007JC004712.
- Wallace J M and Thompson D J, (1998) The Arctic Oscillation signature in wintertime geopotential height and temperature. *Geophysical Research Letters*. Vol. 25, pp.1297-1300.
- Wallace DWR, Bange HW (2014) Introduction to special section: results of the Meteor 55: Tropical SOLAS experiment. *Geophysical Research Letters*, 31, L23S01. doi:10.1029/2004GL02014.
- Wang X, Murtugudde R, Hackert E, Marañón E (2016) Phytoplankton carbon and chlorophyll distributions in the equatorial Pacific and Atlantic: A basin-scale comparative study. *Journal of Marine Systems*, 109–110, 138-148.
- Wasmund N, Nausch G, Hansen A (2014) Phytoplankton succession in an isolated upwelled Benguela water body in relation to different initial nutrient conditions. *Journal of Marine Systems*, 140, 163–174.
- Weijden A J van der, Weijden C H van der (2002) Silica fluxes and opal dissolution rates in the northern Arabian Sea. *Deep-Sea Research*, 1 49, 157–173.
- Weingartner T J, Weisberg R H (1991) On the Annual Cycle of Equatorial Upwelling in the Central Atlantic Ocean. *Journal of Physical Oceanography*, 21, 68-82.
- Weldeab S, Lea D W, Schneider R R, Andersen N (2007) 155,000 years of West African monsoon and ocean thermal evolution. *Science*, 316, 1303–1307.
- WFC (2005) *Fish and Food Security in Africa*. World Fish Center, Penang, Malaysia. 11 pp.
- Wilding J (1939) The oxygen threshold for three species of fish. *Ecology*, 20: 253-263.
- Wyrtki K (1971) *Oceanographic Atlas of the International Indian Ocean Expedition*, National Science Foundation, 531 pp.
- Xue Y, Ales F D, Lau W K M, Boone A, Kyu-Myong K, Mechoso C R, Wang G, Kucharski F, Schiro K, Hosaka M, Li S, Druyan L M, Sanda I, Thiaw W, Zeng N, Comer R E, Lim Y K, Mahanama S, Song G, Gu Y, Hagos S M, Chin M, Schubert S, Dirmeyer P, Leung L R, Kalnay E, Kitoh A, Lu C, Mahowald N, Zhang Z M (2016) West African monsoon decadal variability and surface-related forcings: second West African Monsoon Modeling and Evaluation Project Experiment (WAMME II). *Journal of Climate Dynamics*, 47(11), 3517-3545.
- Zelle H, Appeldoorn G, Burgers G, & van Oldenborgh G J (2004) The relationship between sea surface temperature and thermocline depth in the eastern equatorial Pacific. *Journal of physical oceanography*, 34(3), 643-655.
- Zubkov MV, Sleigh MA, Burkill PH, Leakey RJG (2000) Picoplankton community structure on the Atlantic Meridional Transect: a comparison between seasons. *Prog. Oceanography*, 45, 369-386.

#### 4. GENETIC AND EPIGENETIC CHANGES IN ORGANISMS CARRIED IN BALLAST WATER DURING TRANS-EQUATORIAL TRAVELS IN THE ATLANTIC OCEAN

Eva Garcia-Vazquez<sup>1</sup>, Anastasija Zaiko<sup>2</sup>  
Alba Ardura<sup>3</sup> (not on board)

<sup>1</sup>UOviedo  
<sup>2</sup>UKlaipeda, Cawthron Institute  
<sup>3</sup>UOviedo

**Grant No AWI\_PS102\_00**

##### **Objectives**

Two objectives are sought in this project:

1. To identify and quantify the genetic and epigenetic changes experienced by organisms carried inside the ballast tank of the *Polarstern* across the Equator. During the cruise, the work included sampling ballast water, sorting by species and storing in ethanol the organisms present in the samples, for further molecular analysis in home laboratories.
2. To explore the development of the biofilm/biofouling communities within the ballast tanks, shift in taxonomical composition over the cross-latitudinal transfer and assess their possible contribution to the cross-regional introduction of marine non-indigenous species. The experiment was conducted onboard, by deploying the settlement plates in the ballast tank and sampling the biofilm for further molecular analysis in home laboratories.

##### **Work at sea**

Ballast tank number 7 was filled with offshore sea water in front of Bremerhaven port. Ballast water (BW) samples were taken via the sounding pipe, every day along the travel: before, after and one crossing the Equator, from November 13 to December 10, 2016. At each position, replicate samples were collected by concentrating 100 L of ballast water by filtering through a planktonnet. Onboard, samples were visually analyzed with the microscope, and specimens of the selected taxa were sorted for further molecular analyses. The rest of species were also visually classified from sample aliquots. From each sample, a sub-sample was stored in absolute ethanol for metabarcoding and other in RNA-later for extraction of RNA. Comparison between RNA (a molecule of very short life) and DNA (more resistant molecule) would allow to inferring living organisms. Physic-chemical parameters of the ballast water were monitored once per day over the cruise: pH, salinity, oxygen concentration, temperature, conductivity, ammonia. The temperature increased until the equator, then decreased. The dissolved oxygen decreased until the end of the travel, whereas ammonia concentration increased. As an example, the evolution of the temperature within the tank along the travel is presented below in Fig. 4.1.

An additional parallel experiment in BW was carried out, addressing the hypothesis that the biofilm/biofouling of BW tank walls might be an important vector of Non-Indigenous Species introduction. Three lines with replicate PVC plates (15x15 cm) were suspended vertically in the ballast tank on the day of departure. The biofilm from the plates was sampled 2 times during the voyage: when the tank was opened in las Palmas and upon arrival in Cape Town. For the sampling, a line was retrieved from the tank (at each port call when it was safe to open the manhole), samples were collected as in Pochon et al. (2015) and preserved in DNA/RNA fixative until the further molecular analysis (eDNA, eRNA extraction, metabarcoding) at home laboratories.

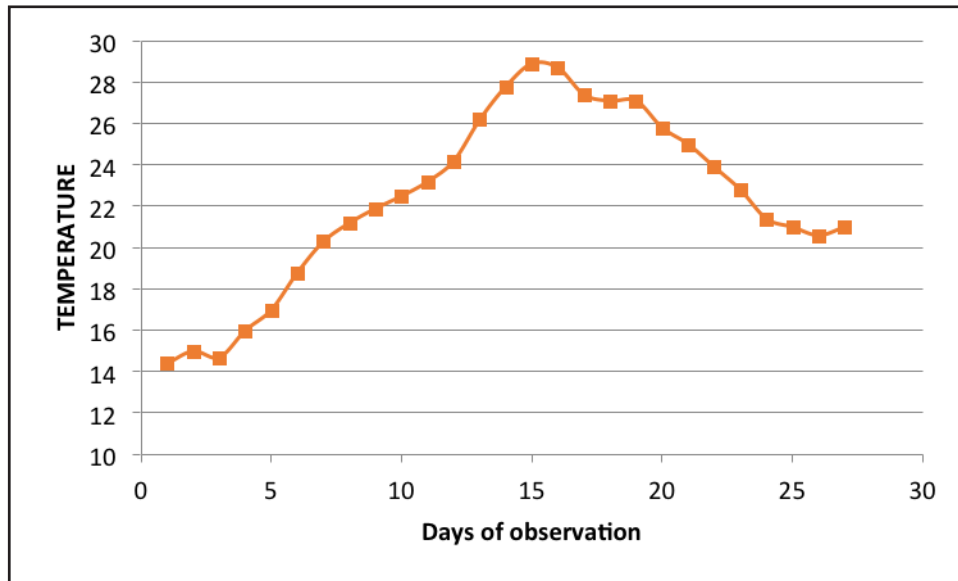


Fig. 4.1: Evolution of water temperature in the ballast tank number 6 of *Polarstern* during the cruise PS102

Garcia-Vazquez and Zaiko did BW sampling in collaboration with *Polarstern* crew complying with all onboard health and safety requirements. Sample preparation and visual sorting was done by researchers during the travel.

#### Preliminary (expected) results

All the samples collected during the *Polarstern* cruise were split in two halves. One half was safely stored in the Laboratory of Natural Resources of the University of Oviedo and the other half at Cawthron Institute (New Zealand). They are placed at the disposal of the scientific community within a maximum of one-year moratorium after the cruise (until 31 December 2017). They are available under request (Eva Garcia-Vazquez: [egv@uniovi.es](mailto:egv@uniovi.es); Anastasija Zaiko: [Anastasija.zaiko@jmtc.ku.lt](mailto:Anastasija.zaiko@jmtc.ku.lt))

The number of individual organisms sampled and stored in DNA or RNA fixative was >300 and corresponded principally to copepods, dinoflagellates and diatoms that were the most abundant eukaryotes in the samples analyzed. Copepods and diatoms increased proportionally until the end of the travel. Copepodites (copepod larvae) were observed until the last day of travel, demonstrating that at least some species were able to reproduce in route within the ballast

tank. DNA from these organisms will be available under request, and this particular point will be clearly stated in the scientific publication/s arising from the project. Entire individuals are not available because they all were very small and were completely smashed for DNA extraction.

DNA Barcoding (COI, 18S and 16S rRNA genes as Barcodes) is being used for species ascertainment from individual samples. NGS Metabarcoding as in Zaiko et al. (2015a,b) is being conducted as well and will serve for describing the plankton and biofilm community. The Ion Torrent and Illumina platforms are being employed. The samples fixed in RNA-later (a fixative of RNA) have been already retro-transcribed into cDNA. NGS Metabarcoding from these samples will be used for determining the fraction of the community –and species catalogue- that is alive in each sample.

### **Data management**

The data obtained from the samples will be essentially DNA sequences. The DNA sequences will be obtained, edited and curated, expectedly will be ready by the end of 2017. They will be submitted to the public repository GenBank (<http://www.ncbi.nlm.nih.gov/genbank/>). The release date will be six months after submission, therefore they will be fully accessible for the scientific community expectedly one year and a half after the cruise end.

The scientific results obtained from the samples collected in the cruise will be analyzed, interpreted and published in peer-refereed scientific journals indexed in SCI. At least one article will arise from the project. The *Polarstern* crew and the Chief Scientist of the expedition as well as the AWI will be acknowledged in all publications and deliverables that may be obtained from the samples obtained in the project. The authors strictly adhere to the Good Scientific Practice in Research and Scholarship of the European Science Foundation ([http://www.esf.org/fileadmin/Public\\_documents/Publications/ESPB10.pdf](http://www.esf.org/fileadmin/Public_documents/Publications/ESPB10.pdf)). The intention of the authors is to publish the results in Open Access journals.

### **References**

- Pochon X, Zaiko A, Hopkins GA, Banks JC, Wood SA (2015) Early detection of eukaryotic communities from marine biofilm using high-throughput sequencing: an assessment of different sampling devices. *Biofouling*, 31(3), 241-251.
- Zaiko A, Martinez JL, Schmidt-Petersen J, Ribicic D, Samuiloviene A, Garcia-Vazquez E (2015a) Metabarcoding approach for the ballast water surveillance - an advantageous solution or an awkward challenge? *Marine Pollution Bulletin* 92, 25-34.
- Zaiko A, Martinez JL, Ardura A, Clusa L, Borrell YJ, Samuiloviene A, Roca A, Garcia-Vazquez E (2015b) Detecting nuisance species using NGST: methodology shortcomings and possible application in ballast water monitoring. *Marine Environmental Research* doi: 10.1016/j.marenvres.2015.07.002.

## 5. AUTONOMOUS MEASUREMENT PLATFORMS FOR ENERGY AND MATERIAL EXCHANGE BETWEEN OCEAN AND ATMOSPHERE (OCEANET): ATMOSPHERE

A. Macke<sup>1</sup> (not on board), R. Engelmann<sup>1</sup> (not on board), H. Deneke<sup>1</sup> (not on board), Heike Kalesse<sup>1</sup>, Moritz Haorig<sup>1</sup>, Stephanie Fiedler<sup>2</sup>

<sup>1</sup>TROPOS  
<sup>2</sup>MPI-M

**Grant No AWI\_PS102\_00**

### Objectives

The net radiation budget at the surface is an important regulator in the climate system of the Earth. Next to well-known greenhouse gas effects it is mainly influenced by the complex spatial distribution of aerosols and clouds (liquid and ice water clouds) in the atmosphere. The complex interaction between aerosol particles and cloud particles still causes many uncertainties in climate models. While aerosol particles can directly scatter and absorb light depending on their type and chemical composition they also act as cloud condensation nuclei (CCN) and ice nuclei (IN).

The TROPOS scientists (H. Kalesse, M. Haorig) were aboard the PS102 transect to primarily collect data for a better understanding of the aerosol and cloud interaction. Therefore several remote-sensing instruments were on board within the OCEANET project. This project delivers valuable atmospheric measurement datasets over the oceans – in regions of the world which are not easily accessible. For the last 7 years a container-based platform has regularly been operated at *Polarstern* to obtain measurements and to contrast atmospheric processes between the anthropogenic polluted northern hemisphere and the more undisturbed southern hemisphere. For the PS102 cruise a renewed container was used and tested for the first time. The container was installed on the Heli-Deck (portside) and measurements were performed underway and continuously.

Additional to the measurements of TROPOS, sun photometer (type MICROTOPS and CALITOO) were made aboard (T. Keck, FU Berlin, S. Fiedler, MPI-Hamburg) to measure the Aerosol Optical Depth (AOD, the aerosol extinction in the entire atmosphere) along the cruise. Measurements with the MICROTOPS are performed within the framework of the Maritime Aerosol Network (MAN) as part of the Aerosol Robotic Network (AERONET).

### *Remote sensing (OCEANET Container)*

The primary instrument is a multiwavelength Raman lidar (type: Polly-XT) which measures profiles of the backscatter coefficient at three wavelengths, of the extinction coefficient and of the depolarisation at two wavelengths as well as of the water-vapour mixing ratio.

The portable lidar Polly-XT performed 24/7 measurements aboard *Polarstern*, whenever the weather conditions were appropriate (i.e., when the sun was not near-zenith). Aerosol particle optical properties in terms of the particle backscatter and extinction coefficient can be determined directly and serve as input for height-resolved inversion methods to estimate the

main microphysical properties (e.g. size distribution) at any measured height. Thus, lofted free-tropospheric aerosol layers can be characterized separately from the marine boundary layer. Typical known free-tropospheric aerosols are anthropogenic emissions from North America, dust from the Saharan region or smoke from biomass burning in Central Africa. These aerosols can be lifted up above land and are transported over the Atlantic Ocean for several days. During this transport aerosols influence the radiation budget of the Earth. Thus, the height-resolved information as derived from lidar is a crucial input for radiative transfer calculations to determine the direct aerosol radiative effect more precisely. In addition, the height-resolved measurements offer the opportunity to determine the extent of simultaneously occurring clouds, as well as the cloud's thermodynamic state of phase (liquid or solid) to investigate aerosol-cloud interactions and to determine the indirect aerosol radiative effect which shows the highest uncertainties in climate research. Latest studies reported that even an estimation of IN is possible from depolarization lidar data.

A Raman lidar like Polly-XT measures the extinction at night time using the vibrational-rotational Raman bands of nitrogen at 607 nm (excited with 532 nm) and 387 nm (excited with 355 nm). Up to now the extinction has been measured only in the UV and the visible, because longer wavelengths are less sensitive to molecules. A new approach uses the rotational Raman bands of nitrogen at 1,053 to 1,062 nm (excited with 1,064 nm) to determine the extinction at 1,064 nm, too. On the *Polarstern* cruise this approach will be tested on Saharan dust, African Biomass burning and pristine marine aerosol.

Additionally, a microwave radiometer (MWR, type: HATPRO) was operated. It measures brightness temperatures in the microwave region and uses absorption bands of water vapour and oxygen to retrieve temperature profiles and humidity profiles up to 10 km altitude height. Humidity profiles were used to derive integrated water vapour (IWV) and the liquid water path (LWP). In combination with the variability of the downward radiative quantities these time series make it possible to observe small scale atmospheric structures and cloud inhomogeneity.

Furthermore, a shadow band radiometer was mounted to the container roof. This radiometer measures the spectral and broadband down-welling radiation (0.3-1.6 micrometer range) from the upper hemisphere. Thanks to its rotating shadow band which blocks the direct sun when scanning over the receiver surface, the global, diffuse, and direct radiation were observed.

Two all sky cameras were also mounted on the roof taking pictures every 20 sec. These photos can be used to estimate the general cloud situation and also help in determining times when the shadow band radiometer data should be used with caution – like when the chimney of the *Polarstern* was continuously blocking the sun during late afternoon hours on the Northern Hemisphere or during CTD stations.

### **Work at sea**

The OCEANET container includes several active- and passive remote sensing instruments for the optical characterisation of aerosols and clouds. The measurements were taken continuously en-route and are not depending on any station work. The OCEANET instrument container was setup in the afternoon of 11 November, 2016 in Bremerhaven after the helicopters were stored in the hangar (Fig. 5.1, Tab. 5.1). After installation, the container was connected to the ships power grid. Two 32A cables were required. The UV1 (“Unterverteilung”) cable is connected directly to the ships grid (A/C, water chiller, blowers), while the UV2 cable is connected to the ships UPS system (all instruments). A 32A connector is not available at the Helideck, so that a 16 A-to-32 A adapter was used. It was found that the 3-phase 16A is enough for the instruments as they are distributed equally over all 3 power phases. The container was connected to the intranet of the vessel.

The Polly-XT lidar was taken into operation during the evening of 11 November 2016. At the same time, the MWR HATPRO was calibrated with liquid nitrogen (25 l). The procedure went as planned and the radiometer has been measuring continuously for the entire transect. The shadow band radiometer started measuring properly on 15 November 2016.

Regular maintenance procedures included daily cleaning on the radiation sensors and the All-Sky-camera dome. The lidar window was also cleaned on a regular basis (about every five days) depending on obvious sea-spray or other contamination. The air condition was not strong enough to keep the air temperature inside the container at 20°C in the tropics, most probable cause to a loss of cooling liquid. On 26 November the temperature inside the container reached 32°C, in the next days up to 36°C. The lidar was turned off some days during noon to prevent further heating. Since 3 December the temperature outside was below 24°C and the air condition worked properly again. During the period from 29 November until 9 December, the lidar was turned off for 2-4 h during noon because of high sun elevation. Direct sunlight must be prevented from entering the 30-cm telescope. Also, the lidar was turned off within the 12 mile zone around Las Palmas at 21 November from 3 am until 5 pm.

The extinction at 1,064 nm was measured with the rotational Raman filter (1,058 nm) during five nights covering Saharan dust (24 and 25 November), low level clouds (1 December), African biomass burning smoke (5 December) and marine conditions (8 December).

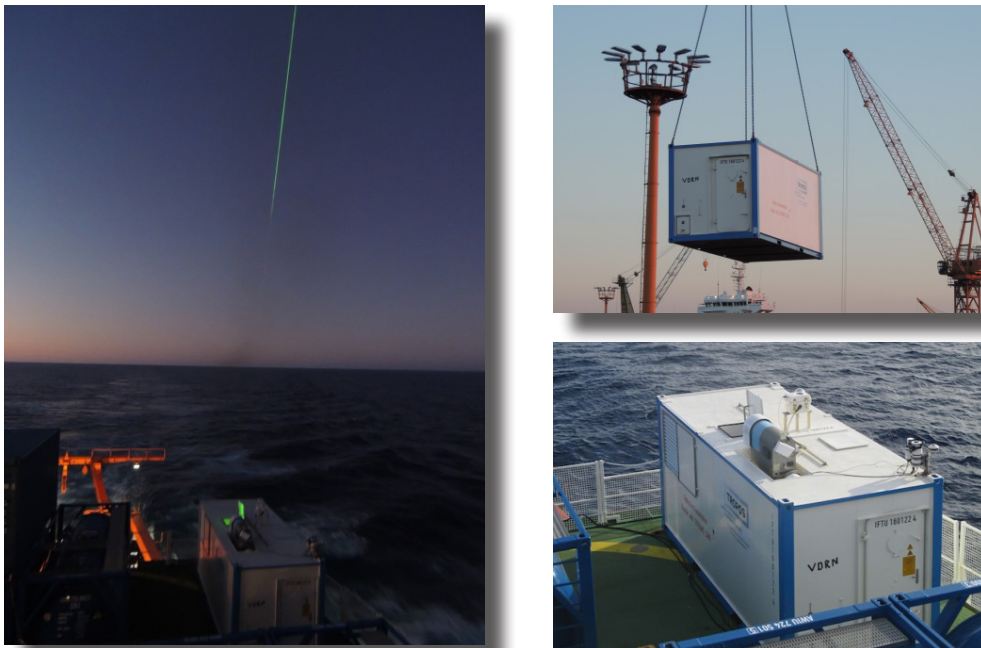


*Fig. 5.1: The new OCEANET remote-sensing container on the Polarstern Heli-deck. a) Night measurement on the ocean. b) Loading of the container in Bremerhaven. c) The grey-blue instrument on the front left corner is the HATPRO microwave radiometer, the instrument on the right front corner is the shadow band radiometer which has a small all-sky camera attached to it. Near the center of the container the all-sky camera is positioned. The open lid is the place where the Polly-XT lidar beam exits the container.*

Measurements with the MICROTOPS and CALITOO sun photometers were performed on a regular basis whenever clear-sky conditions prevailed. Several scientists and the POGO students shared this manual measurement task.

**Tab. 5.1:** Overview of the scientific instruments deployed on the OCEANET container during the PS102 *Polarstern* cruise

Instruments	Time Resolution	Data Availability
Raman lidar Polly-XT	30 s	12.11.2016 – 09.12.2016
HATPRO microwave radiometer (MWR)	1 s/1min	12.11.2016 – 09.12.2016
Shadow band radiometer	1 min	16.11.2016 – 09.12.2016
All sky camera	20s	12.11.2016 – 09.12.2016

### Expected and preliminary results

After leaving Bremerhaven in very cold, but clear conditions the weather in the North Sea and the English Channel till the coast of Portugal was dominated by clouds. Many low clouds and only a few precipitation events were observed with the lidar. Figure 5.2 presents the lidar quicklooks of the range-corrected signal at 1064 nm and the volume depolarization ratio at 532 nm wavelength. The same channel was used for the measurements at 1,064 nm and 1,058 nm. The signal at 1,058 nm is one to two orders of magnitude lower than the signal at 1,064 nm, resulting in much weaker signals in the nights of 24 and 25 November as well as in the nights of 1, 5 and 8 December. Pristine marine conditions without clouds had been observed on the 19 and 20 November, before a lofted plume of Saharan dust above the marine boundary layer appeared on the evening of 20 November. The plume extended from 1,200 m to 2,500 m height. The lidar was turned off in the 12 nautical miles zone of Gran Canaria. At leaving this zone the lidar was turned on again and could further observe the dust. Around 24 November, at the latitude of Cabo Verde, the lidar shows increased depolarization above the marine boundary layer. A dust and smoke mixture reaching up to 4 km dominated the aerosol load in the free troposphere. The ship steadily moved crossed the plume in southward direction so that in the evening of 26 November the region of dust was left behind. On Sunday 27 November *Polarstern* reached the inner tropical convergence zone (ITCZ) at 7°N. Several smoke plumes from West and Central Africa with a maximal vertical extend up to 3.5 km altitude dominated the situation till the evening of 30 November. After that, marine stratocumulus occurred frequently. In the short cloud free areas the lidar showed some lofted layers of continental aerosol, probably smoke. Since 5 December mostly clear sky with some low level cumulus clouds and clean marine aerosol conditions had dominated and it had been possible to detect only thin layers of continental aerosol above. The 9 December was characterized by drizzle, high relative humidity (97 %) and cloud base heights around 100 m.

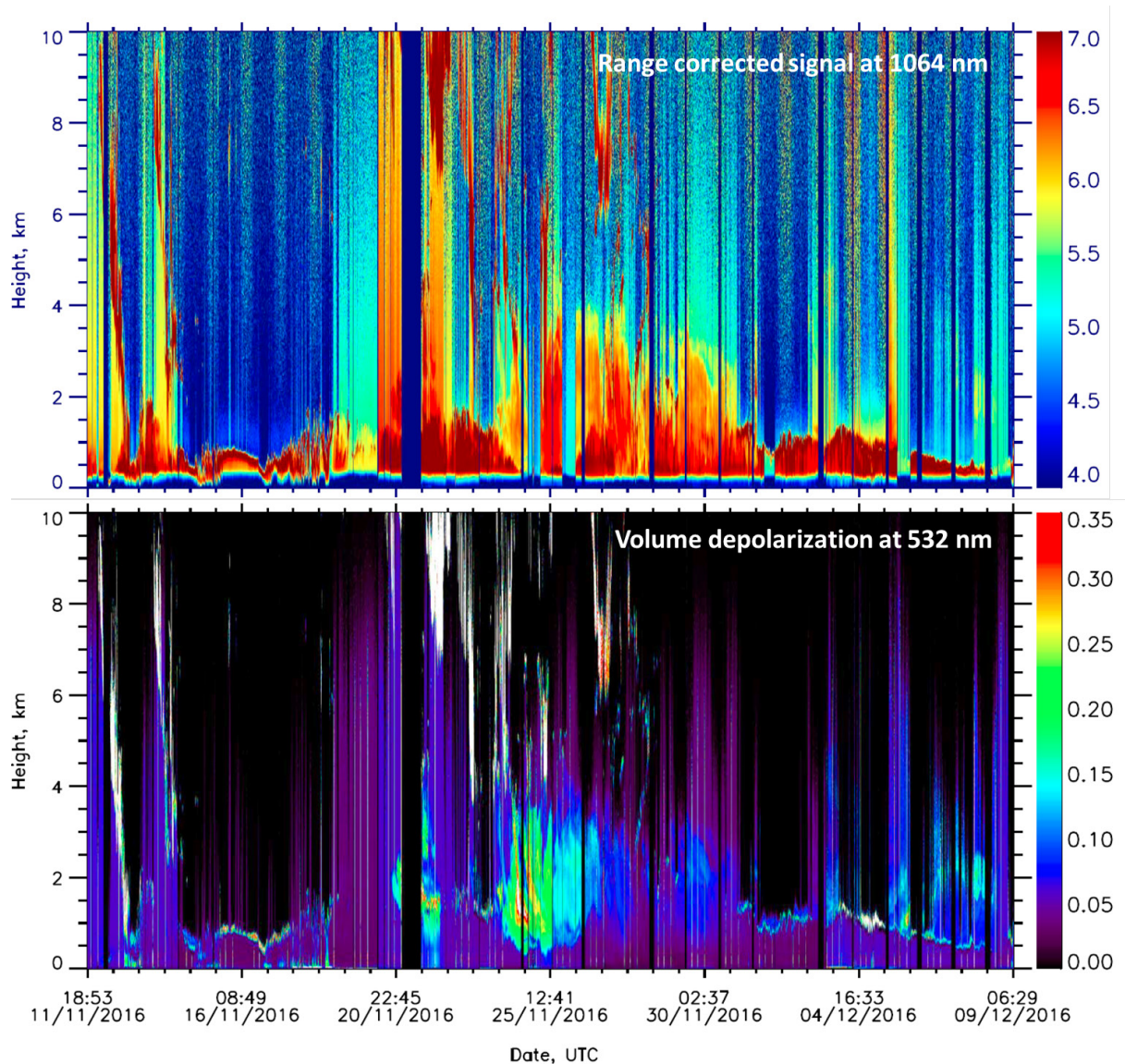


Fig. 5.2: Range-corrected lidar signal at 1064 nm wavelength (top) and volume depolarization ratio at 532 nm wavelength (bottom, preliminary). During the extinction measurements at 1,064 nm (nights of 24, 25 Nov, 1, 5, 8 Dec) the range-corrected signal at 1,058 nm is shown (top).

The microwave radiometer HATPRO measured the integrated water vapour (IWV) and the liquid water path (LWP) along the cruise. Figure 5.3 and 5.4 show quicklooks of these variables. Data presented is preliminary and has to be quality-controlled and reprocessed with the proper retrieval algorithms for finalization. It can already be seen that *Polarstern* has crossed the tropical latitudes around 23 November – 2 December where the IWV increased by a factor of two-three from about 10-20 kg/m<sup>2</sup> to 40-60 kg/m<sup>2</sup>. Narrow peaks in the time series are partly caused by cleaning of the sensors with distilled water on a nearly daily basis or from sampling our own ship plume which has occurred several times along the transect. Observed LWP (Fig. 5.4) ranged from a few tenth of g/m<sup>2</sup> in thin marine stratocumulus clouds to a few hundred g/m<sup>2</sup> in thicker cumulus clouds and peaked at about 1,500-2,000 g/m<sup>2</sup> in cumulus congestus clouds.

The temperature transect (Fig. 5.5) shows that surface temperatures increased from below 5°C to about 30°C in the Inner tropical convergence zone (ITCZ). The 0°C isotherm height increased from 2.5 km at the start of the cruise to about 4 km south of 20°N. A strong low-level inversion which descended over time had started to form on Dec 5.



Fig. 5.3: Integrated water vapour (IWV) during PS102 measured with the microwave radiometer HATPRO

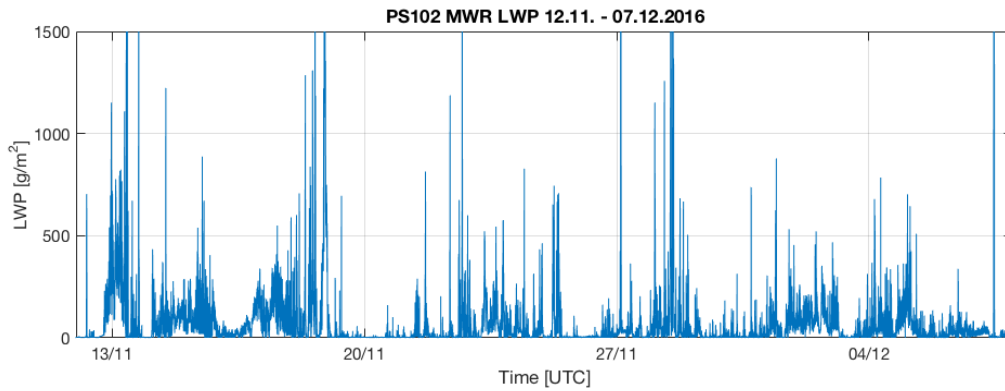


Fig. 5.4: Liquid water path (LWP) during PS102 measured with the microwave radiometer HATPRO

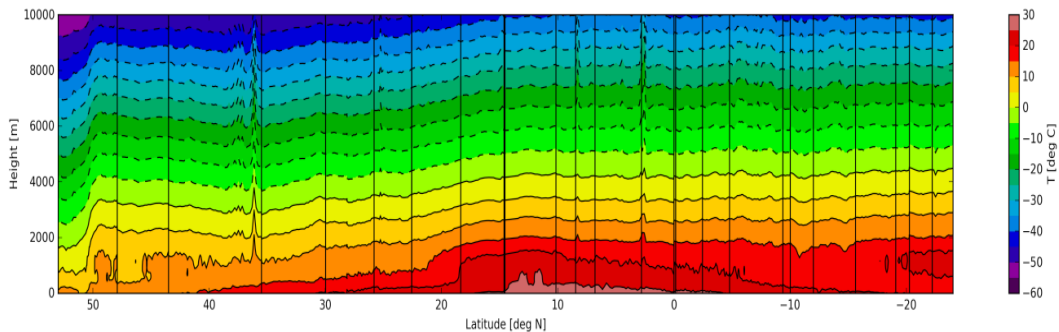


Fig. 5.5: Transect of temperature profiles during PS102 measured with the microwave radiometer HATPRO

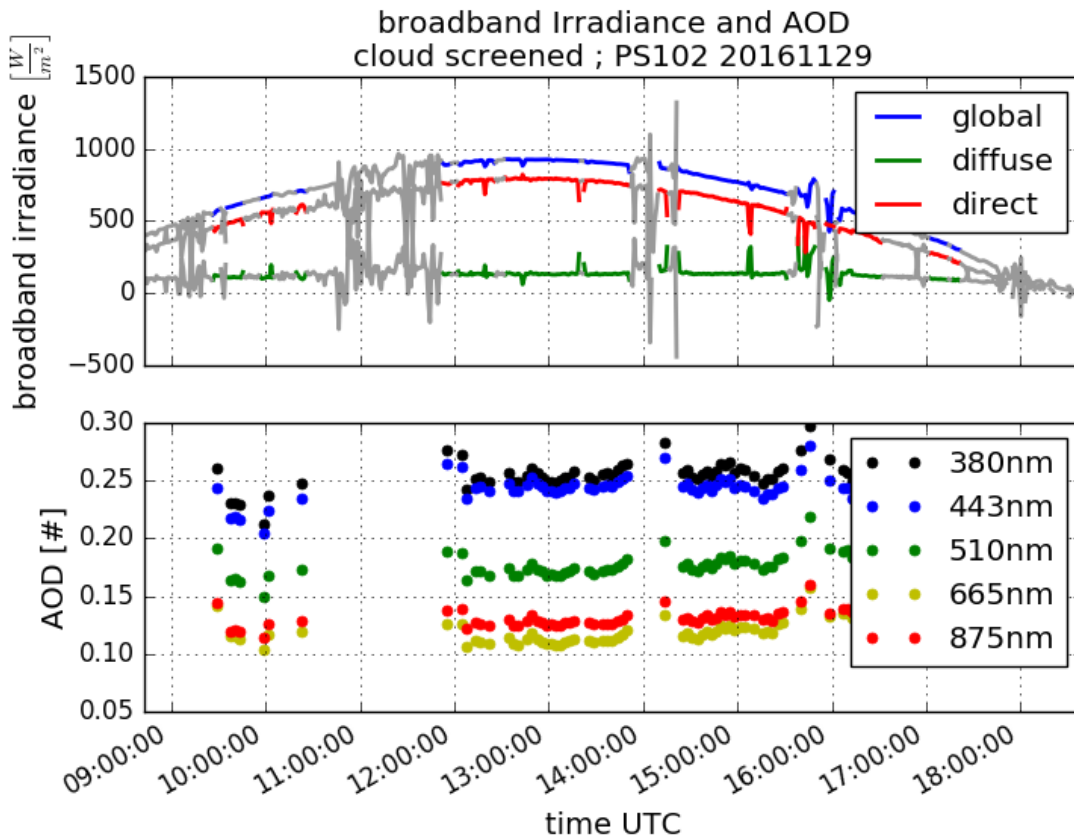


Fig. 5.6: Example of the daily cycle of the broadband solar irradiance (flux density) on November 29, 2016 measured with the shadow band radiometer as well as derived aerosol optical depth.

A typical example (November 29, day of the equator crossing) of the daily broadband solar irradiance (flux density) measured with the shadow band radiometer is shown in Figure 5.6. Solar radiation input reaches its maximum at local noon as can be seen in the global (direct + diffuse) as well as the direct radiation from the sun. Diffuse radiation from the sky does not have a daily cycle. Grey areas of strong fluctuations in the signal indicate clouds. A cloud screening is applied before the determination of aerosol optical depth. Wavelength-dependent aerosol optical depth values on November 29 range between 0.11 (at 665 nm) to 0.25 (at 380 nm). Similar values of aerosol optical depth for that day were obtained with the MICROTOPS sun photometer. Back trajectories calculated for that day show that biomass burning aerosol was advected to the *Polarstern* from central Africa.

A detailed description of the MICROTOPS sun photometer measurements is given by S. Fiedler in chapter 6).

### Data management

All remote-sensing and data processing will be carried out at TROPOS in Leipzig. The primary address for the data access should therefore be TROPOS but as soon as the data are available they can be used by other cruise participants after request. Additionally, it is foreseen to upload the quality checked data to the Pangaea database. However, this data processing and upload procedure might take a few months.

## 6. COLUMN-INTEGRATED OPTICAL MEASUREMENTS OF AEROSOL, WATER VAPOUR AND CLOUDS

Stephanie Fiedler<sup>1</sup>, S. Kinne<sup>1</sup> (not on board) and  
F. Jansen<sup>1</sup> (not on board)

<sup>1</sup> MPI-M

Grant No AWI\_PS102\_00

See chapter 5 for Objectives

Work at sea

*MICROTOPS measurements*

A MICROTOPS instrument had been provided by NASA to do remote sensing of aerosol optical depth (AOD) and water vapour content. The data was submitted and quality checked by the Marine Aerosol Network (MAN) as part of the Aerosol Robotic Network (AeroNet, Smirnov et al., 2009). The small handheld instrument (Fig. 6.1) measures the intensity of incoming solar radiation. It is combined with a GPS to estimate the intensity at the top of the atmosphere. Incoming solar radiation measured onboard the ship has been reduced by absorption and scattering. Based on associated differences in the radiation, properties of atmospheric aerosol and water vapour along the atmospheric path are derived. These measurements rely on direct sunlight, such that the data record is limited to day and intermittent by clouds.

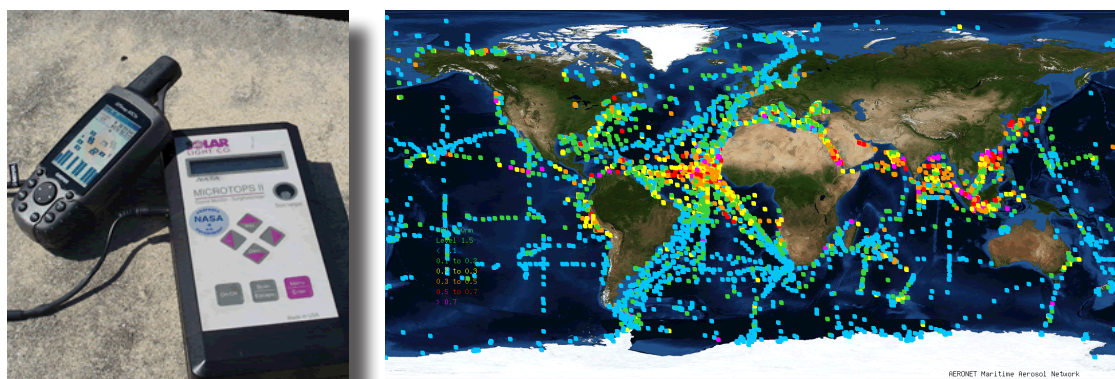


Fig. 6.1: (left) MICROTOPS instrument, (right) network of past observations within Marine Aerosol Network (MAN, [http://aeronet.gsfc.nasa.gov/new\\_web/maritime\\_aerosol\\_network.html](http://aeronet.gsfc.nasa.gov/new_web/maritime_aerosol_network.html))

The MICROTOPS measurements are a contribution to the typically sparse network over remote waters (Fig. 6.1). They help to better understand the Earth radiation budget, e.g. the measurements are used to update the present-day aerosol climatology of MPI-M (MAC, Kinne et al., 2013). This climatology is the basis for the simple plumes parameterisation MACv2.0-SP1.0 for aerosol optical properties for usage in CMIP6 models (Fiedler et al., in review; Stevens et al., 2016). The MICROTOPS measurements from this expedition could be further used for validation and development of satellite products and atmospheric models as well as inter-disciplinary studies on ocean fertilisation.

Aerosol Optical Depth

The AOD is measured for four wavelengths, namely 380 nm, 440 nm, 675 nm, and 870 nm. Determining the Angstrom exponent from the measurements at 440 nm and 870 nm allows to derive the AOD at 500 nm that is commonly used for inter-comparison of measurements and models.

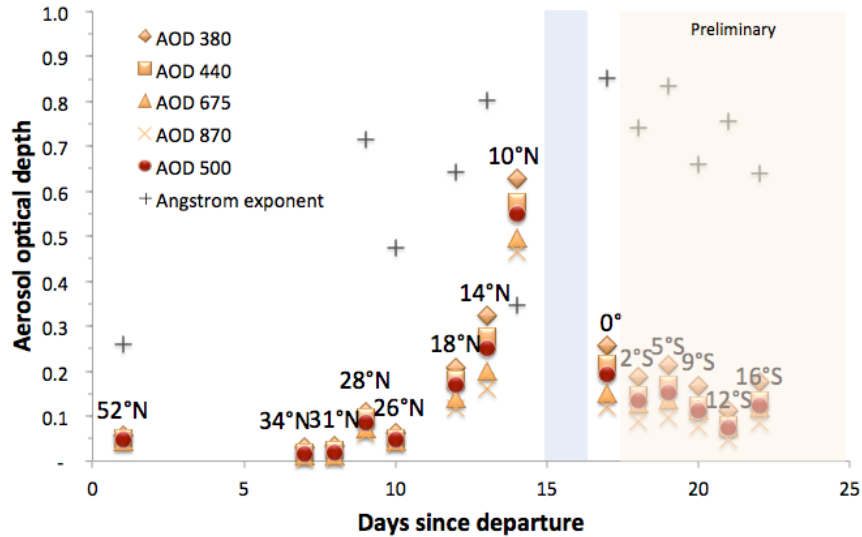


Fig. 6.2: Atlantic transect of aerosol optical depth from MICROTOPS. Shown are daily mean AODs for different wavelengths and the Angstrom exponent for 440 nm/870 nm. Blue shading marks the ITCZ, and yellow shading data that has not yet been quality controlled.

The Atlantic transect of AOD is shown in Fig. 6.2. In Northern mid-latitudes, the measurements indicate pristine ocean background AODs for 500 nm at the order of 0.02 - 0.05. As we approached the Intertropical convergence zone (ITCZ) from the North, AOD increased to a maximum of 0.55. The increasing aerosol is likely associated with a mixture of Saharan dust and anthropogenic aerosol that are typical for offshore regions of North Africa for this season. Anthropogenic aerosol is likely associated with burning of biomass in sub-Saharan Africa (Fig. 6.3, left).

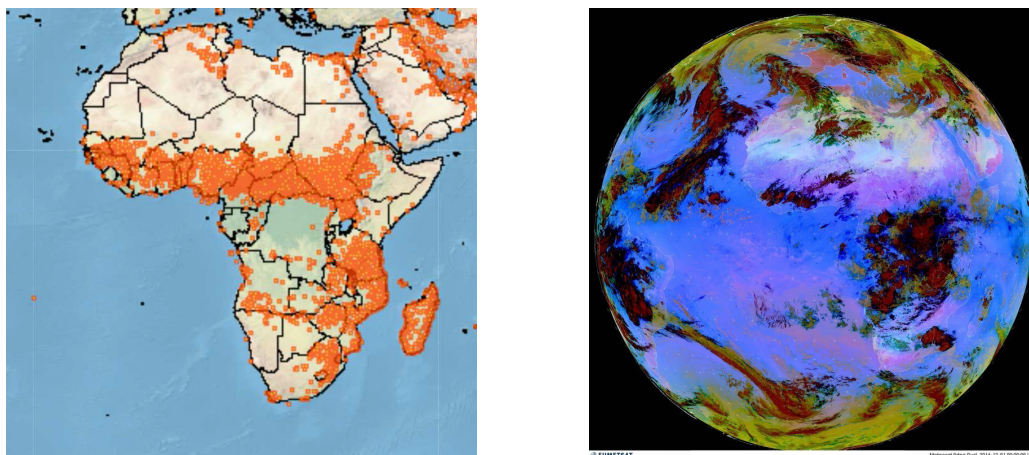


Fig. 6.3: (left) VIIRS (375 m) fire map for 29 - 30 November 2016. Orange dots indicate active fires as retrieved from the satellite observation (NASA FIRMS Web Fire Mapper, as of 2 December 2016). (right) MSG SEVIRI false color product for midnight of 1 December 2016 (EUMETSAT). Dark red indicates clouds, pink desert dust and blue water vapour.

After leaving the ITCZ towards the South, AODs were lower and might at least in parts be associated with biomass burning in southern regions of Africa. Although VIIRS and MODIS do not indicate active fire in the majority of central and western regions of Africa, the presence of clouds likely made a retrieval of active fires difficult, e.g., indicated by clouds in the false color product of MSG SEVRI on 1 December 2016 (Fig. 6.3).

#### Column integrated water vapour

In addition to the AOD, MICROTOPS derives the water vapour content along the atmospheric path. The data shows clearly larger values in the tropics than extra-tropics as one would expect from the higher temperatures in the tropics (Fig. 6.4). Typical values of the water vapour content near the ITCZ are around 4.5 cm in precipitable water equivalent. The maximum in water vapour content is expected at the ITCZ and is one way of defining the ITCZ location. This definition has the advantage of being independent from the somewhat temporally intermittent and spatially variable clouds and rainfall. Unfortunately, water vapour content is not always available, e.g., observation with MICROTOPS has not been possible due to the presence of clouds.

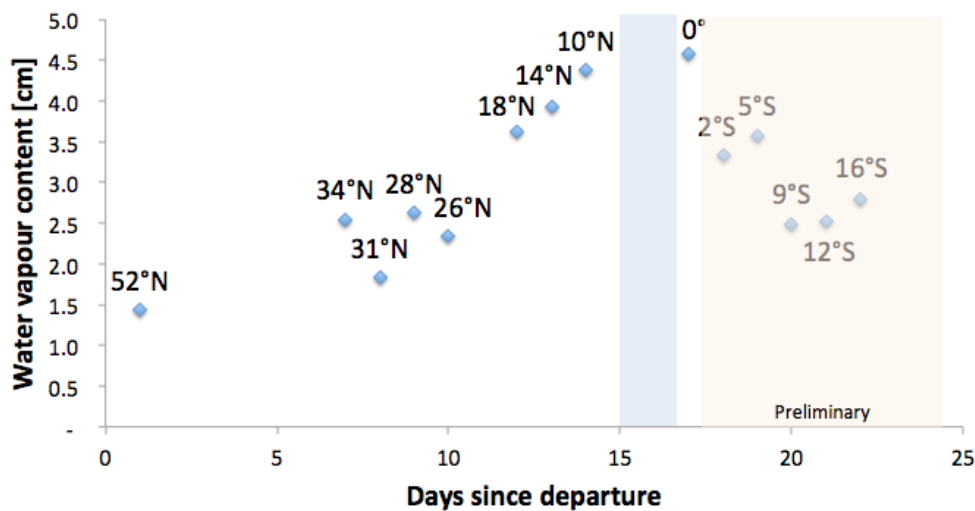


Fig. 6.4: Atlantic transect of water vapour path from MICROTOPS. Shown are daily mean values. Blue shading marks the position of the ITCZ and yellow shading data that has not yet been quality controlled.

#### Calitoo measurements

The new hand-held sun photometer Calitoo had been brought to *Polarstern* for the first time. Coordinated observations with two Calitoo instruments and two MICROTOPS gave a quantitative assessment of the uncertainty in determining AOD from these instruments. The second MICROTOPS has been brought by the 'Freie Universität'. That instrument and the Calitoo had been used by the NoSoAT students to do observations, in parallel to the MICROTOPS instrument brought by MPI-M.

The coordinated measurements were done on 29 and 30 December 2016 from the pile deck. Five times we did simultaneous measurement sequences of ten samples. In between sequences we had breaks of two minutes. Sequences were paused when a cloud moved into the path. Fig. 6.5 shows the inter-comparison of the observations on the two days. The AOD has been interpolated to the same wavelength of 500 nm and daily averaged. The interpolation is done by first calculating the Angstrom exponent from 465 nm/619 nm for Calitoo, and 440 nm/870 nm for MICROTOPS and then applying the exponent with the AODs measured at 540 nm and 440 nm to derive AODs at 500 nm. The results indicate a reasonable agreement of Calitoo with MICROTOPS with an uncertainty of 10 %.

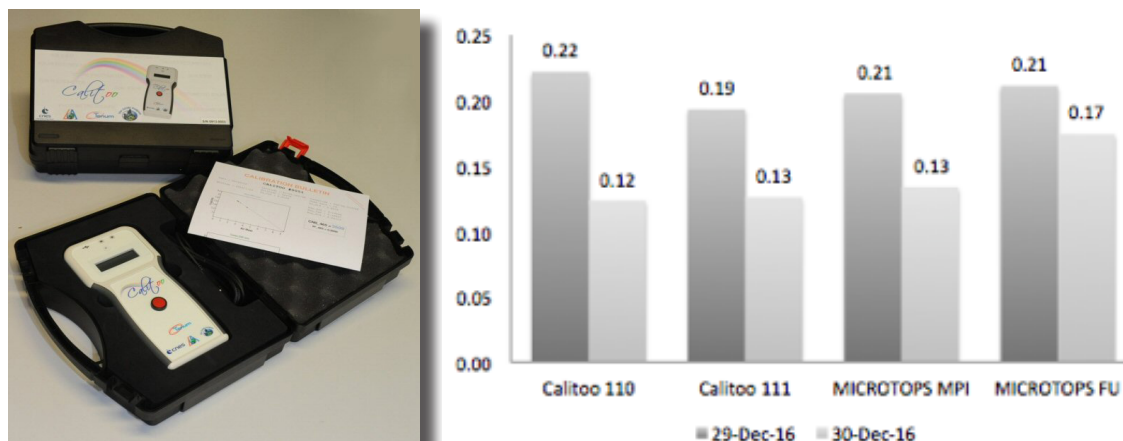


Fig. 6.5: (left) Calitoo instrument (<http://www.calitoo.fr>), (right) Comparison of AOD at 500 nm derived from Calitoo and Microtops measurements of 29 and 30 December 2016.

### Cloud imagers

Two cloud imager systems had been operated during the entire cruise (Fig. 6.6). Both contained two cameras each, one for visible (VIS) and one for near-infrared (NIR) radiation. The systems were installed in the vicinity of each other and pointed towards the sky to continuously record cloud scenes along the ship track. They were placed on the pile deck at the westward facing railing, and were connected to energy supply and computers in the research lab on A level.

All cameras had been in operation from 11 November 2016 until 10 December 2016. The visible cameras recorded throughout day and night. These images will serve to derive cloud fractions during daytime and help to better characterise NIR images. In latitudes of high sun elevations over the horizon, the NIR imagers had to be covered with shields to protect the sensors from direct sunlight. NIR images will be used to derive cloud fraction at night and record brightness temperatures of the cloud base. A derivation of cloud base height and a cloud type classification will be subject of ongoing research.



Fig. 6.6: Photo of the cloud imagers (top left) 'Pinocchio' and (right) 'Dumbo'

## Cool-box Imager 'Dumbo'

### Instrument description and operation

The larger of the two imager systems 'Dumbo' is contained in a cooling box that includes a webcam plus controller, the NIR imager, and a PC to record the data of the cameras (Fig. 6.7). In order to reduce the number of disturbances at the boundary of the imagers, 'Dumbo' has been elevated by a wooden construction of palettes and securely tied to the railing with strings. Rain drops on the sensible NIR lens have been avoided by a thin plastic cover. The cover had to be regularly replaced. Typically, a replacement after a couple of days was sufficient, but during episodes of aerosol deposition the cover had to be daily exchanged, and additionally after heavy rain, e.g., in the ITCZ. At the same time, the lens of the webcam was checked whether cleaning is necessary.

The temperature and humidity inside of the box had to be monitored to be alert of a possibly necessary shut down. In the ITCZ, the imager was approaching a critical temperature level. In order to reduce the temperature to continue the measurements throughout the ITCZ, an improvised ice pack was put into the cooling box. The ice pack was made of three air tight plastic containers filled with crushed ice. To reduce the risk of water leakage or excessive water condensation on the outside of the pack, the plastic boxes were put in one sealed and one unsealed plastic bag, and wrapped into a kitchen towel. The three containers in use had a capacity of 350 ml, 870 ml, and 600 ml and successfully cooled the system so that the imager kept being in operation for the entire cruise.

The system is controlled on a laptop using a remote desktop connection. In order to get a full record from the NIR imager in ASCII format, and JPG images for case studies, the software of the NIR imager was used to convert the system-internal data format. Data of the NIR imager was daily converted and copied to a portable hard disk. The recording frequency for the images is 10 seconds.

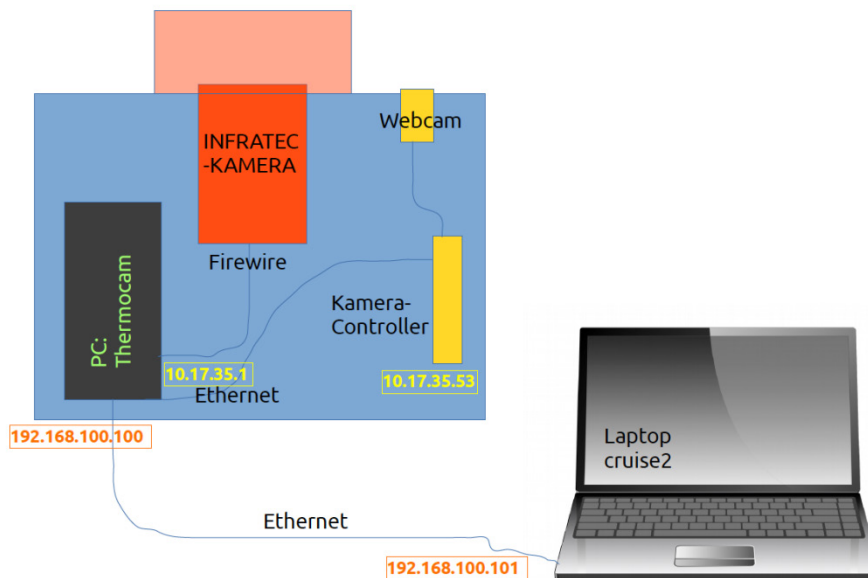


Fig. 6.7: Sketch of 'Dumbo' (F. Jansen)

### Light-weight Imager 'Pinocchio'

#### Instrument description and operation

'Dumbo' is accompanied by a smaller and light-weight imager 'Pinocchio', that had recently been constructed and was in operation for the first time. The NIR imager and webcam are connected to a desktop computer that are situated in the research lab on A level (Fig. 6.8). This construction was not sensitive to the tropical heat. The cameras recorded clouds without interruptions except during small solar zenith angles. During those times, the NIR imager was covered with a three times folded carton to avoid direct sunlight on the sensor during mid-day. Regular maintenance in intervals of 3-4 days included cleaning of the lenses from rain and dust deposition, and copying of the data to a portable hard disk.

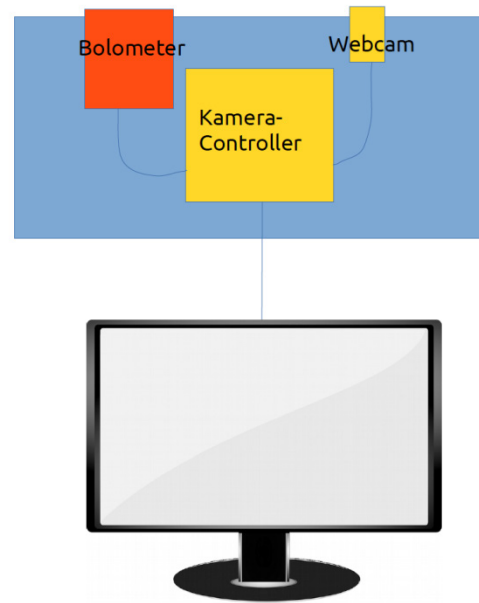


Fig. 6.8: Sketch of 'Pinocchio' (F. Jansen)

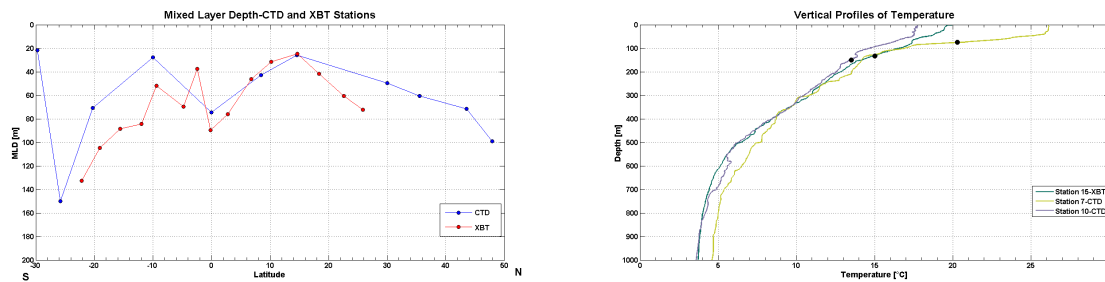


Fig. 6.9: (left) Mask for cutting boundaries of artificial objects. (right) Example of brightness temperature distribution from NIR imager after applying the mask.

### Preliminary and expected results

#### 'Dumbo'

The purpose of 'Dumbo' is to characterise cloud scenes along the ship track to derive an Atlantic transect of cloud types. The infrared camera measures differences in brightness temperature that allow to derive cloud characteristics, such as the cloud base height, and determine the cloud fraction during night.

A preexisting algorithm for for the NIR images (K. Duscha and N. Fuchs) has been adapted to data collected during this cruise to do first quality checks of the produced ASCII files. An example of the boundary mask for cutting non-cloud objects from the images and an example of the brightness temperature plots are shown in Fig. 6.9. The full processing of the data record will be done on a higher performance computer at MPI-M, after the code will have been further developed. The code has already been extended to calculate a cloud inhomogeneity parameter as time series that is written to an ASCII file. Future additions to the will include a derivation of cloud base heights for the most frequently present brightness temperature per image.

**Tab. 6.1:** Case studies with NIR imager of ‘Dumbo’

Time	Weather	Location
16 November 2016 - 17 November 2016	Transition of St to Sc ahead of trailing cold front	Offshore Portugese coast
17 November 2016 - 18 November 2016	Precipitating Sc ahead of trailing cold front	Offshore Portugese coast
21 November 2016 - 22 November 2016	Cirrus in subtropical high	Canary Islands
27 November 2016 - 28 November 2016	ITCZ	Offshore southern West Africa

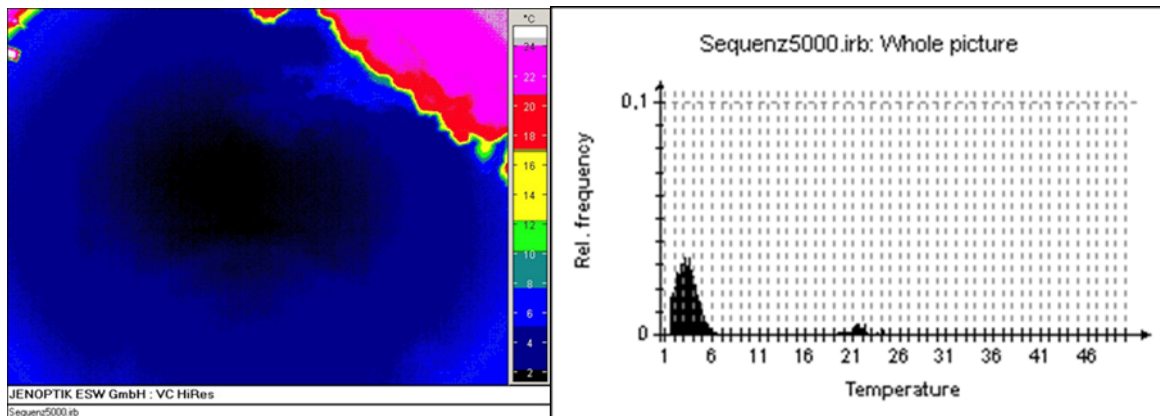


*Fig. 6.10: Example of NIR imager in ITCZ from internal software of ‘Dumbo’ for 28 November 2016 at 22:35:52.*

During the cruise, case studies (Tab. 6.1) were identified for different meteorological regimes to help the validation of the anticipated code development. For each case, NIR images were output as JPG and frequency histograms of brightness temperature were calculated with the imager software. These were produced with a temporal resolution of roughly three hours and matched up with other data, such as LIDAR, HatPro, weather analysis and satellite images available onboard.

The histograms gave a first indication that using the width of the distribution could be suitable for differentiating stratiform from cumuli cloud types, and clear sky. An example is shown in Fig. 6.10, where the clear-sky temperature is clearly distinct from the cloud temperature. In combination with the cloud fraction, this information could be used to derive a simple cloud type classification along the Atlantic transect.

A systematic validation of the method will be needed, in addition to testing different ideas for scaling the clear-sky brightness with air temperature. This scaling will be done with the near-surface and possibly with a vertical correction using data from the weather station and radiosondes from 12 UTC onboard. Reference data for cloud base height are ceilometer measurements from the pile deck that is situated reasonably near to the imagers, but on the other side of the ship such that it might miss the actual height of the clouds above the camera. Presumably for cumuli type clouds, that might be misleading. Further reference data for validating cloud base heights will therefore be used, e.g., from the Hatpro Microwave Radiometer and the PollyXT LIDAR ‘Arielle’ in the Oceanet container on the helicopter deck. Using that data will help to assess the spatial variability in observed cloud-base heights. Refer to the section on Oceanet for a detailed description of that data.

### Light-weight Imager 'Pinocchio'

'Pinocchio' produced continuous series of VIS and NIR cloud images that are stored as JPG files. The recording frequency is one minute. The data will be compared against 'Dumbo' to evaluate whether 'Pinocchio' can be solely used during future cruises. Fig. 6.11 shows an example for mid-night of 7 December 2016. The VIS image shows the lidar beam and stars, while the NIR image indicate clouds. The advantage of 'Pinocchio' would be an easier handling and less logistical effort for transport and installation. One potential drawback is the missing display of the values of the brightness temperatures in the NIR images. Dependent on the application, e.g., for deriving cloud base height, these values would be needed. Comparison against 'Dumbo' will determine whether the colors of the NIR images of 'Pinocchio' can be assigned brightness temperatures from 'Dumbo'.

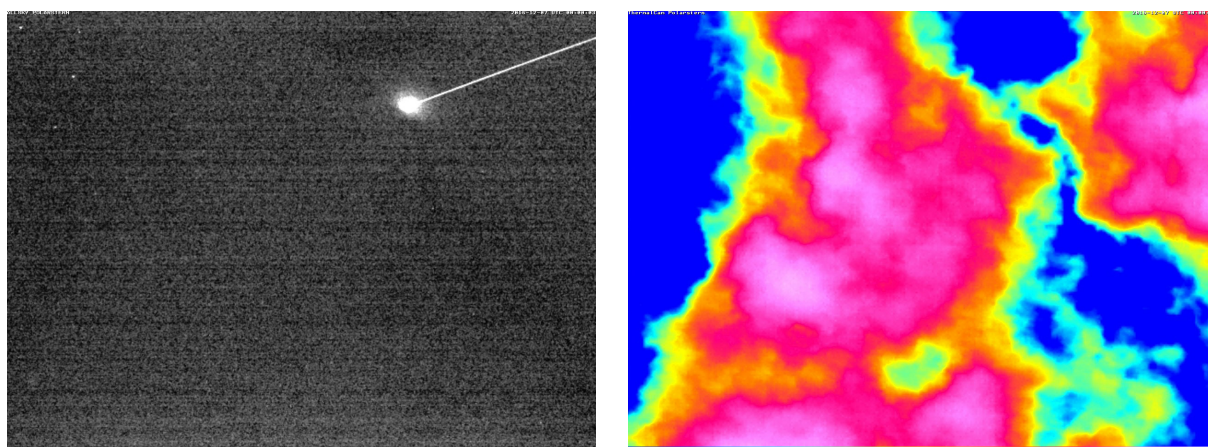


Fig. 6.11: Example of VIS and NIR images from 'Pinocchio' for mid-night of 7 December 2016

See chapter 5 for Data management

### References

- Fiedler S, Stevens B, and Mauritsen T. (in review) On the sensitivity of anthropogenic aerosol forcing to atmospheric variability and parameterizing a Twomey effect.
- Kinne S, O'Donnel D, Stier P, Kloster S, Zhang K, Schmidt H, Rast S, Giorgetta M, Eck T F, Stevens B (2013) MAC-v1: A new global aerosol climatology for climate studies. *Journal of Advances in Modeling Earth Systems*, 5 (4), 704–740, doi: 10.1002/jame.20035.
- Smirnov et al. (2009) Maritime Aerosol Network as a component of Aerosol Robotic Network, *J. Geophys. Res.*, 114, D06204, doi:10.1029/2008JD011257.
- Stevens B., Fiedler S, Kinne S, Peters K, Rast S, Müsse J, Smith S J, Mauritsen T (2016) Simple Plumes: A parameterization of anthropogenic aerosol optical properties and an associated Twomey effect for climate studies, *Geosci. Model Dev. Disc.*, 2016, 1–34, doi:10.5194/gmd-2016-189.

## 7. STABLE N - ISOTOPES OF AMMONIUM AND AMMONIA OVER THE ATLANTIC OCEAN

Heidi Witte Gaedecke, Julia Goedecke,  
G. Gravenhors (not on board)

GAUG

Grant No AWI\_PS102\_00

### Objectives

During the cruise we made field measurements on board to answer the following questions:

1. What  $^{15}\text{N}/^{14}\text{N}$ -isotope ratios are found in ammonium of size separated airborne particles and in gaseous ammonia over the Atlantic?
2. What differences in  $\text{NH}_4^-$  and  $\text{NH}_3$ -concentrations and in N isotope ratios do exist between air over the North Atlantic and the South Atlantic?
3. Can we differentiate  $\text{NH}_3$ -source and -sink regions on the Atlantic?
4. What fingerprint do ammonia and ammonium, dissolved in the surface water of the Atlantic, leave in the atmosphere?

All measurements will be continued over the ice covered Atlantic during the PS103 and on the way from South to North Atlantic during PS105.

### Work at sea

For  $\text{NH}_3^-$  and  $\text{NH}_4^+$  concentration and  $\delta^{15}\text{N-NH}_3$  and  $\delta^{15}\text{N-NH}_4^+$  isotope measurements the  $\text{NH}_4^+$  and  $\text{NH}_3$ -gas molecules have been accumulated on filter pack systems with 90 mm diameter (Fig. 7.1). The filter pack system consists of one teflon-membrane filter in front to collect particles and three acidified membrane filters behind to absorb gas phase ammonia.

Five individual standalone systems (filter pack, gas pump, gas meter, wind direction controller) have been installed on the deck above the bridge.



Fig. 7.1: Four filter pack systems collecting samples of  $\text{NH}_3$  and  $\text{NH}_4^+$

Fig. 7.2: High-volume-impactor (top), the pumps for the filter pack systems and gas meters



For the case of wind blowing from the tail a similar filter pack system was ready to be installed on the stern (Fig. 7.2). During PS102 it has not been necessary to use this extra system because the wind or relative wind came the most time from the front area.

Depending on the  $\text{NH}_4^+$  mass found on each  $\text{NH}_4^+$ -particle filter and on each  $\text{NH}_3$  ammonia filter the solutions of filters will be clumped or kept individually and used for  $\text{NH}_4\text{-N}$  and  $\text{NH}_3\text{-N}$  isotope analyses on land.

Two identical high-volume samplers (ca.  $90 \text{ m}^3/\text{h}$ ) have collected size-fractionated airborne particles with a 5 stage impactor (Fig. 7.2). The 5 stages of the impactor (ca  $< 10 \mu\text{m}$  to  $> 0.1 \mu\text{m}$  radius) have been covered by a teflon foil (Fig. 7.3) and backed up with a teflon membrane filter (filter  $\text{Ø} = 20 \text{ cm}$ , particle  $r < 0.1 \mu\text{m}$  radius). The impactors have been installed on the deck above the bridge.

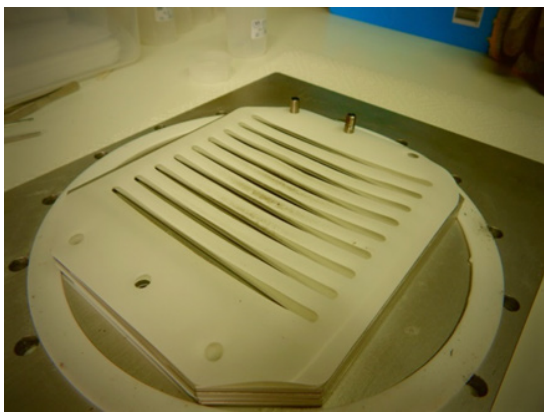


Fig. 7.3: Slotted Teflon foil with particles

3 days of sampling over the North Atlantic and 5 days of sampling over the South Atlantic are necessary to collect enough  $\text{NH}_4\text{-N}$  and  $\text{SO}_4\text{-S}$  for isotope analyses for the different particle size ranges.

All filter samples have been stored in PE-bottles at a temperature of  $4 \text{ }^\circ\text{C}$ .

### Expected Results

The samples will be analysed at home in order to get the  $\text{NH}_3\text{-}$  and the  $\text{NH}_4\text{-}$ concentration and N-isotope ratio.

### Data management

The data observed on board will be stored at PANGAEA database.

## 8. EN-ROUTE TEST OF UPGRADED SHIP DATA MANAGEMENT SYSTEM DSHIP

Peter Gerchow<sup>1</sup> Carsten Schirnick<sup>2</sup>,  
Ralf Günther<sup>3</sup>, Ralf Löwenberg<sup>3</sup>,  
Tim Tomczak<sup>3</sup>

<sup>1</sup>AWI  
<sup>2</sup>GEOMAR  
<sup>3</sup>WERUM

**Grant No AWI\_PS102\_00**

### Objectives

The ship data management system DSHIP from firm WERUM was upgraded to version 3 during ship yard time of *Polarstern* in October/November 2016. The database of previous version has been transferred and adjusted to the new version.

### Work at sea

As the old version shall run as backup, some sensor interfaces must be doubled to provide data to both versions. During the cruise all associated sensors and devices had been switched on to acquire data as usual. The correct receive and storage of these data has been supervised. All tools (e.g. station book, etc.) have been tested and used under real conditions.

As the new version provides more functionality and a more specific device description, these additional properties have been registered in the database. Adjustments of configuration and runtime settings as well as the completion of variable settings have been performed.

The nautical officers got lectures for the new graphical user interface and for operating the new features like station book.

### Data management

The upgrade of Dship system could be finished successfully. The previously version is already running in parallel as backup system. The old version will be deinstalled when the new system is running stable over a longer period.

## 9. TEST OF NEW SEA WATER SUPPLY AND TEST OF ATTACHED SENSORS

Ralf Krockner<sup>1</sup>, Martina Gehrung<sup>2</sup>, Stefan Raimund<sup>3</sup>,  
Sören Krägefsky<sup>1</sup> (not on board)

<sup>1</sup>AWI  
<sup>2</sup>HZG  
<sup>3</sup>SubCtech

**Grant No AWI\_PS102\_00**

### Objectives

During shipyard time of *Polarstern* in May/June 2016 the room G-707 was arranged to be laboratory for water analysis by devices FerryBox from firm 4H-Jena as well as pCO<sub>2</sub> analyzers from firm General Oceanics and from firm SubCtech respectively. During ship yard time in October/November 2016 these installations had been finished and scientific devices had been relocated from the previous place, namely wet-laboratory 1, to the new room. These arrangements were recommended to significantly reduce length of pipes providing sea water and finally to reduce possible chemical or physical processes within sea water prior to the analyzers.

The FerryBox system is analyzing biological parameters of seawater. To avoid damage of cells and organisms by rotary pump a bypass was installed providing seawater alternatively by membrane pump. The oscillating pressure of seawater caused by membrane pump is minimized by downstreamed snubber.

During ship yard time the usual operation of the systems cannot be executed, because the harbour water is polluted by sediments and other particles. A temporarily installed provisory fresh water supply allowed only rudimentary flow tests.

### Work at sea

The correct installation of sea water supply, fresh water supply, reference gases and network connections has been tested under real conditions. The several valves have been adjusted to provide sea water with appropriate flow rate and pressure for each analyzer. The tests have been performed using membrane pump. The provisionally installed rotary pump will be replaced by a more powerful one after the cruise. To externally acquire primary data of OceanPack pCO<sub>2</sub> analyzer for data analysis an additional interface as well as data server (Laptop) was installed. The crew was instructed and short manuals were delivered on how to switch on and off the systems. Data management (see below) was successfully tested.

### Preliminary (expected) results

The sea water supply could be tested successfully. The pressure variations produced by membrane pump are nearly eliminated by snubber. The adjustment of snubber needs to be supervised and adjusted periodically. Pressure regulators for seawater as well as for reference gases will additionally be installed to avoid pressure surges / peaks which may damage the systems. During following cruise PS103 sea water analysis will be performed, to assess the influence of both types of pumps (rotary and membrane) on the biological properties measured by the systems.

### Data management

The data management of FerryBox by means of data delivery to ship data management system and online delivery via satellite to be presented on onshore portal has been successfully tested.

## 10. INTEGRATION OF NEW MOTION SENSOR IXBLUE HYDRINS (PART 2)

Ralf Krockner<sup>1</sup>, Johannes Kässbohrer<sup>2</sup>

<sup>1</sup>AWI

<sup>2</sup>FIELAX

**Grant No AWI\_PS102\_00**

### **Objectives**

During ship yard time of *Polarstern* in May/June 2016 two new motion sensors of type HYDRINS from firm IXBLUE were installed to replace existing sensors MINS from firm Raytheon Anschütz. The provision of motion data for hydroacoustic sensors was already performed in June. As the number of output interfaces of HYDRINS devices is limited, not all necessary data formats for recipient devices could directly be provided. For this reason interface boxes have been created by firm FIELAX to duplicate and reformat the output strings of the motion sensor for the associated recipients.

### **Work at sea**

As converter boxes have been installed, all sensors receiving new established input data streams. All these systems have been operated to test and confirm the correct receive of input data. The correct functionality of all associated sensors and devices could be confirmed.

The HYDRINS sensors have been registered in Dship system to be the new source for motion data.

### **Data management**

All necessary data streams can be provided from both motion sensors HYDRINS 1 and HYDRINS 2. Data streams which are not directly provided by motion sensors are converted and provided by appropriate interface box.

No device/sensor is receiving data from previously installed sensors of type MINS / MINS interface anymore, but interfaces still exists as backup. Both MINS sensors will stay on board as backup at least during next arctic season.

## **11. ACKNOWLEDGEMENTS**

We would like to express our gratitude to the AWI, POGO, SMART, and the Nippon foundation for supplying past research as well as funding and facilitating the North South Atlantic Training Transect 2016. We would like to offer our sincerest thanks to Captain Wunderlich and all the crew, who helped make this a wonderful, enriching and enjoyable cruise. We are very grateful to all the teaching/instructors and technical staff who made this cruise an interesting, fun and inspiring learning platform. We are deeply indebted to chief scientist, Professor Dr. Karen Wiltshire for the educational programme and for her constant support and encouragement.

## **APPENDIX**

- A.1 Teilnehmende Institute / Participating Institutions**
- A.2 Teilnehmer / Participants**
- A.3 Schiffsbesatzung / Ship's Crew**
- A.4 Stationsliste PS102 / Station List PS102**

## A.1 TEILNEHMENDEINSTITUTE/PARTICIPATINGINSTITUTIONS

	<b>Address</b>
AWI	Alfred-Wegener-Institut Helmholtz-Zentrum für Polar- und Meeresforschung Am Handelshafen 12 27570 Bremerhaven Germany
CAU	Christain-Albrechts-Universität Kiel Christian-Albrechts-Platz 4 24118 Kiel Germany
DWD	Deutscher Wetterdienst Geschäftsbereich Wettervorhersage Seeschiffahrtsberatung Bernhard Nocht Str. 76 20359 Hamburg Germany
FIELAX	FIELAX Gesellschaft für wissenschaftliche Datenverarbeitung mbH Schleusenstr. 14 D-27568 Bremerhaven Germany
FUB	Freie Universität Berlin Kaiserswerther Str. 16-18 14195 Berlin Germany
GAUG	Georg-August-Universität Göttingen Wilhelmsplatz 1 37073 Göttingen Germany
GEOMAR	GEOMAR Helmholtz-Zentrum für Ozeanforschung Kiel Wischhofstr. 1-3 24148 Kiel Germany
HZG	Helmholtz-Zentrum Geesthacht Zentrum für Material- und Küstenforschung Max-Planck-Straße 1 21502 Geesthacht Germany

---

	<b>Address</b>
JUB	Jacobs University Bremen Campus Ring 1 28759 Bremen Germany
MPI-M	Max Planck Institute for Meteorology Bundesstrasse 53 20146 Hamburg Germany
NU	Northumbria University 2 Ellison Pl NE1 8ST Newcastle upon Tyne United Kingdom
NUIG	National University of Ireland Galway, University Road, Galway Ireland
PU	Plymouth University Drake Circus PL4 8AA Plymouth United Kingdom
RSHU	Russian State Hydrometeorological University Malookhtinskaya naberezhnaya 98 St Petersburg Russia
SubCtech	SubCtech GmbH Wellseedamm 3 24145 Kiel Germany
TROPOS	Leibniz Institute for Tropospheric Research Permoserstrasse 15 04318 Leipzig Germany
UAlg	University of the Algarve Campus da Penha, 8005-139 Faro Portugal

	<b>Address</b>
UAlex	Alexandria University El-Gaish Rd Alexandria Egypt
UdA	Universidade dos Acores Ladeira da Mãe de Deus 9501-855 Ponta Delgada Portugal
UdBA	Universidad de Buenos Aires Viamonte 430 1053 Buenos Aires Argentina
UCC	University College Cork Western Road Cork Ireland
UGhent	University Ghent St. Pietersnieuwstraat 33 9000 Gent Belgium
UHB	Universität Bremen Bibliothekstraße 1 28359 Bremen Germany
UiT	Universitetet i Tromsø Hansine Hansen veg 18 9019 Tromsø Norway
UKlaip	Klaipėda University Herkus Mantas str. 84 LT-92294 Klaipėda Lithuania
UKeny	UKeny University Kenyatta Kenya Drive Nairobi City Kenya
Uni Oviedo	University Oviedo Calle San Francisco, 1, 33003 Oviedo, Asturia Spain

	<b>Address</b>
UPD	University of the Philippines Dillman Diliman Quezon City 1101 Metro Manila Philippines
UPMC	University Pierre et Marie Curie 4 Place Jussieu 75005 Paris, France
UPVD	University of Perpignan Via Domitia 52 Av. Paul Alduy 66100 Perpignan France
UWien	University of Vienna Universitätsring 1 1010 Wien Austria
WERUM	WERUM Software & Systems AG Wulf-Werum-Str. 3 21337 Lüneburg Germany
WWU	Westfälische Wilhelms-Universität Schlossplatz 2 48149 Münster Germany
ZEU	Zhejiang University 38 Zheda Rd, Xihu 310027 Hangzhou, Zhejiang China

## A.2 FAHRTTEILNEHMER / CRUISE PARTICIPANTS

### LEG1

<b>Name/ Last name</b>	<b>Vorname/ First name</b>	<b>Institut/ Institute</b>	<b>Beruf/ Profession</b>	<b>Discipline/ Fachrichtung</b>
Wiltshire	Karen	AWI	Chief Scientist	Oceanography
Lemke	Peter	AWI	Scientist	Physics
Adeleye	Adedayo	ZEU	Student	Chemistry
Amorim	Katherine	UAlg/ CAU	Student	Biology
Brodte	Eva-Maria	AWI	Scientist	Biology
Carstens	Kristine	AWI	Technician	Biology
Copeland	William	UiT	Student	Oceanography
Cronin	Abigail	UCC	Student	Oceanography
Croot	Peter	NUIG	Scientist	Oceanography
Curran	Michelle	NUIG	Student	Physics
Daly	Eoghan	NUIG	Student	Biology
Deschepper	Inge	Galway Mayo Institute of Technology & UGhent	Student	Oceanography
Ehrhardt	Sophie	UHB	Student	Geosciences
Espinosa Lagunes	Carla	UHB	Student	Chemistry
Fiedler	Stephanie	MPI-M	Scientist	Physics
Gajigan	Andrian	UPD	Student	Oceanography
Garcia- Vazquez	Eva	Uni Oviedo	Scientist	Biology
Gehrung	Martina	HZG	Engineer	Logistics
Geisen	Carla	UPMC	Student	Biology
Gerchow	Peter	AWI	Engineer	Logistics
Giunta	Valeria	UdBA	Student	Oceanography
Goedecke	Julia	GAUG	Student	Chemistry
Gregory	Clynton	NUIG	Student	Biology
Günther	Ralf	WERUM	Engineer	Logistics
Haarig	Moritz	TROPOS	Scientist	Physics
Höpker	Sebastian	UHB	Student	Geosciences
Kaessbohrer	Johannes	FIELAX	Engineer	Logistics
Kalesse	Heike	TROPOS	Scientist	Physics
Keck	Therese	FUB	Scientist	Physics
Krocker	Ralf	AWI	Scientist	Logistics
Löwenberg	Ralf	WERUM	Engineer	Logistics
Maarouf	Rabie	UAlex	Student	Geosciences
Magalhães Loureiro	Clara	UdA	Student	Biology
Miller	Max	DWD	Technician	Meteorology
O'Donovan	Sarit	UAlg	Student	Oceanography

<b>Name/ Last name</b>	<b>Vorname/ First name</b>	<b>Institut/ Institute</b>	<b>Beruf/ Profession</b>	<b>Discipline/ Fachrichtung</b>
O'Sullivan	Hugh	PU	Student	Biology
Playford	Lionel	NU	Photographer	Public outreach
Raimund	Stefan	SubCtech	Engineer	Logistics
Reichardt	Aurelia	UHB	Student	Biology
Rick	Johannes	AWI	Scientist	Biology
Ruhtz	Thomas	FUB	Scientist	Physics
Sagero	Philip	UKeny	Student	Chemistry
Sarker	Subrata	JUB	Student	Biology
Schirnack	Carsten	GEOMAR	Engineer	Logistics
Schlacke	Sabine	WWU	Scientist	Legal profession
Shestakova	Elena	RSHU	Student	Oceanography
Sonnabend	Hartmut	DWD	Scientist	Meteorology
Thabet	Walaa	UAlex	Student	Chemistry
Tomczak	Tim	WERUM	Engineer	Logistics
Wilson	Annette	AWI	Scientist	Oceanography
Witte- Gaedeke	Heidi	GAUG	Scientist	Chemistry
Yirgaw	Daniel Gebregiorgis	GEOMAR	Student	Geosciences
Zaiko	Anastasija	UKlaip	Scientist	Biology
Zambalos	Helena	UWien	Student	Biology

**LEG2**

<b>Name/ Last name</b>	<b>Vorname/ First name</b>	<b>Institut/ Institute</b>	<b>Beruf/ Profession</b>	<b>Discipline/ Fachrichtung</b>
Wiltshire	Karen	AWI	Chief Scientist	Oceanography
Lemke	Peter	AWI	Scientist	Physics
Adeleye	Adedayo	ZEU	Student	Chemistry
Amorim	Katherine	UAlg/ CAU	Student	Biology
Brodte	Eva-Maria	AWI	Scientist	Biology
Carstens	Kristine	AWI	Technician	Biology
Copeland	William	UiT	Student	Oceanography
Cronin	Abigail	UCC	Student	Oceanography
Croot	Peter	NUIG	Scientist	Oceanography
Curran	Michelle	NUIG	Student	Physics
Daly	Eoghan	NUIG	Student	Biology
Deschepper	Inge	Galway Mayo Institute of Technology & UGhent	Student	Oceanography
Ehrhardt	Sophie	UHB	Student	Geosciences
Espinosa Lagunes	Carla	UHB	Student	Chemistry
Fiedler	Stephanie	MPI-M	Scientist	Physics
Gajigan	Andrian	UPD	Student	Oceanography
Garcia- Vazquez	Eva	Uni Oviedo	Scientist	Biology
Geisen	Carla	UPMC	Student	Biology
Giunta	Valeria	UdBA	Student	Oceanography
Goedecke	Julia	GAUG	Student	Chemistry
Gregory	Clynton	NUIG	Student	Biology
Haarig	Moritz	TROPOS	Scientist	Physics
Höpker	Sebastian	UHB	Student	Geo sciences
Kalesse	Heike	TROPOS	Scientist	Physics
Kuster	Ulrich	FU Berlin	Scientist	Physics
Maarouf	Rabie	UAlex	Student	Geo sciences
Magalhães Loureiro	Clara	UdA	Student	Biology
Miller	Max	DWD	Technician	Meteorology
O'Donovan	Sarit	UAlg	Student	Oceanography
O'Sullivan	Hugh	PU	Student	Biology
Playford	Lionel	NU	Photographer	Public outreach
Preusker	Rene	FUB	Scientist	Physics
Reichardt	Aurelia	UHB	Student	Biology
Rick	Johannes	AWI	Scientist	Biology
Sagero	Philip	UKeny	Student	Chemistry
Sarker	Subrata	JUB	Student	Biology
Schlacke	Sabine	WWU	Scientist	Legal profession

<b>Name/ Last name</b>	<b>Vorname/ First name</b>	<b>Institut/ Institute</b>	<b>Beruf/ Profession</b>	<b>Discipline/ Fachrichtung</b>
Shestakova	Elena	RSHU	Student	Oceanography
Sonnabend	Hartmut	DWD	Scientist	Meteorology
Thabet	Walaa	UAlex	Student	Chemistry
Witte- Gaedeke	Heidi	GAUG	Scientist	Chemistry
Yirgaw	Daniel Gebregiorgis	GEOMAR	Student	Geosciences
Zaiko	Anastasija	UKlaip	Scientist	Biology
Zambalos	Helena	UWien	Student	Biology

### A.3 SCHIFFSBESATZUNG / SHIP'S CREW

No.	Name	Rank
01	Wunderlich, Thomas	Master
02	Lauber, Felix	1. Offc.
03	Ziemann, Olaf	Ch. Eng.
04	Spielke, Steffen	2. Offc.
05	Kentges, Felix	2. Offc.
06	Peine, Lutz	3. Offc.
07	Scholl, Thomas	Doctor
08	Hofmann, Jörg	R. Offc.
09	Schnürch, Helmut	2. Eng.
10	Buch, Erik Torsten	2. Eng.
11	Rusch, Torben	2. Eng.
12	Brehme, Andreas	Elec. Eng.
13	Ganter, Armin	ELO
14	Markert, Winfried	ELO
15	Winter, Andreas	ELO
16	Feiertag, Thomas	ELO
17	Schröter, Rene	Boatsw.
18	Neisner, Winfried	Carpenter
19	Clasen, Nils	A.B.
20	Schröder, Norbert	A.B.
21	Burzan, Gerd-Ekkehard	A.B.
22	Hartwig-Labahn, Andreas	A.B.
23	Fölster, Michael	A.B.
24	Müller, Steffen	A.B.
25	Brickmann, Peter	A.B.
26	Sedlak, Andreas	A.B.
27	Beth, Detlef	Storek.
28	Plehn, Markus	Mot-man
29	Klein, Gert	Mot-man
30	Krösche, Eckard	Mot-man
31	Dinse, Horst	Mot-man
32	Watzel, Bernhard	Mot-man
33	Meißner, Jörg	Cook
34	Tupy, Mario	Cooksmate
35	Möller, Wolfgang	Cooksmate
36	Wartenberg, Irina	1. Stwdess
37	Schwitzky-Schwarz, Carmen	Stwdess/N.
38	Hischke, Peggy	2. Stwdess
39	Grigull, Elke	2. Steward
40	Krause, Tomasz	2. Stwdess
41	Hu, Guo Yong	2. Steward
42	Chen, Quan Lun	2. Stwdess
43	Ruan, Hui Guang	Laundrym.

## A.4 STATIONSLISTE / STATION LIST PS102

Station	Date	Time	Latitude	Longitude	Depth (m)	Gear	Action	Comments
PS102_0_Underway-1	2016-11-14	08:30	50,25997	-1,57161	57,00000	ADCP_150	profile start	
PS102_0_Underway-1	2016-12-11	12:12	-33,85925	18,44498	14,60000	ADCP_150	profile end	
PS102_0_Underway-2	2016-11-15	09:25	48,32809	-7,66701	176,00000	FBOX	profile start	
PS102_0_Underway-2	2016-11-20	21:00	29,45393	-15,11848	3574,00000	FBOX	profile end	
PS102_0_Underway-2	2016-11-21	17:45	27,57490	-15,32500	2141,00000	FBOX	profile start	
PS102_0_Underway-2	2016-12-10	14:07	-32,04142	15,45743	2027,00000	FBOX	profile end	
PS102_0_Underway-3	2016-11-15	09:48	48,28265	-7,78059	174,00000	TSG_KEEL	profile start	
PS102_0_Underway-3	2016-11-20	21:40	29,36829	-15,13011	3576,00000	TSG_KEEL	profile end	
PS102_0_Underway-3	2016-11-21	15:13	27,96556	-15,22788	1062,00000	TSG_KEEL	profile start	
PS102_0_Underway-3	2016-12-11	06:12	-33,48141	17,78953	173,00000	TSG_KEEL	profile end	
PS102_0_Underway-4	2016-11-13	09:00	52,90636	3,25105	31,60000	PCO2_GO	profile start	
PS102_0_Underway-4	2016-11-20	22:10	29,30384	-15,13862	3574,00000	PCO2_GO	profile end	
PS102_0_Underway-4	2016-11-21	17:45	27,57490	-15,32500	2141,00000	PCO2_GO	profile start	
PS102_0_Underway-4	2016-12-02	12:00	-7,23432	-4,17480	4358,00000	PCO2_GO	profile end	
PS102_0_Underway-5	2016-11-12	11:40	53,83026	8,08616	15,10000	PCO2_SUB	profile start	
PS102_0_Underway-5	2016-11-20	21:00	29,45393	-15,11848	3574,00000	PCO2_SUB	profile end	
PS102_0_Underway-5	2016-11-21	17:45	27,57490	-15,32500	2141,00000	PCO2_SUB	profile start	
PS102_0_Underway-5	2016-12-10	14:07	-32,04219	15,45869	2026,00000	PCO2_SUB	profile end	
PS102_0_Underway-6	2016-11-12	09:00	53,56819	8,55368	15,60000	WST	profile start	
PS102_0_Underway-7	2016-11-12	09:00	53,56819	8,55368	15,60000	OCEANET	profile start	
PS102_0_Underway-7	2016-11-21	03:00	28,68895	-15,22028	3585,00000	OCEANET	profile end	
PS102_0_Underway-7	2016-11-21	16:45	27,72319	-15,20881	1904,00000	OCEANET	profile start	
PS102_0_Underway-7	2016-12-09	21:00	-30,60148	13,21195	3226,00000	OCEANET	profile end	
PS102_0_Underway-8	2016-11-12	09:00	53,56819	8,55368	15,60000	SPM	profile start	

**A.4 Stationsliste / Station List PS102**

Station	Date	Time	Latitude	Longitude	Depth (m)	Gear	Action	Comments
PS102_0_Underway-8	2016-12-09	21:00	-30,60148	13,21195	3226,00000	SPM	profile end	
PS102_0_Underway-9	2016-11-12	09:00	53,56819	8,55368	15,60000	UAS	profile start	
PS102_0_Underway-9	2016-12-11	06:16	-33,48643	17,79758	171,00000	UAS	profile end	
PS102_0_Underway-10	2016-11-12	09:00	53,56819	8,55368	15,60000	UWS	profile start	
PS102_0_Underway-10	2016-12-10	07:00	-31,48571	14,56727	2704,00000	UWS	profile end	
PS102_1-1	2016-11-15	07:03	48,58481	-7,02308	143,00000	BUCKET	station start	
PS102_2-1	2016-11-15	13:38	47,92866	-8,65788	2035,00000	CTDOZE	station start	
PS102_2-1	2016-11-15	14:17	47,92739	-8,65945	1970,00000	CTDOZE	at depth	
PS102_2-1	2016-11-15	15:11	47,92810	-8,66094	1940,00000	CTDOZE	station end	
PS102_2-2	2016-11-15	15:23	47,92804	-8,65980	1972,00000	PLA	station start	
PS102_2-2	2016-11-15	15:34	47,92731	-8,66080	1936,00000	PLA	at depth	
PS102_2-2	2016-11-15	15:46	47,92702	-8,66005	1951,00000	PLA	station end	
PS102_3-1	2016-11-16	08:00	45,36610	-10,39930	3013,00000	BUCKET	station start	
PS102_4-1	2016-11-16	19:49	43,49997	-11,62777	5031,00000	CTDOZE	station start	
PS102_4-1	2016-11-16	21:30	43,50087	-11,63216	5022,00000	CTDOZE	at depth	
PS102_4-1	2016-11-16	23:37	43,50225	-11,63573	5022,00000	CTDOZE	station end	
PS102_4-2	2016-11-16	23:48	43,50286	-11,63546	5022,00000	PLA	station start	
PS102_4-2	2016-11-16	23:58	43,50208	-11,63546	5021,00000	PLA	at depth	
PS102_4-2	2016-11-17	00:08	43,50205	-11,63541	5024,00000	PLA	station end	
PS102_5-1	2016-11-17	08:00	42,17884	-12,01425	5692,00000	BUCKET	station start	
PS102_6-1	2016-11-18	07:59	38,28080	-13,10979	NA	BUCKET	station start	
PS102_7-1	2016-11-19	00:43	35,50050	-13,85359	4821,00000	CTDOZE	station start	
PS102_7-1	2016-11-19	02:15	35,49660	-13,84810	4824,00000	CTDOZE	at depth	
PS102_7-1	2016-11-19	04:04	35,49131	-13,84074	4829,00000	CTDOZE	station end	
PS102_7-2	2016-11-19	04:11	35,49091	-13,84041	4828,00000	PLA	station start	
PS102_7-2	2016-11-19	04:14	35,49075	-13,84029	4829,00000	PLA	at depth	
PS102_7-2	2016-11-19	04:33	35,48983	-13,83913	4824,00000	PLA	station end	
PS102_8-1	2016-11-19	08:01	34,92230	-13,98329	4128,00000	BUCKET	station start	
PS102_9-1	2016-11-20	08:01	30,96739	-14,84066	3699,00000	BUCKET	station start	
PS102_10-1	2016-11-20	14:02	29,99356	-15,04459	3312,00000	CTDOZE	station start	
PS102_10-1	2016-11-20	15:10	29,99234	-15,04483	3315,00000	CTDOZE	at depth	
PS102_10-1	2016-11-20	16:24	29,99647	-15,04379	3311,00000	CTDOZE	station end	
PS102_10-2	2016-11-20	16:29	29,99615	-15,04342	3312,00000	PLA	station start	
PS102_10-2	2016-11-20	16:43	29,99620	-15,04235	3309,00000	PLA	at depth	
PS102_10-2	2016-11-20	16:56	29,99581	-15,04136	NA	PLA	station end	
PS102_11-1	2016-11-22	10:59	25,81808	-17,97913	3310,00000	BUCKET	station start	
PS102_11-2	2016-11-22	11:03	25,81465	-17,98431	3309,00000	XBT	station start	
PS102_11-2	2016-11-22	11:04	25,81447	-17,98454	3308,00000	XBT	profile start	
PS102_11-2	2016-11-22	11:11	25,80872	-17,99328	3302,00000	XBT	profile end	
PS102_12-1	2016-11-23	10:57	22,58354	-20,56343	4156,00000	XBT	station start	

Station	Date	Time	Latitude	Longitude	Depth (m)	Gear	Action	Comments
PS102_12-1	2016-11-23	10:58	22,58324	-20,56355	4156,00000	XBT	profile start	
PS102_12-1	2016-11-23	11:04	22,57313	-20,56753	4155,00000	XBT	profile end	
PS102_12-2	2016-11-23	11:10	22,56951	-20,56345	4156,00000	XBT	station start	
PS102_12-2	2016-11-23	11:10	22,56951	-20,56345	4156,00000	XBT	profile start	
PS102_12-2	2016-11-23	11:17	22,57432	-20,55557	4149,00000	XBT	profile end	
PS102_12-3	2016-11-23	11:19	22,57596	-20,55279	4150,00000	BUCKET	station start	
PS102_13-1	2016-11-24	10:56	18,34763	-21,45144	3115,00000	XBT	station start	
PS102_13-1	2016-11-24	10:56	18,34773	-21,45136	3116,00000	XBT	profile start	
PS102_13-1	2016-11-24	11:04	18,35371	-21,44342	3114,00000	XBT	profile end	
PS102_13-2	2016-11-24	11:05	18,35507	-21,44136	3114,00000	BUCKET	station start	
PS102_14-1	2016-11-25	06:41	14,63955	-20,99670	4242,00000	XBT	station start	
PS102_14-1	2016-11-25	06:43	14,63736	-20,99646	4243,00000	XBT	profile start	
PS102_14-1	2016-11-25	06:48	14,62950	-20,99514	4244,00000	XBT	profile end	
PS102_14-2	2016-11-25	06:53	14,62169	-20,99472	4247,00000	BUCKET	station start	
PS102_15-1	2016-11-25	07:27	14,55285	-20,98533	4247,00000	CTDOZE	station start	
PS102_15-1	2016-11-25	08:53	14,55696	-20,98812	4251,00000	CTDOZE	at depth	
PS102_15-1	2016-11-25	10:28	14,56128	-20,98810	4252,00000	CTDOZE	station end	
PS102_15-2	2016-11-25	10:37	14,56180	-20,98801	4252,00000	PLA	station start	
PS102_15-2	2016-11-25	10:43	14,56235	-20,98794	4253,00000	PLA	at depth	
PS102_15-2	2016-11-25	10:50	14,56301	-20,98776	4252,00000	PLA	station end	
PS102_16-1	2016-11-26	10:58	10,15662	-20,05012	4695,00000	XBT	station start	
PS102_16-1	2016-11-26	10:58	10,15686	-20,05009	4696,00000	XBT	profile start	
PS102_16-1	2016-11-26	11:04	10,16712	-20,04971	4715,00000	XBT	profile end	
PS102_16-2	2016-11-26	11:06	10,17002	-20,04979	4721,00000	BUCKET	station start	
PS102_16-3	2016-11-26	11:19	10,15867	-20,05208	4703,00000	UCTD	station start	
PS102_16-3	2016-11-26	11:19	10,15837	-20,05201	4701,00000	UCTD	profile start	
PS102_16-3	2016-11-26	11:23	10,14683	-20,04969	4682,00000	UCTD	at depth	
PS102_16-3	2016-11-26	11:45	10,09224	-20,03560	4638,00000	UCTD	profile end	
PS102_16-3	2016-11-26	11:45	10,09182	-20,03546	4638,00000	UCTD	station end	
PS102_17-1	2016-11-26	20:56	8,48062	-19,46613	4497,00000	CTDOZE	station start	
PS102_17-1	2016-11-26	22:23	8,48235	-19,46458	4497,00000	CTDOZE	at depth	
PS102_17-1	2016-11-26	23:58	8,48279	-19,46588	4497,00000	CTDOZE	station end	
PS102_17-2	2016-11-27	00:04	8,48272	-19,46588	4497,00000	PLA	station start	
PS102_17-2	2016-11-27	00:17	8,48345	-19,46587	4497,00000	PLA	at depth	
PS102_17-2	2016-11-27	00:31	8,48385	-19,46532	4497,00000	PLA	station end	
PS102_18-1	2016-11-27	10:55	6,82217	-18,58980	4702,00000	XBT	station start	
PS102_18-1	2016-11-27	10:56	6,82195	-18,58967	4702,00000	XBT	profile start	
PS102_18-1	2016-11-27	11:02	6,81319	-18,58517	4701,00000	XBT	profile end	
PS102_18-2	2016-11-27	11:05	6,80974	-18,58306	4703,00000	BUCKET	station start	
PS102_19-1	2016-11-27	16:39	5,86858	-18,08578	4758,00000	UCTD	station start	
PS102_19-1	2016-11-27	16:58	5,81472	-18,05757	4969,00000	UCTD	station end	
PS102_20-1	2016-11-28	11:00	2,83307	-16,48798	4761,00000	XBT	station start	
PS102_20-1	2016-11-28	11:00	2,83247	-16,48765	4762,00000	XBT	profile start	
PS102_20-1	2016-11-28	11:03	2,82860	-16,48561	4762,00000	XBT	profile end	

A.4 Stationsliste / Station List PS102

Station	Date	Time	Latitude	Longitude	Depth (m)	Gear	Action	Comments
PS102_20-2	2016-11-28	11:04	2,82766	-16,48511	4762,00000	BUCKET	station start	
PS102_20-2	2016-11-28	11:09	2,82089	-16,48153	4761,00000	BUCKET	station end	
PS102_20-3	2016-11-28	11:10	2,81994	-16,48103	4762,00000	XBT	station start	
PS102_20-3	2016-11-28	11:11	2,81897	-16,48052	4761,00000	XBT	profile start	
PS102_20-4	2016-11-28	11:17	2,81071	-16,47600	4759,00000	XBT	station start	
PS102_20-4	2016-11-28	11:17	2,81057	-16,47593	4759,00000	XBT	profile start	
PS102_20-4	2016-11-28	11:24	2,80207	-16,47150	4758,00000	XBT	profile end	
PS102_21-1	2016-11-28	16:32	1,98998	-16,04508	5159,00000	UCTD	station start	
PS102_21-1	2016-11-28	16:53	1,93733	-16,01708	4641,00000	UCTD	station end	
PS102_22-1	2016-11-29	05:27	0,00045	-15,00135	3775,00000	CTDOZE	station start	
PS102_22-1	2016-11-29	06:47	0,00009	-15,00127	3775,00000	CTDOZE	at depth	
PS102_22-1	2016-11-29	08:23	0,00067	-15,00107	3774,00000	CTDOZE	station end	
PS102_22-2	2016-11-29	08:29	0,00060	-15,00117	3774,00000	PLA	station start	
PS102_22-2	2016-11-29	08:45	0,00137	-15,00341	3774,00000	PLA	at depth	
PS102_22-2	2016-11-29	08:57	0,00268	-15,00510	3773,00000	PLA	station end	
PS102_23-1	2016-11-29	10:57	-0,14017	-14,79067	4065,00000	XBT	station start	
PS102_23-1	2016-11-29	10:58	-0,14039	-14,79038	4064,00000	XBT	profile start	
PS102_23-1	2016-11-29	11:04	-0,14465	-14,78386	4063,00000	XBT	profile end	
PS102_23-2	2016-11-29	11:05	-0,14580	-14,78222	4059,00000	BUCKET	station start	
PS102_24-1	2016-11-29	16:35	-0,63921	-14,04625	3982,00000	UCTD	station start	
PS102_24-1	2016-11-29	17:05	-0,68572	-13,97639	3658,00000	UCTD	station end	
PS102_25-1	2016-11-30	10:56	-2,44019	-11,35760	3466,00000	XBT	station start	
PS102_25-1	2016-11-30	10:56	-2,44026	-11,35748	3466,00000	XBT	profile start	
PS102_25-1	2016-11-30	11:02	-2,44524	-11,35001	3550,00000	XBT	profile end	
PS102_25-2	2016-11-30	11:04	-2,44692	-11,34750	3551,00000	BUCKET	station start	
PS102_26-1	2016-11-30	16:24	-2,96419	-10,57430	3546,00000	UCTD	station start	
PS102_26-1	2016-11-30	16:49	-3,00582	-10,51252	3586,00000	UCTD	station end	
PS102_27-1	2016-12-01	10:55	-4,78496	-7,85078	3663,00000	XBT	station start	
PS102_27-1	2016-12-01	10:55	-4,78507	-7,85062	3663,00000	XBT	profile start	
PS102_27-1	2016-12-01	11:01	-4,79091	-7,84220	3798,00000	XBT	profile end	
PS102_27-2	2016-12-01	11:03	-4,79278	-7,83936	3823,00000	BUCKET	station start	
PS102_28-1	2016-12-01	16:29	-5,31179	-7,06142	3963,00000	UCTD	station start	
PS102_28-1	2016-12-01	16:50	-5,34731	-7,00897	3987,00000	UCTD	station end	
PS102_29-1	2016-12-03	09:56	-9,37460	-0,94707	5566,00000	XBT	station start	
PS102_29-1	2016-12-03	09:56	-9,37469	-0,94692	5565,00000	XBT	profile start	
PS102_29-1	2016-12-03	10:02	-9,38019	-0,93881	5567,00000	XBT	profile end	
PS102_29-2	2016-12-03	10:03	-9,38142	-0,93681	5568,00000	BUCKET	station start	
PS102_30-1	2016-12-03	16:30	-9,99957	0,00010	5570,00000	CTDOZE	station start	
PS102_30-1	2016-12-03	18:21	-10,00058	-0,00015	5570,00000	CTDOZE	at depth	
PS102_30-1	2016-12-03	20:16	-10,00084	-0,00119	5571,00000	CTDOZE	station end	
PS102_30-2	2016-12-03	20:22	-10,00085	-0,00143	5571,00000	PLA	station start	
PS102_30-2	2016-12-03	20:30	-10,00088	-0,00137	5570,00000	PLA	at depth	
PS102_30-2	2016-12-03	20:39	-10,00105	-0,00168	5571,00000	PLA	station end	
PS102_31-1	2016-12-04	09:53	-11,99570	1,21414	5552,00000	XBT	station start	

Station	Date	Time	Latitude	Longitude	Depth (m)	Gear	Action	Comments
PS102_31-1	2016-12-04	09:53	-11,99587	1,21424	5554,00000	XBT	profile start	
PS102_31-1	2016-12-04	10:00	-12,00445	1,21916	5549,00000	XBT	profile end	
PS102_31-2	2016-12-04	10:03	-12,00786	1,22127	5552,00000	BUCKET	station start	
PS102_32-1	2016-12-05	09:55	-15,60358	3,43298	5479,00000	XBT	station start	
PS102_32-1	2016-12-05	09:55	-15,60373	3,43308	5478,00000	XBT	profile start	
PS102_32-1	2016-12-05	10:01	-15,61138	3,43747	5478,00000	XBT	profile end	
PS102_32-2	2016-12-05	10:05	-15,61617	3,44048	5478,00000	XBT	station start	
PS102_32-2	2016-12-05	10:05	-15,61639	3,44062	5478,00000	XBT	profile start	
PS102_32-2	2016-12-05	10:10	-15,62340	3,44532	5478,00000	XBT	profile end	
PS102_32-3	2016-12-05	10:12	-15,62598	3,44676	5477,00000	BUCKET	station start	
PS102_33-1	2016-12-06	08:53	-19,06913	5,60567	5285,00000	XBT	station start	
PS102_33-1	2016-12-06	08:53	-19,06920	5,60583	5285,00000	XBT	profile start	
PS102_33-1	2016-12-06	08:58	-19,07286	5,61324	5280,00000	XBT	profile end	
PS102_33-2	2016-12-06	09:01	-19,07512	5,61786	5278,00000	BUCKET	station start	
PS102_34-1	2016-12-06	14:20	-19,88730	6,11921	1965,00000	UCTD	station start	
PS102_34-1	2016-12-06	14:37	-19,93155	6,14735	3501,00000	UCTD	station end	
PS102_35-1	2016-12-06	16:47	-20,25004	6,35139	4710,00000	CTDOZE	station start	
PS102_35-1	2016-12-06	18:20	-20,24987	6,34998	4705,00000	CTDOZE	at depth	
PS102_35-1	2016-12-06	20:03	-20,25015	6,34968	4709,00000	CTDOZE	station end	
PS102_35-2	2016-12-06	20:11	-20,25018	6,34958	4708,00000	PLA	station start	
PS102_35-2	2016-12-06	20:23	-20,24953	6,34969	4702,00000	PLA	at depth	
PS102_35-2	2016-12-06	20:37	-20,24888	6,34965	4697,00000	PLA	station end	
PS102_36-1	2016-12-07	08:54	-22,21169	7,51512	2935,00000	XBT	station start	
PS102_36-1	2016-12-07	08:54	-22,21186	7,51545	2935,00000	XBT	profile start	
PS102_36-1	2016-12-07	09:01	-22,21631	7,52394	2938,00000	XBT	profile end	
PS102_36-2	2016-12-07	09:03	-22,21789	7,52729	2940,00000	BUCKET	station start	
PS102_37-1	2016-12-07	14:17	-23,04368	8,00966	4003,00000	UCTD	station start	
PS102_37-1	2016-12-07	14:34	-23,08775	8,03622	3731,00000	UCTD	station end	
PS102_38-1	2016-12-08	07:41	-25,83009	9,70094	7383,00000	CTDOZE	station start	
PS102_38-1	2016-12-08	09:14	-25,82946	9,70163	4651,00000	CTDOZE	at depth	
PS102_38-1	2016-12-08	10:58	-25,83052	9,70023	4652,00000	CTDOZE	station end	
PS102_38-2	2016-12-08	11:05	-25,83026	9,70011	4650,00000	PLA	station start	
PS102_38-2	2016-12-08	11:27	-25,82998	9,70019	4651,00000	PLA	at depth	
PS102_38-2	2016-12-08	11:46	-25,82886	9,70035	4650,00000	PLA	station end	
PS102_39-1	2016-12-08	14:23	-26,25261	9,97941	4669,00000	UCTD	station start	
PS102_39-1	2016-12-08	14:44	-26,30391	10,01337	4669,00000	UCTD	station end	
PS102_40-1	2016-12-09	06:59	-29,08815	11,88159	4016,00000	UCTD	station start	
PS102_40-1	2016-12-09	06:59	-29,08853	11,88183	4016,00000	UCTD	profile start	
PS102_40-1	2016-12-09	07:02	-29,09436	11,88576	4003,00000	UCTD	at depth	
PS102_40-1	2016-12-09	07:19	-29,13209	11,91114	3969,00000	UCTD	profile end	
PS102_40-1	2016-12-09	07:20	-29,13405	11,91258	3965,00000	UCTD	station end	
PS102_41-1	2016-12-09	08:57	-29,39514	12,09085	3832,00000	XBT	station start	
PS102_41-1	2016-12-09	08:57	-29,39528	12,09092	3835,00000	XBT	profile start	
PS102_41-1	2016-12-09	09:03	-29,40339	12,09601	3828,00000	XBT	profile end	

**A.4 Stationsliste / Station List PS102**

Station	Date	Time	Latitude	Longitude	Depth (m)	Gear	Action	Comments
PS102_41-1	2016-12-09	09:04	-29,40434	12,09642	3826,00000	XBT	station start	
PS102_41-2	2016-12-09	09:05	-29,40583	12,09627	3822,00000	BUCKET	station start	
PS102_42-1	2016-12-09	11:09	-29,70590	12,33940	3735,00000	CTDOZE	station start	
PS102_42-1	2016-12-09	12:25	-29,70478	12,34144	3734,00000	CTDOZE	at depth	
PS102_42-1	2016-12-09	13:54	-29,70451	12,34057	3734,00000	CTDOZE	station end	
PS102_42-2	2016-12-09	14:01	-29,70467	12,34043	3734,00000	PLA	station start	
PS102_42-2	2016-12-09	14:11	-29,70495	12,34047	3736,00000	PLA	at depth	
PS102_42-2	2016-12-09	14:23	-29,70519	12,34071	3733,00000	PLA	station end	

Gear ab breviations	Gear
ADCP_150	Vessel mounted Acoustic Doppler Current Profiler 150 kHz
BUCKET	Bucket Water Sampling
CTDOZE	CTD AWI-OZE
FBOX	FerryBox
OCEANET	Atmosphere Observatory
PCO2_GO	pCO2 GO
PCO2_SUB	pCO2 Subctech
PLA	Plankton Recorder / Net
SPM	Sun Photometer
TSG_KEEL	Thermosalinograph Keel
UAS	Underway Air Sampling
UCTD	Underway CTD
UWS	Underway Water Sampling
WST	Weatherstation
XBT	Expendable Bathythermograph

Die **Berichte zur Polar- und Meeresforschung** (ISSN 1866-3192) werden beginnend mit dem Band 569 (2008) als Open-Access-Publikation herausgegeben. Ein Verzeichnis aller Bände einschließlich der Druckausgaben (ISSN 1618-3193, Band 377-568, von 2000 bis 2008) sowie der früheren **Berichte zur Polarforschung** (ISSN 0176-5027, Band 1-376, von 1981 bis 2000) befindet sich im electronic Publication Information Center (**ePIC**) des Alfred-Wegener-Instituts, Helmholtz-Zentrum für Polar- und Meeresforschung (AWI); see <http://epic.awi.de>. Durch Auswahl "Reports on Polar- and Marine Research" (via "browse"/"type") wird eine Liste der Publikationen, sortiert nach Bandnummer, innerhalb der absteigenden chronologischen Reihenfolge der Jahrgänge mit Verweis auf das jeweilige pdf-Symbol zum Herunterladen angezeigt.

The **Reports on Polar and Marine Research** (ISSN 1866-3192) are available as open access publications since 2008. A table of all volumes including the printed issues (ISSN 1618-3193, Vol. 377-568, from 2000 until 2008), as well as the earlier **Reports on Polar Research** (ISSN 0176-5027, Vol. 1-376, from 1981 until 2000) is provided by the electronic Publication Information Center (**ePIC**) of the Alfred Wegener Institute, Helmholtz Centre for Polar and Marine Research (AWI); see URL <http://epic.awi.de>. To generate a list of all Reports, use the URL <http://epic.awi.de> and select "browse"/"type" to browse "Reports on Polar and Marine Research". A chronological list in declining order will be presented, and pdf icons displayed for downloading.

#### **Zuletzt erschienene Ausgaben:**

#### **Recently published issues:**

**713 (2017)** The Expedition PS102 of the Research Vessel POLARSTERN to the Atlantic Ocean in 2016, by Karen Wiltshire, Eva-Maria Brodte, Annette Wilson and Peter Lemke

**712 (2017)** The Expedition PS104 of the Research Vessel POLARSTERN to the Amundsen Sea in 2017, by Karsten Gohl

**711 (2017)** Mid-Range forecasting of the German Waterways streamflow based on hydrologic, atmospheric and oceanic data, by Monica Ionita

**710 (2017)** The Expedition PS103 of the Research Vessel POLARSTERN to the Weddell Sea in 2016/2017, edited by Olaf Boebel

**709 (2017)** Russian-German Cooperation: Expeditions to Siberia in 2016, edited by Pier Paul Overduin, Franziska Blender, Dmitry Y. Bolshiyarov, Mikhail N. Grigoriev, Anne Morgenstern, Hanno Meyer

**708 (2017)** The role of atmospheric circulation patterns on the variability of ice core constituents in coastal Dronning Maud Land, Antarctica, by Kerstin Schmidt

**707 (2017)** Distribution patterns and migratory behavior of Antarctic blue whales, by Karolin Thomisch

**706 (2017)** The Expedition PS101 of the Research Vessel POLARSTERN to the Arctic Ocean in 2016, edited by Antje Boetius and Autun Purser

**705 (2017)** The Expedition PS100 of the Research Vessel POLARSTERN to the Fram Strait in 2016, edited by Torsten Kanzow

**704 (2016)** The Expeditions PS99.1 and PS99.2 of the Research Vessel POLARSTERN to the Fram Strait in 2016, edited by Thomas Soltwedel

**703 (2016)** The Expedition PS94 of the Research Vessel POLARSTERN to the central Arctic Ocean in 2015, edited by Ursula Schauer

**702 (2016)** The Expeditions PS95.1 and PS95.2 of the Research Vessel POLARSTERN to the Atlantic Ocean in 2015, edited by Rainer Knust and Karin Lochte



**ALFRED-WEGENER-INSTITUT**  
HELMHOLTZ-ZENTRUM FÜR POLAR-  
UND MEERESFORSCHUNG

**BREMERHAVEN**

Am Handelshafen 12  
27570 Bremerhaven  
Telefon 0471 4831-0  
Telefax 0471 4831-1149  
[www.awi.de](http://www.awi.de)

